




Universitetet
i Stavanger

Faculty of Science and Technology

Master's Thesis

Study program/specialization: Petroleum Engineering Reservoir Technology	Spring semester, 2019 Open access
Author: Markus Lindanger	 (authors signature)
Supervisors: Skule Strand Tina Puntervold Iván Darío Piñerez Torrijos	
Thesis title: Production of Smart Water by Acid Flooding in Chalk Cores: Oil Recovery Effects at Intermediate Temperature	
Credits (ECTS): 30	
Keywords: Enhanced Oil Recovery Acid Flooding Ion Chromatography Smart Water Wettability Alteration	Number of pages: 110 + supplemental material: 20 Stavanger, 14th of June 2019

MASTER'S THESIS

**Production of Smart Water by
Acid Flooding in Chalk Cores**

Oil Recovery at Intermediate Temperature

By:
MARKUS LINDANGER



FACULTY OF SCIENCE AND ENGINEERING
DEPARTMENT OF ENERGY RESOURCES

June 14, 2019

Acknowledgements

This experimental thesis has been a great learning experience for me, and I would like to thank associate professors Skule Strand and Tina Puntervold for giving me an interesting and challenging topic. The guidance from both have been excellent, and their office doors have always been open whenever I needed to discuss something. I am also very grateful for the supervision from Dr. Iván Darió Piñerez Torrijos, both in the laboratory and for help regarding the thesis.

It has been a joy to work in the Smart Water EOR laboratory and I would like to thank my fellow lab-partners Agnes, Amalie, Erlend and Katarina for making it so, with good music, jokes and fruitful discussions. Finally, a huge thank you to all students in Petroleum Engineering at the University of Stavanger. Many good times have been shared together during these five years, and it would not have been the same without you.

I also acknowledge The National IOR Centre of Norway for the funding and collaboration.

Abstract

Considering that most carbonates are of low water wetness, it is of great interest to inject a brine that can alter the wettability to enhance oil production. Smart Water injection has therefore become the most meaningful EOR flooding technique in chalk reservoirs in recent years. The EOR technology is based on tuning the ionic composition of the injection brine to increase the water-wetness of the reservoir, which induces stronger capillary forces and increased microscopic sweep efficiency. Injection of seawater (SW) has already proven to be a great success at the chalk reservoir Ekofisk, and is considered as an excellent wettability modifier. However, research has shown that SW enriched in SO_4^{2-} and Ca^{2+} and depleted in monovalent ions is even more efficient at wettability alteration (Fathi, 2012).

The purpose of this thesis is therefore to test if an improved Smart Water can be produced by injecting sulphuric acid into chalk outcrop cores. The acid will then provide SO_4^{2-} -ions, and dissolution of chalk will add Ca^{2+} -ions to the solution. The produced Smart Water then contains the necessary potential determining ions and at the same time is of low salinity.

In the first part of the experiment, sulphuric acid concentrations of 9.7, 13.3 and 16.7 mM were flooded at 70 °C, while 4.9 and 8.5 mM were flooded at 130 °C. Ion chromatography (IC) analysis of the effluent from the acid flooding was then performed to evaluate the composition of the produced Smart Water. In the second part, oil recovery by spontaneous and forced imbibition was conducted at 90 °C with Smart Water and SW. Gypsum was used as Smart Water to represent the brine produced by acid flooding, to simplify the experimental test. FW was imbibed at 70 °C to have a reference where no wettability alteration takes place. The experiments were performed to study the performance of the Smart Water relative to SW. Three cores saturated with $S_{wi} = 10\%$ VBOS and $S_{oi} = 90\%$ oil with AN=0.5 mgKOH/g with permeabilities 4.65-5.14 mD and porosities 48-49 % were used for the experiment. In the third part of the experiment, the effect temperature has on wettability alteration was investigated, by comparing the performance of Smart Water and SW at 90 °C, with a parallel study performed at 70 °C with the exact same fluids.

The IC-analysis of the effluent from the acid flooding, show that the Smart Water acquires a composition of SO_4^{2-} and Ca^{2+} in a 1:1 proportion. The oil recovery by spontaneous imbibition for FW, SW and Smart Water were, 10 %, 24% and 27 % OOIP, respectively. The corresponding modified Amott water index for the fluids in the same order, was $I_{W-SI}^* = 0.13$, $I_{W-SI}^* = 0.31$ and $I_{W-SI}^* = 0.36$. The same trend was seen with the Amott water index, with $I_W = 0.18$, $I_W = 0.44$ and $I_W = 0.49$, for FW, SW and Smart Water. The temperature show a clear effect on the wettability alteration with both Smart Water and SW producing 14-16 % more at 90 °C compared at 70 °C by spontaneous imbibition.

Results from the experiments therefore confirm that a Smart Water of low salinity can be produced by injecting sulphuric acid into Stevns Klint chalk outcrop cores. When the acid solution is transported across the core, it establishes an equilibrium with the chalk surface and obtains an equal proportion of Ca^{2+} -ions and SO_4^{2-} -ions. Based on the imbibition rate and ultimate recovery from the spontaneous imbibition, along with the modified Amott water index and normal Amott water index, a conclusion can be made that the Smart Water is slightly more efficient than SW at increasing the water wetness at 90 °C.

Contents

Acknowledgements	i
Abstract	ii
List of Figures	vi
List of Tables	vii
Nomenclature	viii
1 Introduction	1
1.1 Objective	4
2 Theory	6
2.1 Recovery of Hydrocarbons	6
2.2 Displacement Efficiency	7
2.3 Displacement Forces	7
2.3.1 Gravity Forces	8
2.3.2 Viscous Forces	8
2.3.3 Fluid Flow in Porous Media	9
2.3.4 Capillary Forces	10
2.4 Surface Forces	13
2.4.1 Electrical Double Layer	13
2.4.2 Disjoining Pressure	13
2.5 Wettability	14
2.5.1 Wettability Measurements	15
2.5.2 Amott Method	16
2.5.3 United States Bureau of Mines	18
2.5.4 Chromatographic Wettability Test	19
2.5.5 Spontaneous Imbibition Method	20
2.6 Dissolution and Solubility	22
2.6.1 Chemical Equilibrium	22
2.6.2 Acid Dissociation in Aqueous Solutions	23
2.6.3 Strength of Acids and Bases	24
2.6.4 Solubility Equilibrium	25
2.7 Solubility and Influencing Factors	26
2.7.1 Carbonate Acid System	27

3	Chalk Wettability and Wettability Alteration by Smart Water	30
3.1	Carbonate Reservoirs	30
3.1.1	Carbonate Rocks	30
3.2	Initial Wettability of Chalk	33
3.3	Potential Determining Ions in Chalk	38
3.4	Smart Water EOR Mechanism	40
3.5	Temperature Effect on Wettability Alteration	42
3.6	Modified Seawater for EOR	43
3.7	Production of Smart Water	46
3.7.1	Smart Water Production by Membranes	46
3.7.2	Production of Smart Water by Sulphuric Acid	48
4	Experimental	49
4.1	Materials	49
4.1.1	The Outcrop Rock	49
4.1.2	Preparation of Oil	50
4.1.3	Brines	52
4.2	Analyses	54
4.2.1	Viscosity Measurement	54
4.2.2	IFT Measurement	54
4.2.3	pH Measurements	54
4.2.4	Density Measurements	55
4.2.5	Acid-Number (AN) and Base-Number (BN)	55
4.2.6	PHREEQC	55
4.2.7	Scanning Electron Microscope with EDX	56
4.2.8	Ion Chromatography Analyses of Brines	57
4.3	Methodology	58
4.3.1	Chalk Core Cleaning	58
4.3.2	Permeability and Porosity Measurements	59
4.4	Core Restoration for SI and FI Experiments	60
4.4.1	Establishing Initial Water Saturation	60
4.4.2	Establishing Initial Oil Saturation	61
4.4.3	Ageing	61
4.5	Oil Recovery by Spontaneous Imbibition	62
4.6	Oil Recovery by Forced Imbibition	62
4.7	Bulk Solution Test	63
4.7.1	Synthetic Production of H ₂ SO ₄ Based Smart Water	65
4.8	Acid Flooding	66
5	Results and Discussion	69
5.1	Acid Flooding	70
5.1.1	Acid Flooding at 70°	71
5.1.2	Acid Flooding at 130°	75

5.1.3	Summary of Acid Flooding	77
5.1.4	PHREEQC Simulation - Improvements to Smart Water	80
5.2	Scanning Electron Microscope Analysis	82
5.2.1	Chalk Characterization	82
5.2.2	Investigation of Acid-Dissolution	84
5.3	Smart Water EOR in Chalk	87
5.3.1	Initial Wetting of the SK Cores	88
5.3.2	Initial Wetting State of the Restored SK Cores	89
5.3.3	Comparison of SW and Smart Water	91
5.3.4	Spontaneous Imbibition - Discussion	92
5.3.5	Forced Imbibition - Discussion	98
5.4	Temperature Effect on Wettability Alteration	100
5.4.1	Temperature Effect - Spontaneous Imbibition	100
5.4.2	Temperature Effect - Forced Imbibition	101
6	Conclusions and Future Work	102
6.1	Conclusions	102
6.2	Future Work	103
	Bibliography	110
	Appendix	111
A	Poster	112
B	Chemicals and Brine Recipes	114
B.1	Acid Number Solutions	114
B.2	Base Number Solutions	115
B.3	Brine Recipes	116
C	Imbibition Data	117
C.1	Imbibition Data for SK5	117
C.1.1	Spontaneous Imbibition Data - SK5	117
C.1.2	Forced Imbibition Data - SK5	118
C.2	Imbibition Data for SK6	120
C.2.1	Spontaneous Imbibition Data - SK6	120
C.2.2	Forced Imbibition Data - SK6	121
C.3	Imbibition Data for SK2	123
C.3.1	Spontaneous Imbibition Data - SK2	123
C.3.2	Forced Imbibition Data - SK2	124
C.4	pH of Effluent During Acid Flooding	126
C.5	Ion Chromatography Results	127
C.5.1	IC Analysis of Effluent from 6 mM H ₂ SO ₄ (130°)	127
C.5.2	IC Analysis of Effluent from 8 mM H ₂ SO ₄ (130°)	127

C.5.3	IC Analysis of Effluent from 12 mM H ₂ SO ₄ (70°)	128
C.5.4	IC Analysis of Effluent from 15 mM H ₂ SO ₄ (70°)	128
C.5.5	IC Analysis of Effluent from 18 mM H ₂ SO ₄ (70°)	129

D PHREEQC 130

D.1	PHREEQC - SO ₄ ²⁻ equilibrated with CaCO ₃ (s)	130
D.2	PHREEQC - SO ₄ ²⁻ and Mg ²⁺ equilibrated with CaCO ₃ (s)	130

List of Figures

1.1	Waterflooding and Smart Water flooding comparison.	1
1.2	Optimal SW composition for wettability alteration in chalks.	2
2.1	A bundle of capillary tubes	8
2.2	Capillary tube in a water/air system.	10
2.3	Capillary tube in an oil/water system.	11
2.4	Force balance on water, oil and solid in equilibrium.	14
2.5	Capillary pressure curve for Amott and Harvey wettability test.	17
2.6	Illustration of a spontaneous imbibition test.	20
2.7	Hexamminecobalt(II)	26
2.8	Bjerrum plot	29
3.1	Distribution of wettability on 161 carbonate cores	31
3.2	Image of the chalk surface taken by the scanning electron microscope	32
3.3	Effect of FW composition on the initial wetting state of Stevns Klint cores.	34
3.4	Oil production vs Time for oils with different AN-numbers by spontaneous imbibition.	35
3.5	Effect of crude oil AN and aging temperature on water wet surface area.	36
3.6	Acid number of effluent crude oil versus PV flooded.	37
3.7	Zeta potential on Stevns Klint chalk as a function of Ca^{2+} and SO_4^{2-} concentration.	38
3.8	Interaction of the divalent ions SO_4^{2-} , Ca^{2+} and Mg^{2+}	39
3.9	Illustration of the Smart Water mechanism.	41
3.10	Adsorption of sulfate on chalk at different temperatures.	42
3.11	Comparison of modified SW at 70 °C and 90 °C.	43
3.12	Oil Recovery as a function of SW composition at 90 °C.	44
3.13	Illustration of Smart Water production from SW using NF membranes	46
3.14	Distribution of ion rejection by the NF membrane.	47
4.1	Scanning electron microscope (SUPRA V35) and Palladium coating on chalk samples.	56
4.2	Determination of permeability.	59
4.3	Set-up used to establish oil saturation.	61
4.4	Experimental set-up of the spontaneous imbibition.	62

4.5	Trend plot for determination of SO_4^{2-} -concentration at 90 °C.	65
4.6	Chemical structure of the sulphuric acid H_2SO_4	66
4.7	Illustration of core flooding setup used during experiments.	67
5.1	Injection of DI-water with increasing H_2SO_4 -concentration at 70 °C with a rate of 12 PV/d = 0.32 ml/min.	71
5.2	pH measurements of the brines at 70 °C	73
5.3	Plots from the ion chromatography data.	75
5.4	pH measurements of the brines at 130 °C	76
5.5	Simulation of Precipitation of Anhydrite in DI-water performed in PHREEQC, without Mg	80
5.6	Simulation of Precipitation of Anhydrite in DI-water performed in PHREEQC with Mg present	81
5.7	Image of the chalk surface magnified 1000 times of a Stevns Klint core.	82
5.8	SEM-image of the chalk surface magnified 10 000 of a Stevns Klint Core.	83
5.9	Comparison of dissolution between inlet and outlet of a chalk core flooded with acid	84
5.10	SEM-image of the inlet of chalk core flooded with acid.	85
5.11	SEM-image of the outlet of chalk core flooded with acid.	86
5.12	Spontaneous imbibition at 25 °C with DI for core SKWW	88
5.13	Spontaneous imbibition at 70 °C with FW for core SK2	89
5.14	Comparison of SW and Smart Water by spontaneous imbibition at 90 °C.	91
5.15	Comparison of SW, FW and Smart Water on spontaneous imbibition performance.	92
5.16	Oil recovery by forced imbibition of FW and Smart Water at 70 °C .	95
5.17	Oil recovery by forced imbibition of SW and Smart Water at 90 °C .	96
5.18	Oil recovery by forced imbibition of Smart Water at 90 °C	97
5.19	Comparison of SW and Smart Water by spontaneous imbibition at 70 °C and 90 °C.	100

List of Tables

2.1	Summary of equilibrium constants in the carbonate acid system . . .	29
3.1	Ionic composition of retentate and permeate with the nanofiltration membrane, NF 270	47
4.1	Stevns Klint Cores used during this thesis with physical parameters. .	49
4.2	Properties of the oils used in this experimental study, showing measured AN and BN.	51
4.3	Interfacial tension of oil in equilibrium with FW, SW and Smart Water at 23 °C.	51
4.4	Composition of the formation water at Valhall (VB0S), seawater (SW) and Smart Water.	53
4.5	DI-water with H ₂ SO ₄ equilibrated with CaCO ₃	64
4.6	pH and H ₂ SO ₄ concentration of the injected acid solutions.	64
5.1	Summary of the effluent ion concentration and pH from the acid flooding.	79
5.2	EDX-analysis on a chalk piece from a Stevns Klint core which comes straight from an outcrop block.	82
5.3	EDX-analysis on chalk piece from the inlet slice post acid-flooding. .	85
5.4	EDX-analysis on chalk piece from the outlet slice post acid-flooding. .	86
5.5	Oil recovery by spontaneous imbibition comparison of completely water-wet core, FW, SW and Smart Water.	94
5.6	Results from oil recovery by forced imbibition experiments.	98
5.7	Summary of oil recoveries by spontaneous imbibition conducted at temperatures of 70 °C and 90 °C.	101
B.1	Chemicals for acid number measurements	114
B.2	Chemicals for base number measurements	115
B.3	Composition of the formation water at Valhall without sulphate, VB0S, synthetic seawater SW and Smart Water.	116
C.1	Spontaneous imbibition data of SK5 with SSW.	117
C.2	Forced imbibition data of SK5 with SSW and CaSO ₄	118
C.3	Spontaneous imbibition data of SK6 with Smart Water.	120
C.4	Forced imbibition data of SK6 with Smart Water.	121
C.5	Spontaneous imbibition data of SK2 with FW (VB0S).	123

C.6	Forced imbibition data of SK2 with FW (VB0S) and later switched to CaSO ₄	124
C.7	pH of effluent during acid flooding of core SK1	126
C.8	Ion chromatography analysis of effluent from 6 mM H ₂ SO ₄	127
C.9	Ion chromatography analysis of effluent from 8 mM H ₂ SO ₄	127
C.10	Ion chromatography analysis of effluent from 12 mM H ₂ SO ₄	128
C.11	Ion chromatography analysis of effluent from 15 mM H ₂ SO ₄	128
C.12	Ion chromatography analysis of effluent from 18 mM H ₂ SO ₄	129
D.1	Simulation of SO ₄ ²⁻ equilibrated with CaCO ₃ (s).	130
D.2	Simulation of SO ₄ ²⁻ and Mg ²⁺ equilibrated with CaCO ₃ (s).	130

Nomenclature

A	Cross-sectional area	[m ²]
A_1	Grey filled area under forced drainage curve	
A_2	Grey filled area under forced imbibition curve	
$A_{heptane}$	Area between sulfate and tracer curve for reference core	
A_{wett}	Area between sulfate and tracer curve for sample core	
C_1	Concentration of stock solution	[moles/L]
C_2	Concentration of diluted solution	[moles/L]
E	Overall displacement efficiency	
E_D	Microscopic displacement efficiency	
E_V	Macroscopic displacement efficiency	
H	Height of a liquid column	[cm]
I	Relative displacement index	
I_O	Amott wettability index to oil	
I_{USBM}	USBM wettability index	
I_W	Amott wettability index to water	
K	Equilibrium constant	
K_a	Acid-dissociation constant	
K_{sp}	Solubility product constant	
M	Mobility factor	
PV	Pore volume	[ml]
P_{atm}	Atmospheric pressure	[Pa]
P_b	Pressure in the liquid bulk phase	[Pa]
P_c	Capillary pressure	[Pa]

P_f	Pressure in the liquid film	[Pa]
P_o	Oil phase pressure	[Pa]
P_w	Water phase pressure	[Pa]
Q	Reaction quotient	
R	Radius of the inter-granular pore throats	[cm]
S_{oi}	Initial oil saturation	
S_{or}	Residual oil saturation	
S_w	Water saturation	
V_1	Volume of stock solution	[L]
V_2	Volume of diluted solution	[L]
WI	Chromatographic wettability index	
W_{target}	Predefined target weight	[g]
ΔP	Differential pressure	[Pa]
ΔP_g	Pressure difference due to gravity	[Pa]
ΔS_{OF}	Saturation change during forced imbibition of oil	
ΔS_{OS}	Saturation change during spontaneous imbibition of oil	
ΔS_{WF}	Saturation change during forced imbibition of water	
ΔS_{WS}	Saturation change during spontaneous imbibition of water	
ΔS_w	Change in water saturation	
$\Delta \rho$	Density difference	[kg/m ³]
Ω	Saturation state	
Π	Disjoining pressure	[Pa]
ΣF_y	Sum of forces in y-direction	[N]
\bar{v}	Average velocity	[cm/s]
μ	Viscosity	[mPas]
μ_o	Viscosity of oil	[mPas]
μ_w	Viscosity of water	[mPas]

ρ_{VB0S}	Density of valhall formation water	[kg/m ³]
ρ_a	Density of air	[kg/m ³]
ρ_o	Density of oil	[kg/m ³]
ρ_w	Density of water	[kg/m ³]
σ	Interfacial tension	[N/m]
σ_{os}	Interfacial tension between oil and solid	[N/m]
σ_{ow}	Interfacial tension between oil and water	[N/m]
σ_{ws}	Interfacial tension between water and solid	[N/m]
θ	Wetting angle	
dp/dx	Pressure gradient	[Pa/m]
g	Gravity constant	[m/s ²]
g_c	Conversion factor	
h	Height from free water level to meniscus	[cm]
h_1	Height from surface to oil-water interface	[cm]
k	Permeability	[md]
k_{ro}	Relative permeability of oil	
k_{rw}	Relative permeability of water	
q	Flow rate	[cm ³ /s]
r	Radius of capillary tube	[cm]
AN	Acid number of the crude oil	[mgKOH/g]
BN	Acid number of the crude oil	[mgKOH/g]
DI	Deionized water	
EOR	Enhanced oil recovery	
FI	Forced imbibition	
FW	Formation water	
IFT	Interfacial tension	
OOIP	Original oil in place	

SI Spontaneous imbibition
SW Seawater
TDS Total dissolved solids [g/L]
VB0S Synthetic Valhall formation water without sulfate

1 | Introduction

Waterflooding has historically been implemented when the natural energy of the reservoir no longer can sustain enough pressure to displace hydrocarbons towards the well. The injected water prolong the production by maintaining the reservoir pressure and by increasing the oil displacement efficiency. The recovery from waterflooded reservoirs can be very high, in some cases over 50 % (Dake, 1978). In chalk reservoirs however, natural fractures exist with permeabilities up to 100 times higher than the matrix permeability (Graue et al., 2002). Since the water follows the path of least resistance, it will flow through the high permeable fractures rather than through the matrix, as seen in figure 1.1 (a). The water will only displace oil in the fractures and not the oil residing in the matrix, leading to an overall low recovery factor. Consequently, the process of absorbing water into the rock matrix without pressure support seen in figure 1.1 (b), is a fundamental recovery method for chalk fields. This absorption process is known as spontaneous imbibition (SI), and it is a capillary driven mechanism. The SI process can only happen when the capillary forces are positive, which means that the rock has to be water-wet. Considering that most carbonates are oil-wet (Chilingar and Yen, 1983), it is of great importance to alter the wettability toward a more water-wet state. Studies have shown that injection brines containing Ca^{2+} -ions and SO_4^{2-} -ions, are able to disturb the chemical equilibrium in the reservoir, leading to an alteration in wettability (Zhang, 2006).



(a) Standard waterflooding.

(b) Spontaneous imbibition

Figure 1.1: With positive capillary pressure, the water imbibes spontaneously into the matrix, thus displacing an increased fraction of oil.

Seawater (SW) contains both of these ions, and have already proven to be an excellent fluid for wettability alteration in chalk (Strand et al., 2005; Zhang et al., 2006; Austad et al., 2009). Recently it has been found that certain modifications to

SW can make it even more efficient in increasing the water wetness in chalks (Fathi, 2012; Puntervold et al., 2015). One way of improving SW, is to deplete it in NaCl while maintaining Ca^{2+} , Mg^{2+} and SO_4^{2-} -concentration. This modified SW, termed as SW0Na, gives a higher recovery than SW by spontaneous imbibition, as given in figure (1.2). Hence, there appears to be a salinity effect associated with wettability alteration in chalks. Furthermore, will SW depleted in NaCl and spiked in SO_4^{2-} be of even higher efficiency, with 20 % OOIP more than SW.

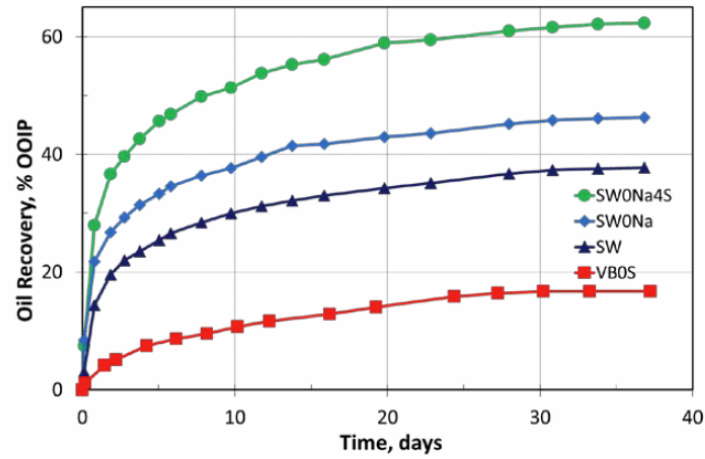


Figure 1.2: Optimal SW composition for wettability alteration in chalks. Figure by (Fathi, 2012).

Smart Water Definition

With many different companies and researchers, there have been correspondingly many names for brines that work as wettability modifiers in chalk reservoirs. Hence, a short introduction to some of the names, in addition to a definition of the Smart Water term is given here.

BP call their technology *LoSal*, and focuses on brines with low salinity in sandstones. The LoSal technology will be implemented on Clair Ridge in the near future, with an expected additional oil recovery of 40 million barrels due to the low salinity brine (BP, 2019). Exxon named their technology *Advanced Ion Management*, which modifies injection water by addition, removal or dilution of ions for carbonate reservoirs (Vo et al., 2012). While Shell call their technology *Designed Water Flood*, with the emphasis on low salinity water injection (Shell, 2019).

The EOR group at the University of Stavanger have proposed their water technology "Smart Water". In contrast to the companies above which focuses solely on either low salinity or addition/removal of ions, Smart Water is rather a broad definition of a brine with *a specific ionic composition that can change the wettability of the rock* (Austad et al., 2017). Hence, Smart Water can be SW which is injected into the carbonate reservoir at Ekofisk and it can be a low salinity brine in sandstone reservoirs.

By altering the wettability of the chalk towards a more water-wet state, Smart Water enhances the fluid flow and increases the oil recovery. This is attributed to the increase in capillary forces which allow for improved water imbibition into smaller pores. Oil from the smaller pores then flow through larger pores and fractures that act as transport veins for the oil to producer. Smart Water is made by modifying the composition of ions of the injected fluid. Subsequently, no chemicals are added, such as polymers or surfactants making it rather cheap and environmentally friendly (Austad, Strand, and Puntervold, 2017).

1.1 Objective

In this thesis work we will investigate further the salinity effect, and evaluate if a Smart Water brine can be made by injecting fresh water containing sulphuric acid (H_2SO_4) into chalk cores, and study if it is more efficient than SW in altering the wettability. Acid-dissociation will provide SO_4^{2-} -ions to the brine, and dissolution of chalk will release Ca^{2+} -ions to the brine. With no other salts added the salinity could be held at a minimum. Spontaneous- and forced imbibition experiments are performed on mixed wet outcrop chalk cores from Stevns Klint to evaluate the efficiency of H_2SO_4 in fresh water as Smart Water at 90 °C in this thesis compared with corresponding results obtained by Andreassen (2019) at 70 °C. Since SW already is considered a Smart Water in chalk, oil recovery by spontaneous and forced imbibition is compared to SW.

In terms of practicality, reverse osmosis membranes can be used on the rigs to desalinate SW to make fresh water. Sulphuric acid on the other hand, is readily available on the international market, and can be bought in large quantities, making it very cheap. According to Alibaba.com, one ton of high quality industrial grade H_2SO_4 can be bought for between \$ 200-400 USD (Alibaba, 2019).

The work-flow for this experimental thesis is shown as a bullet list, to summarize the work involved in this thesis:

- An acid flooding experiment is set-up, where sulphuric acid (H_2SO_4) dissolved in deionized water (DI) is injected at different concentrations at 70 °C and 130 °C. Effluent is analysed by ion chromatograph to evaluate optimized H_2SO_4 concentration to avoid precipitation of anhydrite $\text{CaSO}_4(\text{s})$, and to verify if dissolution of chalk is possible in core experiments.
- If production of Smart Water is confirmed to work by acid flooding and an equal proportion of SO_4^{2-} - and Ca^{2+} -ions is obtained in the effluent brines, gypsum ($\text{CaSO}_4 \cdot 2 \text{H}_2\text{O}$) will be used to synthetically produce the Smart Water to simplify the spontaneous and forced imbibition experiments.
- Oil recovery experiments by spontaneous imbibition at 90 °C is conducted to evaluate the performance of the Smart Water compared to SW. Since a parallel study is conducted at 70 °C by Andreassen (2019), a core experiment with formation water (FW) imbibition is shared between these studies. The shared core experiment will verify initial core wettability as no wettability alteration is taking place with FW. In addition, can the wettability alteration of SW and Smart Water be compared relative to FW. A modified Amott water index is used to quantify the wettability alteration.
- A parallel study is performed at 70 °C by Andreassen (2019) with all experimental parameters held equal as in the experiment conducted at 90 °C. As a result, the temperature effect on wettability alteration can also be investigated for SW and the Smart Water.
- After spontaneous imbibition experiments, the cores are subjected to forced imbibition at 90 °C for SW and Smart Water, while FW is injected at 70 °C. Oil recovery is then continued by applying a pressure gradient across the core. By conducting forced imbibition, the Amott water index is obtained. By using the Amott water index, the extent of wettability alteration by the different fluids at different temperatures can be quantified.
- Modelling in PHREEQC is also utilized to examine if a higher H_2SO_4 -concentration can be achieved for chalk reservoirs, by adding Mg^{2+} -ions to the injected brine. The concentration of SO_4^{2-} -ions is limited by the solubility of anhydrite (CaSO_4). Recall from earlier that SW spiked with SO_4^{2-} -ions is the most efficient Smart Water, it is therefore of great interest to investigate this matter further.

2 | Theory

2.1 Recovery of Hydrocarbons

Oil recovery has traditionally been divided into three stages that occur at different times during the lifetime of a well.

Primary Recovery

Primary recovery is the first production stage, where the drive mechanisms displacing the oil are naturally existing in the reservoir. The most common mechanisms are: solution-gas drive, gas-cap drive, fluid and rock expansion, expansion of aquifer and gravitational drainage. Since all these processes are associated with decline in reservoir pressure, primary recovery is often called pressure depletion (Muskat, 1949).

Secondary Recovery

After the initial production stage, secondary recovery is initiated to ensure pressure maintenance through waterflooding, but also includes gas injection (to maintain gas cap). The additional energy provided to the reservoir, extends the lifetime of the well and displaces oil towards the producers.

Enhanced Recovery Processes

The third recovery stage used to be known as tertiary production. However, since some reservoirs requires this stage from the start (for instance heavy oils might need thermal energy), it is more preferred by the industry to name it enhanced oil recovery (EOR). The objective with EOR-processes, is to increase sweep efficiency by extracting hydrocarbons that the two first production stages left behind. EOR-processes involves injection of fluids that interact in a favourable way with the oil and rock in the reservoir, and thereby increases the overall recovery. The categories of EOR processes are: thermal, miscible, chemical, immiscible gas drives and other (Green and Willhite, 1998). In 2017, Hopkins proposed an additional category called "wettability alteration", where the main mechanism is to increase capillary forces which leads to increased microscopic sweep efficiency (with Smart Water being in this group) (Hopkins, 2017).

2.2 Displacement Efficiency

The overall performance of any oil recovery displacement process consists of two components, the microscopic displacement efficiency, E_D , and the macroscopic displacement efficiency, E_V . Expressed in equation form, the overall displacement efficiency, E , is the product of the two components:

$$E = E_D E_V. \quad (2.1)$$

Where the microscopic displacement efficiency describes to what extent the EOR fluid is able to mobilize oil at the pore scale. While the macroscopic displacement efficiency, measures how effective the EOR agent is at contacting the pore volume (Green and Willhite, 1998).

Smart Water has the ability to affect the microscopic sweep efficiency, by altering the wettability toward a more water-wet state which induces spontaneous imbibition. When water imbibes into the small chalk pores, it mobilizes oil that were previously unattainable. As a result, the residual oil saturation, S_{or} is reduced. By looking at the formula for microscopic displacement efficiency, E_D ,

$$E_D = \frac{S_{oi} - S_{or}}{S_{oi}}, \quad (2.2)$$

where S_{oi} is initial oil saturation, one can see that Smart Water increases the microscopic displacement efficiency, E_D , by lowering S_{or} .

2.3 Displacement Forces

During waterflooding, several forces affect the overall displacement efficiency. The forces of greatest significance are the capillary forces, the gravity forces and the viscous forces. They control mechanisms such as: phase trapping and mobilization, segregation due to density differences and pressure drop during oil production. For spontaneous imbibition, the two most important forces, are the capillary forces and the gravity forces. Where the capillary forces are the dominating force at high interfacial tension, σ , with gravity force becoming increasingly dominating as σ decreases (Austad and Milter, 1997).

2.3.1 Gravity Forces

Gravity forces are important for movement of oil, and have especially effect in tilted reservoirs. If the flow path for oil is steep enough, it can cause segregation of gas from oil due to density differences. Subsequently, the oil can be produced with a lower gas-oil ratio, and the reservoir energy is therefore conserved with the outcome of prolonged production from the reservoir (Hall, 1961). Gravity forces are also reported by Austad and Milter, (1997) to be important for oil flow when the interfacial tension between oil and water is low, and when the height of the matrix containing the reservoir fluids increases. The pressure difference between oil and water caused by gravity, ΔP_g , can be expressed as follows:

$$\Delta P_g = \Delta\rho \cdot g \cdot H, \quad (2.3)$$

where $\Delta\rho$ is the difference in density between oil and water (kg/m^3), g acceleration due to gravity (m/s^2) and H is the height of the liquid column in m.

2.3.2 Viscous Forces

Whenever a fluid is flowing through a porous media, it will experience resistance to flow due to viscous forces, which causes the pressure to drop. A way of measuring the magnitude of the viscous forces, is by approximating the reservoir channels as a bundle of capillary tubes of equal size and shape like in figure (2.1).

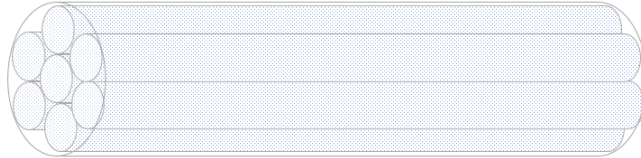


Figure 2.1: Bundle of capillary tubes.

Then by further assuming laminar flow through a single tube depicted above, the pressure drop across a single tube, ΔP , can be found by Poiseuille's law,

$$\Delta P = -\frac{8\mu L\bar{v}}{r^2 g_c}. \quad (2.4)$$

The pressure drop is proportional to the viscosity of the fluid, μ , the length of the tube, L and the average velocity, \bar{v} . While being inverse proportional to the radius, r and the conversion factor g_c .

2.3.3 Fluid Flow in Porous Media

Darcy's law is an equation that originates from Henry Darcy's experiments on fluid flow through sand packs in the 1850's. He found that the flow rate was proportional to the pressure drop across the sand pack while it was inversely proportional to the viscosity. From his studies he also observed that by changing filters on the sand packs, the constant, known as permeability, k , varied, and depended on the filters. In terms of reservoirs, the permeability is a constant which describes the ease at which a fluid permeates through a formation. The equation is given as,

$$q = -\frac{Ak}{\mu} \frac{dp}{dx}, \quad (2.5)$$

where q is the flow rate, A is the cross-sectional area, μ the viscosity of the fluid, k is the permeability and dp/dx is the pressure gradient. The equation is valid under horizontal flow of an incompressible fluid in 100 % saturated porous media. The flow regime must be laminar and no chemical reactions can occur between the fluid and the porous media (Zolotukhin, 2000).

An important aspect of fluid flow in porous media and displacement of oil, is the mobility factor, M . The factor is defined as,

$$M = \frac{k_{rw}/\mu_w}{k_{ro}/\mu_o}, \quad (2.6)$$

where k_{rw} and k_{ro} are the relative permeabilities of water and oil, respectively. While μ_w and μ_o are the viscosities of water and oil. The mobility factor describes the mobility of the water relative to the mobility of the oil. In an ideal water flood, water should flow behind the oil and displace the oil in a piston like manner. This can only happen if $M < 1$. On the other hand, if $M > 1$, the mobility of water will be greater than oil, resulting in a poor displacement process known as viscous fingering. The consequence of viscous fingering, is that the waterflooding will be less effective, with water bypassing a considerable volume of recoverable oil.

2.3.4 Capillary Forces

The capillary forces can dictate whether or not oil recovery will be high or low in reservoirs. In sandstones, strong capillary forces can lead to trapping of oil droplets causing low recoveries. Whereas in chalk reservoirs, strong capillary forces will work in favour for spontaneous imbibition leading to high recoveries. The critical role of the capillary forces, makes them the most important displacement forces for fluid flow in porous media.

Capillary forces are a combination of fluid-fluid interactions of two immiscible phases causing interfacial tension, and fluid-rock interactions associated with wettability of the system. Depending on the surface energy at the interface between oil and water, the rock mineral and the pore throat size, these forces will have a direct impact on fluid saturations, the distribution of fluids and the displacement efficiency of oil (Green and Willhite, 1998).

It is a well known phenomena that when a capillary tube is placed in a container with water, the water is drawn up the tube without any external support as seen in figure (2.2).

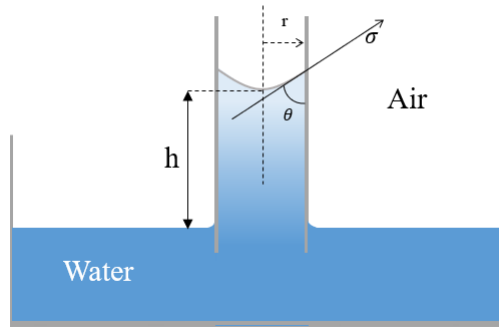


Figure 2.2: Capillary tube redrawn after (Green and Willhite, 1998). The diameter of tube has been exaggerated for illustration purposes.

The water will continue to rise until the capillary forces are neutralized by the weight of the column of water in the capillary tube below the interface. When the system has reached equilibrium, the sum of the forces in the vertical direction, ΣF_y , must be zero. Subsequently this can be used to measure the surface tension, σ :

$$\sigma \cos \theta \cdot 2\pi r = \pi r^2 (\rho_w - \rho_a) gh. \quad (2.7)$$

Here θ is the contact angle between the capillary tube and the water, r is the radius of the tube in cm. The height from free water level to meniscus is, h . Density of water and air are ρ_w and ρ_a in g/cm^3 , and the gravity constant is given as g in cm/s^2 . Then by expressing the equation in terms of the surface tension, σ , we get

the following equation, with unit dynes/cm:

$$\sigma = \frac{rh(\rho_w - \rho_a)g}{2 \cos \theta}. \quad (2.8)$$

With equation (2.8) in mind, a different system is introduced, consisting of air, oil and water. By studying the system in figure (2.3) at static conditions, a simple force balance can be used to find an expression for capillary pressure.

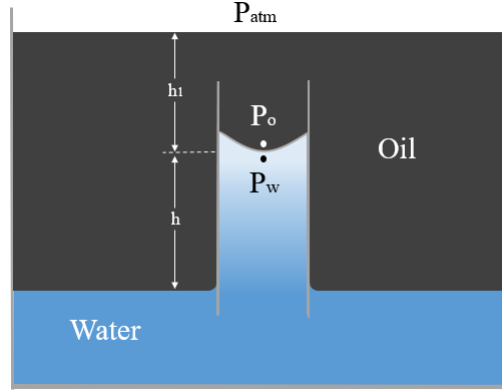


Figure 2.3: Capillary tube in a oil/water system, redrawn after (Green and Willhite, 1998). The diameter of tube has been exaggerated for illustration purposes.

The pressure in the oil phase at the point above the interface is given as,

$$P_o = P_{atm} + \rho_o g h_1, \quad (2.9)$$

and for water the pressure just below the interface is

$$P_w = P_{atm} + \rho_o g (h_1 + h) - \rho_w g h. \quad (2.10)$$

The atmospheric pressure, P_{atm} , is given in units dynes/cm². The height from the surface to the interface is h_1 in cm, while the height from the interface down to the free water level is h , also in cm. The densities ρ_o and ρ_w are density of oil and water respectively and have units g/cm³. The gravity acceleration constant is g , and has unit cm/s². By taking the difference between the oil and water pressure:

$$P_o - P_w = (P_{atm} + \rho_o g h_1) - (P_{atm} + \rho_o g (h_1 + h) - \rho_w g h), \quad (2.11)$$

the following equation becomes

$$P_o - P_w = (\rho_w - \rho_o) g h, \quad (2.12)$$

where the pressure difference between oil and water is termed as the capillary pressure, P_c .

By utilizing equation (2.8), and noting that now the non-wetting phase is oil instead of air, we can solve it with respect to the density difference, $\rho_w - \rho_o$, and insert it into equation (2.12) and we get:

$$P_c = \frac{2\sigma_{ow} \cos \theta}{r}. \quad (2.13)$$

Consequently, the capillary rise seen in (2.2) are dependent on three variables. The radius of the capillary tube, r , which is inversely related to P_c . The wettability of the system expressed through the contact angle θ and the interfacial tension between oil and water, σ_{ow} (Green and Willhite, 1998).

2.4 Surface Forces

2.4.1 Electrical Double Layer

If a charged solid and a fluid are in contact with each other, two characteristic layers with opposite charges will form in vicinity of the solid surface, known as the electrical double layer. An electrical potential therefore exists across the interface. In the first layer, ions are chemically bound (van Der Waals) to the surface of opposite charge, creating an inner region of immobile ions, known as the Stern layer. A second layer of counter ions is then formed, consisting of ions that are attracted to the surface charge by electrical forces (coulombically). The electric attraction allow ions in the second layer to move freely, hence the second layer is known as the diffusive layer. The ion concentration decreases with distance from the interface between the Stern layer and the diffusive layer. When the ion concentration is the same as in the bulk solution, the electrical potential becomes zero (Donaldson and Alam, 2008). The plane separating the immobile ions from the mobile ions, is by convention termed the slipping plane. By measuring the potential difference at the slipping plane and in the bulk solution, one can calculate the zeta-potential (Derjaguin, Churaev, and Muller, 1987).

2.4.2 Disjoining Pressure

A thin liquid film lying between a solid surface and the bulk phase of the liquid, may have a pressure which is different from that within the bulk phase. The difference in pressure is known as the disjoining pressure, Π , and was defined by (Derjaguin, Churaev, and Muller, 1987), as:

$$\Pi = P_f - P_b. \quad (2.14)$$

Where P_f is the pressure in the liquid film, while P_b is the pressure in the bulk phase of the liquid. The disjoining pressure consist of van Der Waals forces (attractive) and electrostatic forces (attractive/repulsive), and together these forces regulate the film thickness (Donaldson and Alam, 2008). The disjoining pressure is therefore a function of film thickness, $\Pi = \Pi(h)$. When the disjoining pressure is negative the two interfaces in the film (solid/film and film/bulk phase) will attract each other, and the film begins to thin. If, the disjoining pressure is positive however, the film thickness will increase, since the two interfaces repel each other.

2.5 Wettability

In a multiphase reservoir, the fluids occupying the pore space will have different affinities for the mineral surfaces, based on ageing, temperature and the surface charge. As a result, there will be a distribution of fluids at the pore scale. The phenomena is called wettability, and it has a direct impact on important parameters such as: relative permeability, k_r , capillary pressure and initial distribution of phases. Since it governs the multiphase flow properties, it is a key parameter for a successful waterflood. Wettability can be defined as *the tendency of one fluid to spread and adhere to a solid surface in the presence of other immiscible fluids* (Craig, 1971). The phase which adheres to the reservoir rock, is termed the wetting phase.

In order to determine which phase is the wetting phase, we can study a single water drop on a solid surface as seen in figure (2.4). Before the system reaches equilibrium, the water drop can either spread or contract on the solid surface, forming an oil/water/solid contact angle, θ , between 0° to 180° . When the forces are balanced and the water drop has stopped moving, the sum of the interfacial forces must be zero:

$$\sigma_{os} - \sigma_{ws} = \sigma_{ow} \cos \theta. \quad (2.15)$$

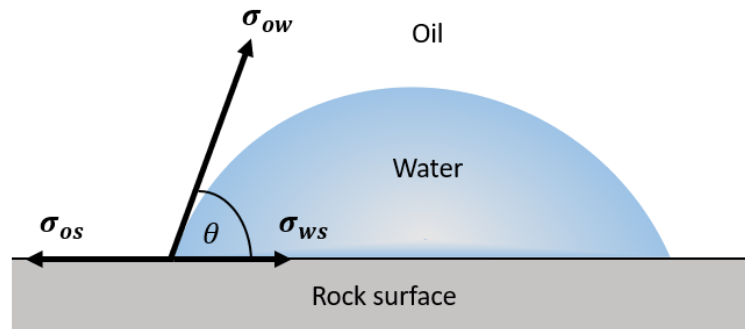


Figure 2.4: Force balance on water, oil and solid in equilibrium. Redrawn after (Green and Willhite, 1998)

Equation (2.15) is called Young's equation, and it is simply a force balance at the intersection line of the solid, oil and water. Where σ_{os} is the interfacial tension between oil and solid, σ_{ws} is the interfacial tension between water and solid, and σ_{ow} is the interfacial tension between oil and water.

By measuring the contact angle θ through the denser phase, which is water in figure (2.4), one can determine the wettability of the system. If the water drop makes an angle with the reservoir rock that is $\theta < 90^\circ$, it is essentially spreading over the surface. Water will then cover most of the mineral surfaces in the reservoir and also reside in the smaller pores, making the reservoir preferentially water-wet. Oil is then distributed in the centre of the pores with water above and below it. However, when the contact angle $\theta > 90^\circ$, the reservoir is preferentially oil-wet. The water drop will contract (minimize the surface area), since the cohesive forces becomes stronger than the adhesive forces. The opposite scenario will then happen, where oil covers most of the surfaces and resides in the smaller pores of the reservoir, with water in the centre of the pore. In some cases the contact angle is close to 90° , which means that there is no preference for any of the fluids, and it is a neutral wettability (Green and Willhite, 1998).

Although wettability can be categorized into; oil-wet, water-wet and neutral-wet, they all imply a homogeneous wettability, where the wetting fluid is continuous. However it is reasonable to believe that there exist a heterogeneous wetting state in many reservoirs, considering that reservoir rocks consist of different minerals, each with their own surface chemistry (Anderson, 1986).

In 1956, Brown and Fatt proposed the idea that wettability of the total surface area could be divided into one preferentially oil-wet fraction and a preferentially water-wet fraction (Brown and Fatt, 1956). This heterogeneous wetting state, also called fractional wettability, implies that the same rock can adsorb polar oil components in one part of the rock, while other parts have a water film at the surface. A subgroup of fractional wettability was later suggested by (Salathiel, 1973), called mixed wettability. In this wetting state, water is preferentially wetting phase in the grain contacts and smaller pores, while the surfaces of the larger pores are oil-wet, forming continuous paths of the oil phase. Consequently, there are 5 wetting states: water-wet, oil-wet, neutral-wet, fractional wetting and mixed wetting.

2.5.1 Wettability Measurements

An accurate assessment of the wettability in a reservoir, is important for any reservoir management. The wettability will dictate how the waterflooding performance will be, the distribution of fluids and also determine whether or not a reservoir is a good candidate for wettability alteration. The angle measurement was mentioned above, however, it is taken at a flat surface in the laboratory. Considering that reservoirs in reality consists of pore structures that are rather complex, the angle measurement is not adequate. However, several methods are capable of measuring the wettability, and the most extensive are presented below.

2.5.2 Amott Method

The Amott method measures the average wettability of a core through application of spontaneous imbibition (SI) and forced imbibition (FI) (Anderson, 1986). By combining the two methods, parameters like relative permeability, viscosity and initial saturation of the rock are negated. Hence, the number of variables which could affect the performance of the test are removed, while the governing parameter becomes the wettability of the system.

The method can be divided into two parts, with the first part associated with oil as the displacing fluid and the latter part with water as the displacing fluid. In the first part, a fully water saturated core is immersed in oil, oil then displaces water as it spontaneously imbibes into the core. When the imbibition process is complete, the volume of water is measured. Subsequently, the core is either centrifuged or flooded to residual water saturation, S_{wr} . The volume of effluent water collected is noted, and hence the total volume is the sum of the two processes. In the second part the roles are reversed, as water is now the displacing fluid, while oil is in the core. The same sequence is executed as explained above.

The results from the experiments are then given as two Amott wettability indexes, I_O , and I_W , for oil and water respectively:

$$I_O = \frac{\Delta S_{OS}}{\Delta S_{OS} + \Delta S_{OF}}, \quad (2.16)$$

where I_O is the Amott wettability index to oil, ΔS_{OS} is the saturation change during spontaneous imbibition of oil, and ΔS_{OF} is the saturation change during forced imbibition of oil. While the Amott wettability index to water, I_W , is given as,

$$I_W = \frac{\Delta S_{WS}}{\Delta S_{WS} + \Delta S_{WF}}. \quad (2.17)$$

Where ΔS_{WS} is the saturation change during spontaneous imbibition of water, and ΔS_{WF} is the saturation change during forced imbibition of water. The ratios I_O , and I_W can be understood as follows: As I_O increases towards 1, the cores are correspondingly more and more oil-wet. Conversely, as I_W increases towards 1 they are more water-wet.

Amott-Harvey

This is a modified version of the Amott method, and it differs from the original method in the preparation stage. The preparation step can be seen in figure (2.5) as number 1, and is related to establishment of S_{wr} by forced displacement of oil into the core. Figure (2.5) displays the capillary pressure, P_c , on the y-axis versus the water saturation, S_w , on the x-axis, in addition to the whole Amott-Harvey test cycle. Each number is associated with a process in the Amott-Harvey test, which is explained below.

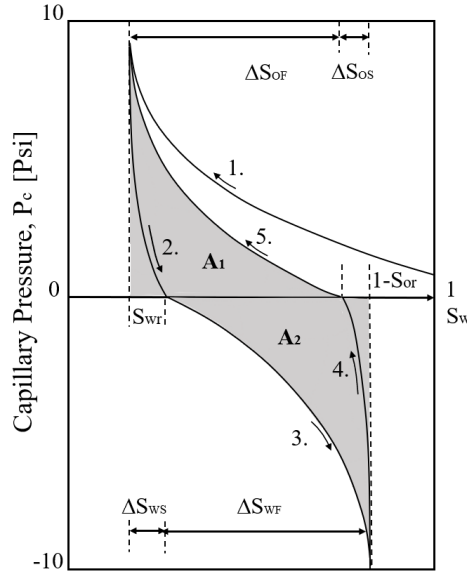


Figure 2.5: Capillary pressure curve for Amott and Harvey wettability test. Redrawn after Tina Puntervold (2008).

In figure (2.5), 5 processes are involved in the Amott-Harvey wettability test:

1. Establishment of S_{wr} through forced imbibition of oil into a water saturated core.
2. Spontaneous imbibition of water
3. Forced imbibition of water
4. Spontaneous imbibition of oil
5. Forced imbibition of oil

A new parameter known as the relative displacement index, I_{AH} , is introduced. It is simply the difference between the ratios given in equation (2.17) and (2.16):

$$I_{AH} = I_W - I_O, \quad (2.18)$$

it gives a number between +1 and -1. Where +1 implies a core which is completely water wet, while -1 is completely oil-wet. The scale was further narrowed down by (Cuiec, 1984) into; slightly oil wet (-0.3 to -0.1), neutral wet (-0.1 to +0.1) and slightly water wet (+0.1 to +0.3).

One of the disadvantages with the Amott Method, is that it is based on fluids that spontaneously imbibe into the core. Consequently, it cannot measure around neutral wettability, since no fluid will spontaneously imbibe (Anderson, 1986).

2.5.3 United States Bureau of Mines

The United States Bureau of Mines (USBM) wettability test developed by (Donaldson et al, 1969), is solely based on forced displacement and does not require the fluid to spontaneously imbibe. Consequently, the wettability of systems close to neutral wettability can be measured as opposed to the Amott method (Donaldson, Thomas, and Lorenz, 1969).

The physical principle of the USBM test, is based on the amount of work it takes for one fluid to displace the other. The work necessary for the non-wetting fluid to displace the wetting fluid and vice-versa, is proportional to the gray filled areas, \mathbf{A}_1 and \mathbf{A}_2 , respectively, in figure (2.5). In a water-wet rock, the work required to increase water saturation is smaller than the work required to increase oil saturation, since a lower differential pressure is needed. Subsequently, if the system is water-wet, the area representing the forced drainage \mathbf{A}_1 , is always larger than the area \mathbf{A}_2 , associated with the forced imbibition. Hence, by utilizing the ratio of the areas, wettability of the system can be quantified.

In order to produce the capillary pressure curve for the USBM wettability test, the cores have to undergo forced drainage and forced imbibition through centrifuging. During forced imbibition, the core is placed in brine and then centrifuged by increasing the speed stepwise until the measured capillary pressure is -10 psi. The capillary pressure and average water saturation are measured at each increment of speed. Subsequently, forced drainage continues by placing the cores in oil, and centrifuging until a capillary pressure of 10 psi is reached. The capillary pressure curve obtained from this test, can then be used to calculate the USBM index, I_{USBM} , which is defined as:

$$I_{USBM} = \log \frac{A_1}{A_2}. \quad (2.19)$$

When the USBM index, $I_{USBM} > 0$, it corresponds to a water-wet core since it requires less effort to increase the water saturation than the oil saturation, hence $\mathbf{A}_1 > \mathbf{A}_2$. Conversely, if the ratio is less than zero, more work is required to increase the water saturation than oil saturation, $\mathbf{A}_1 < \mathbf{A}_2$, and the core is oil-wet. A ratio close to zero, $\mathbf{A}_1 = \mathbf{A}_2$, indicates that the wetting state is neutral (Anderson, 1986).

2.5.4 Chromatographic Wettability Test

Strand et al.(2006) presented a new method of measuring the wetting state of the porous medium for carbonate cores. As opposed to the Amott test and the USBM wettability index, where the wetting state is determined on the basis of processes like spontaneous imbibition and forced imbibition. The chromatographic wettability test is rather based on surface chemistry, where it quantifies the wettability in terms of the fraction of chalk surface which is covered by either oil or water. By flooding a core with a brine containing sulfate ions, SO_4^{2-} , which readily adsorbs onto water-wet surfaces and also having a non-adsorbing tracer such as thiocyanate, SCN^- , the fluid flow of SO_4^{2-} will be retarded relative to the SCN^- . As a result a chromatographic separation of the effluent concentration profiles is obtained, which can be further used to calculate the fraction of water-wet surface.

Cores aged with oil are placed in Hassler core holders and flooded with a brine without SO_4^{2-} and SCN^- to S_{or} . Afterwards the cores are flooded with a minimum of 2 PV with a brine containing SO_4^{2-} and SCN^- . During flooding, effluent samples are collected and analysed in the ion chromatograph mentioned in section (4.2.8). The relative concentration of SO_4^{2-} and SCN^- in each sample is plotted against pore volume injected. The lag of the SO_4^{2-} -curve relative to the SCN^- -curve is proportional to the water-wet surfaces that are capable of adsorbing ionic species. Hence, by taking a ratio of the area between SO_4^{2-} and SCN^- curves of the sample being tested, A_{wett} , and the area between SO_4^{2-} and SCN^- curves in a completely water-wet reference core containing heptane, $A_{heptane}$, the wettability index, WI , can be defined as:

$$WI = \frac{A_{wett}}{A_{heptane}}. \quad (2.20)$$

The area between the curves can be found by calculating the area under each curve with the trapezoidal method, and subtracting the area under the SCN^- - curve from the SO_4^{2-} -curve. The wettability index, will give values in a window between 0 - 1, and they are classified as:

$WI = 1.0$ completely water-wet system

$WI = 0.5$ neutrally wetted system

$WI = 0.0$ completely oil-wet system

The advantages with the chromatography wettability test, is that the test is relatively fast (do not need to wait on spontaneous imbibition), it can assess wettability in the total wetting range, and is sensitive around neutral wettability.

2.5.5 Spontaneous Imbibition Method

The spontaneous imbibition method is a qualitative method, which gives a relative wettability measurement. It is a frequently used method in the industry due to its simplicity in terms of equipment and execution (Anderson, 1986).

The method begins by placing a core at S_{wi} in a brine, and then allowing it to spontaneously imbibe the brine. The rate at which oil is produced and the total volume produced are measured during the test. If considerable amounts of oil is produced at a fast rate, the core is strongly water-wet. However, if the rate and volume of oil produced is lower, the core is less water-wet. Alternatively, if the core cannot imbibe water, the core is immersed in oil at S_{or} . The same assessment apply as above, only now the rate and volume at which water is produced determines the degree of oil-wetting. When neither oil or water can spontaneously imbibe into the core, it is in a neutral wetting state with no preference for any fluid.

On account that wettability and the imbibition-rate are both dependent on factors such as: relative permeability, IFT, viscosity, the porous structure and the initial saturation of the core, it is important to have a reference core which is strongly-water wet, in order to have results that can be interpreted (Denekas et al, 1959, Anderson 1986). In figure (2.6), an illustration is shown where one system is strongly water-wet while the other system is less water-wet. From the figure there are two noticeable differences between the curves. In the strongly water-wet case, the gradient is steeper than the gradient of the sample, which means that the initial imbibition rate is higher for the reference core. Secondly, the higher plateau of the green curve, signifies a stronger water-wet system, which is capable of imbibing more fluid than the sample. Consequently, by supplying several imbibition curves to a plot like figure (2.6), the wettability can be assessed based on the shape and placement relative to the reference curve.

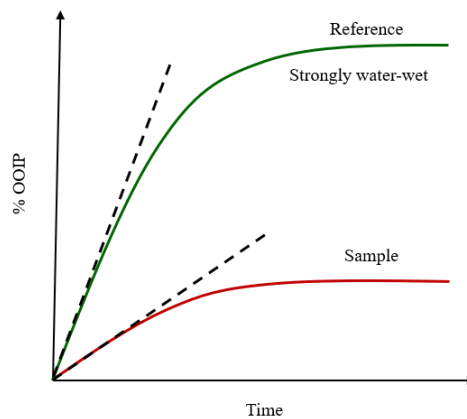


Figure 2.6: Illustration of a spontaneous imbibition test. The green curve represents a strongly water-wet core, while the red curve represents the sample being tested.

Wettability Index based on Spontaneous Imbibition

As discussed above, spontaneous imbibition is used as a qualitative method of measuring the wettability of oil/brine/rock systems. However, the degree of wettability can also be measured quantitatively by spontaneous imbibition, by introducing a modified Amott water index, I_{W-SI}^* (Piñerez Torrijos et al., 2019).

$$I_{W-SI}^* = \frac{SI_C}{SI_{WWC}}. \quad (2.21)$$

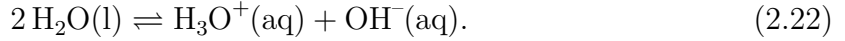
Where SI_{WWC} is the oil recovery (% OOIP) by spontaneous imbibition in a strongly water-wet reference core, while SI_C is the oil recovery (% OOIP) by spontaneous imbibition in the core where the wetting state is evaluated. When $I_{W-SI}^* = 1$, the system is strongly water-wet, while $I_{W-SI}^* = 0$, corresponds to a system that is neutral-wet.

2.6 Dissolution and Solubility

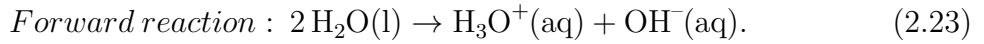
One of the primary processes occurring during production of Smart Water by acid flooding into chalk reservoirs, is dissolution of the chalk surface. The extent of the dissolution process is closely related to the chemical equilibrium which is established between the injected brine and the chalk surface. In addition, will solubility of minerals such as anhydrite, $\text{CaSO}_4(\text{s})$, and calcite, $\text{CaCO}_3(\text{s})$ control the supply of potential determining ions, SO_4^{2-} and Ca^{2+} , to the brine. Important chemical processes related to Smart Water EOR are therefore introduced in this section.

2.6.1 Chemical Equilibrium

Most chemical reactions in nature have a forward and a reversible direction. An example of a reversible reaction can be studied by looking at water. One would expect that pure water only consisted of H_2O molecules. However, considering that it has a small conductivity, there must be free ions available that can carry electrical charge in the water. The process accounting for this, is self-ionization of water, which can be seen in the reaction below,



A minute number of water molecules dissociate into one hydronium, $\text{H}_3\text{O}^+(\text{aq})$, and one hydroxide, OH^- ion, yielding free ions. The reaction is going two ways, and can be decomposed into one forward reaction, and one reverse reaction:



When the forward and reversible reactions above are advancing at equal rates, chemical equilibrium is reached (Brown et al., 2000). The net change in concentration of the species above becomes zero, since dissociation of water molecules is happening at the same rate as water molecules are produced. Consequently, the kinetics of the forward and reversible reactions governs when chemical equilibrium is established.

The relationship between concentrations of reactants and products at equilibrium can be expressed through the law of mass action. Given a general reaction at chemical equilibrium,



where a, b, d, e are the stoichiometric coefficients of the species A, B, D, E. The law of mass action states that the distribution of reactants and products is given by,

$$K = \frac{[\text{D}]^d [\text{E}]^e}{[\text{A}]^a [\text{B}]^b}. \quad (2.26)$$

K , is known as the equilibrium constant. It is a valuable constant, which can indicate whether the equilibrium favors the reactants or the products. It can also be used to calculate concentrations of reactants and products at equilibrium. The brackets are there to indicate that the concentrations are in molarity (mol/L) (Chang and Goldsby, 2014). The equilibrium constant is temperature dependent, thus depending on whether the reaction is exothermic or endothermic, it will either decrease or increase with temperature respectively (Brown et al., 2000).

2.6.2 Acid Dissociation in Aqueous Solutions

In 1923, Brønsted and Lowry defined an acid as a substance capable of donating a proton, and a base capable of accepting a proton (Brown et al., 2000). Like almost all reactions, equilibrium is established when an acid is dissolved in water. Dissociation of acetic acid is an example of that and is given by the following reaction:

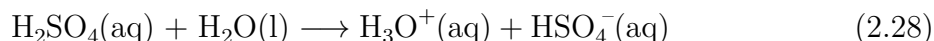


Acid Base Conjugate base Conjugate acid

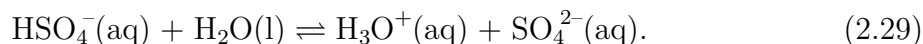
In the reaction above, transferring of proton is happening in both the forward and the reverse reaction. In the forward reaction, acetic acid acts like a Brønsted acid as it is donating a proton to the water molecule. In the reverse reaction, acetate is capable of accepting a proton from the hydronium, making it a Brønsted base. This is known as a conjugate acid-base pair. All Brønsted acids have a conjugate base, which is the leftover after the acid has donated a proton.

2.6.3 Strength of Acids and Bases

The dissociation strength of acids varies, as some acids are better than others to donate protons. The strongest acids ionize completely, which is reflected in a very large equilibrium constant (eq. 2.26) that favours the products over the reactants. Sulphuric acid is characterized as a strong acid, consequently when dissolved in water, it will ionize completely:



Since the equilibrium constants favour the products heavily, the equilibrium reaction is written with one arrow. Sulphuric acid is a diprotic acid, as a result it can donate another proton in a second reaction through the hydrogen sulfate ion, HSO_4^- . In contrast to the sulfuric acid, hydrogen sulfate is a weak acid. Consequently, it will not ionize completely which is characterized by the equilibrium arrows:



To measure the degree of ionization, the equilibrium constant is again used. For reaction (2.29), the law of mass action (2.26) gives the following equilibrium expression:

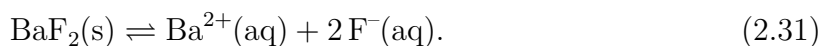
$$K_a = \frac{[\text{H}_3\text{O}^+][\text{SO}_4^{2-}]}{[\text{HSO}_4^-]}. \quad (2.30)$$

Where H_2O has been excluded as it is the solvent of which the acid is dissolved in. Since the equilibrium is associated with an acid-base reaction, the equilibrium constant is denoted, K_a , and is called the acid-dissociation constant for HSO_4^- . For hydrogen sulfate the acid-dissociation constant, $K_a = 1.2 \times 10^{-2}$. Considering that the range for weak acids is between 10^{-2} to 10^{-10} , it is a relatively strong, albeit weak acid (Brown et al., 2000).

2.6.4 Solubility Equilibrium

Water is an excellent solvent due to its polarity, hence when salt is added to water, it will dissolve the salt and still look clear and unaffected. However, if too much salt is added, precipitation may happen through nucleation, crystal growth and ultimately formation of ripened rod-like particles. If the rate of dissolution equals the rate of precipitation, solubility equilibrium has been established. The solution is then called a saturated solution since no additional salt can be dissolved.

When a salt is at solubility equilibrium, the extent of solubility can be expressed through the solubility product constant, K_{sp} . For instance when barium fluoride, BaF_2 , is added to a saturated solution of barium fluoride the following equilibrium is established,



Considering that the concentration of the salt is approximately constant, it can be omitted from the equilibrium constant, hence the expression becomes,

$$K_{sp} = [\text{Ba}^{2+}][\text{F}^{-}]^2 \quad (2.32)$$

For salts such as NaCl which dissolves easily, the solubility constant is very high, whereas for salts which dissolves with increasing difficulty, it decreases correspondingly.

Estimating the Saturation State

It is not always evident what state a solution is in, as it can be under-saturated, saturated and supersaturated. Subsequently, a reaction quotient, Q , is introduced. It is used in the same regard as the solubility constant, however, contrarily to the K_{sp} , the input concentrations do not have to be at equilibrium. The saturation state, Ω , is given as the ratio between the solubility constant and the reaction quotient:

$$\Omega = \frac{Q}{K_{sp}}, \quad (2.33)$$

if $\Omega < 1$, the solution is under-saturated, conversely, $\Omega > 1$ and the solution is supersaturated and when $\Omega = 1$ the solution is at equilibrium.

2.7 Solubility and Influencing Factors

The Common-Ion Effect

The solubility of $\text{BaF}_2(\text{s})$ in reaction (2.31) above, will be reduced if Ba^{2+} or 2F^- are present initially in the solution. The equilibrium is then shifted towards the left according to Le Châteliers principle. This effect is known as the common-ion effect.

Formation of Complex Ions

Formation of complexes can influence the solubility of ionic compounds, since they can reduce the activity of free ionic species in solutions. Below in figure (2.7), is an example of the metal ion Cobalt, Co, which forms a complex with ammonia, NH_3 .

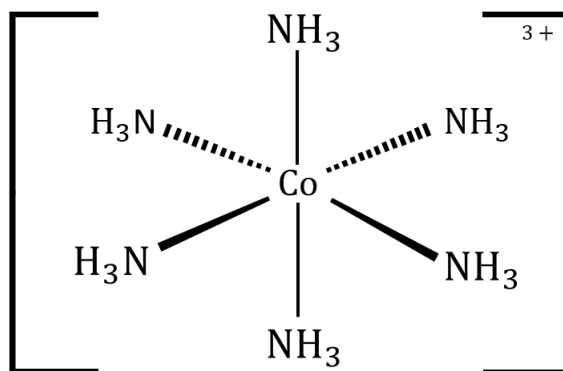
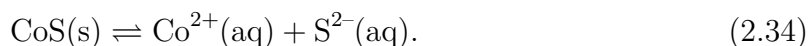


Figure 2.7: Hexamminecobalt(II), illustration of a complex which increases the solubility of ionic compounds with cobalt ions.

Complexes consists of a central metal ion with surrounding ligands (ions or molecules). When they form in solution, the metal ion concentration decreases, which results in higher solubility of ionic compounds consisting of the same metal. An example of a complex ion is Hexaamminecobalt(III), $[\text{Co}(\text{NH}_3)_6]^{3+}$. In this complex, Cobalt is the central metal ion, which is attached to six ammonia ligands as seen above. When for example Cobalt(II) Sulfide is mixed into water, very little dissociation will happen, which is also expressed through the small solubility constant, $K_{sp} = 4.0 \times 10^{-21}$.



However, if ammonia is put into solution, the complex in the figure above can be formed and thereby reduce the ion concentration of Cobalt. The equilibrium will shift towards right, making the salt more soluble in water.

2.7.1 Carbonate Acid System

The carbonate acid system is introduced in this section along with the Bjerrum plot, shown in figure (2.8). The system is very practical to use, since all the equilibrium constants involved in the system, can be used to relate the pH of a brine to the relative concentration of carbonic species in the brine. Consequently, when pH is measured of the effluent brine in the acid flooding experiment, it is possible to track the relative distribution of carbonic species in the Bjerrum plot.

Water in equilibrium with the atmosphere will have gaseous $\text{CO}_2(\text{g})$ dissolved into the water:



The aqueous carbon dioxide will then react with liquid water (H_2O) and form carbonic acid, H_2CO_3 :



It is common to summarize the above equation (2.36) as simply, H_2CO_3^* , since the concentration of $\text{CO}_2(\text{aq})$ is a lot higher than the H_2CO_3 -concentration. Hence, by combining the reactions (2.35) and (2.36), they can be expressed as:



The corresponding equilibrium constant, K_H for the reaction above is given as:

$$K_H = \frac{[\text{H}_2\text{CO}_3^*]}{[\text{CO}_2]}. \quad (2.38)$$

Since carbonic acid is a diprotic acid, H_2CO_3^* , it will provide two protons by dissociating in two stages:



The release of protons, means that the concentration of carbonate species are dependent on the pH of the solution. Hence the Bjerrum plot accordingly shows the relative concentration of carbonic species versus pH. The strength of these two acid dissociation processes, are expressed through their respective acid-dissociation constants, K_{a1} and K_{a2} , respectively.

$$K_{a1} = \frac{[\text{HCO}_3^-][\text{H}^+]}{[\text{H}_2\text{CO}_3^*]}. \quad (2.41)$$

$$K_{a2} = \frac{[\text{CO}_3^{2-}][\text{H}^+]}{[\text{HCO}_3^-]}. \quad (2.42)$$

At 25°C, the values for the two constants are $K_{a1} = 10^{-6.3}$ and $K_{a2} = 10^{-10.3}$ (Appelo and Postma, 2005). Furthermore, water will self-ionize, and is therefore also part of the carbonate acid system,



The corresponding equilibrium constant for water, $K_w = 10^{-14.0}$, and is given as:

$$K_w = [\text{H}^+][\text{OH}^-]. \quad (2.44)$$

All the equilibrium constants, K_{a1} , K_{a2} , K_H and K_w , can be related to pH by use of the Henderson-Hasselbach equation, here shown with a general weak acid/conjugate base pair:

$$\text{pH} = \text{pKa} + \log \left(\frac{[\text{A}^-]}{[\text{HA}]} \right). \quad (2.45)$$

The relation between all the equilibrium constants, are then used to compute the distribution shown in the Bjerrum plot. At any given pH, the plot will tell what the relative concentration of the carbonate species are. Furthermore, it is possible to track the response of the equilibrium solution, when acid is injected into the chalk core.

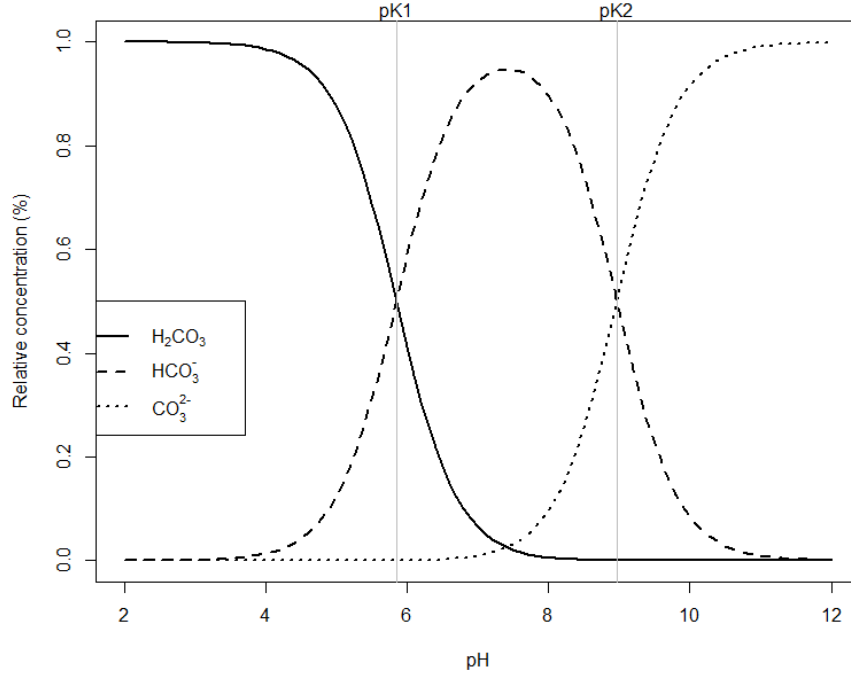
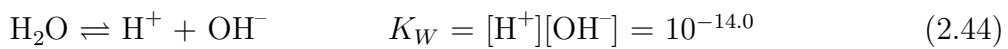
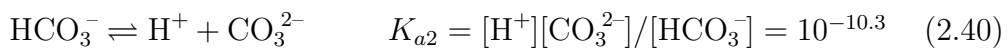
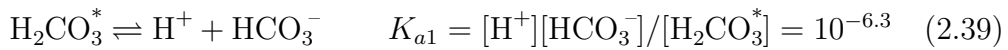
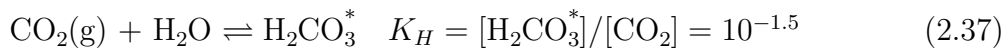


Figure 2.8: Bjerrum plot showing the relative concentrations of species in the carbonate system. The plot has been drawn with the package "seacarb" in R program, by using the Bjerrum function.

Table 2.1: Summary of equilibrium constants in the carbonate acid system, with corresponding equilibrium values at 25°C (Appelo and Postma, 2005).



3 | Chalk Wettability and Wettability Alteration by Smart Water

3.1 Carbonate Reservoirs

Considerable amounts of oil and gas are found in carbonate reservoirs, with over 60 % of the world's oil and 40 % of the world's gas (Montaron, 2008). One of the largest reservoirs in Norway is a carbonate reservoir, Ekofisk, which is a naturally fractured chalk with low matrix permeability but high porosity. Carbonate reservoirs exhibit a large degree of heterogeneity in permeability and porosity, with permeabilities ranging between 0.01 md - 1D and porosities between 1-35% (Lucia, 2007). The low permeability is often translated into low recovery factors, and for carbonate reservoirs it is on average below 30 % (Zhang and Austad, 2005). The low recovery factor is an enormous inspiration for researchers that are trying to improve the oil recovery in carbonates through cost effective EOR-methods. Only a few extra percentages in recovery equivalents to large amounts of money.

3.1.1 Carbonate Rocks

Carbonate rocks are predominantly formed by sediments produced from carbonate-secreting organisms, and partially from chemical precipitation. These organisms, such as corals and algae, thrive in marine environments where it is abundant with sunlight and warmth, and the water is shallow and clear. Hence, most carbonate sediments today are found at 30° latitude, north and south of the equator (Wilson, 1975). Since most carbonates are produced by living organisms, they are often termed as biogenic. In contrast to sandstones, where the sediments are transported and sorted over long distances, carbonate sediments are deposited locally by different organisms. In addition to local deposition, will texture and composition of the sediments be altered through diagenesis. Carbonate rocks therefore have heterogeneous properties.

Chilingar and Yen (1983) published a paper on carbonate reservoir rocks, which showed that the majority of carbonate rocks are oil-wet. The research involved angle measurements to determine wettability, and was conducted on 161 carbonate cores from all over the world. Results from this paper is given in the figure below:

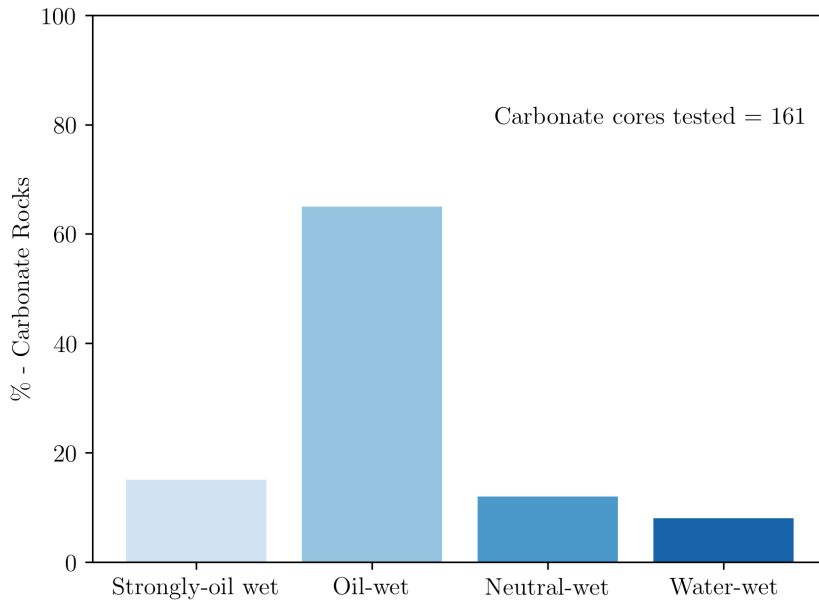


Figure 3.1: Distribution of wettability on 161 carbonate cores examined by Chilingar and Yen (1983).

The building block of carbonate minerals is the carbonate ion, CO_3^{2-} , which forms ionic bonds with divalent cations. The most common divalent ions that bond with the carbonate ion, are; Ca^{2+} , Mg^{2+} and Fe^{2+} . Together with the carbonate ion, they form minerals such as: Calcium carbonate (CaCO_3), Magnesium carbonate (MgCO_3) and Siderite (FeCO_3) (Fairbridge et al., 1967). The minerals orient themselves in either a rhombohedral or a orthorhombic crystal lattice, depending on the size of the divalent ions. For cations that are less than 1 Å, like Fe^{2+} and Mg^{2+} , they will form a rhombohedral lattice. As for Ca^{2+} , it has a size close to 1 Å, and can therefore end up in either a rhombohedral or orthorhombic crystal lattice (Bjørlykke, 2015).

In general, a rock containing more than 50 % of carbonate minerals is defined as a carbonate rock. Among the different carbonate minerals, the calcite mineral (CaCO_3) and the dolomite mineral (MgCO_3) are the most common. Rocks consisting of more than 50 % of calcite are described as limestones, while rocks containing more than 50 % of the dolomite mineral, are known as dolomite rocks or dolostones (Bissell and Chilingar, 1967).

Chalk is a finely composed limestone rock consisting primarily of calcareous plates from the coccolithophore algae and a small amount of pelagic foraminifera. The calcareous plates are known as coccoliths and they are made of calcite crystals of low Mg-content that are between 0.25-1.00 μm in diameter (Friedman, 1996). The calcite crystals are stacked in a spiral pattern which gives the coccoliths a platy look. An image taken by the scanning electron microscope of one of the chalk cores used in this study, show an abundance of coccoliths, either as whole plates or as partial rings in figure (3.2). The image was taken at a magnification of 10 000, and it also shows how small the pores are, with many of the pores being just a few $\mu\text{-meters}$ in size (green scale is 2 μm). Chalk reservoirs are often highly porous (40-50 %) due to micropores, but have very low permeability ~ 1 md (Bjørlykke, 2015). They exert large capillary forces due to small grain size. Furthermore, they also have a large reactive surface area which is positively charged below pH of 8 (Frykman, 2001; Pierre et al., 1990). The only reason why fields like Ekofisk and Valhall can be productive, is due to extensive fractures which acts like transport routes (Bjørlykke, 2015).

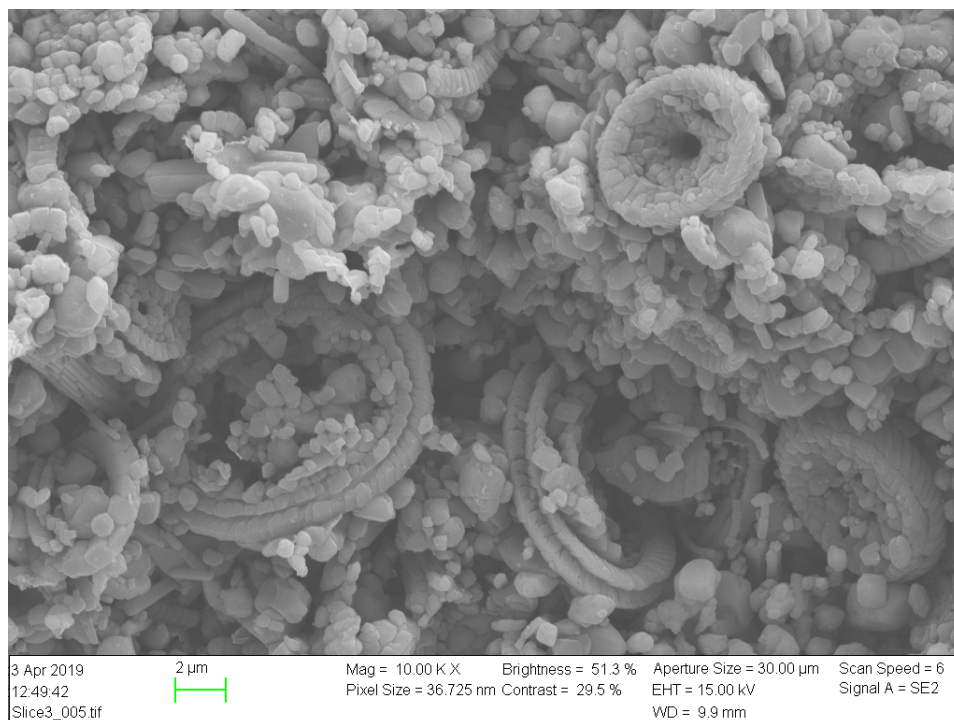


Figure 3.2: Image of the chalk surface taken by the scanning electron microscope at 10 000 magnification. Several coccolith rings are visible in the image. The dark spots are the pore throats. The scale of pore throats, grains and coccoliths in the image are given by the green line of 2 μm .

3.2 Initial Wettability of Chalk

The initial wettability of chalk depends on several factors such as; presence of cations in the formation water, stability of the brine film, acid number (AN) of the crude oil, initial presence of sulphate and temperature. A thorough understanding of how these affect wettability of chalk is of huge importance in terms of reservoir management, but can also serve as guidance in determining the potential of Smart Water injection. It is apparent from capillary pressure curves, that almost all reservoirs are initially water-wet before oil migration. In the upper parts of reservoirs, the P_c - curves display a high oil saturation with residual water saturation, and then as depth increases, there is a gradual transition towards higher water saturation at the bottom of the reservoir. However, research has shown that the majority of carbonate reservoirs are oil-wet, which was displayed in figure (3.1), hence oil must be able to change the wettability when it migrates into the reservoir.

The wetting state of reservoirs has often been associated with the stability of the brine film covering the mineral surfaces. If the film is unstable it can break, with the result of adsorption of polar components from the oil phase. In terms of film stability, a large disjoining pressure is favourable, while a low disjoining pressure will cause the film to thin out and break (Dubey and Doe, 1993). When oil migrates into the reservoir, pressure increases in the porous medium, and the water film becomes surrounded by two interfaces comprised of a crude oil/brine phase and a mineral/brine phase. The interfaces can either have equal or opposite charge, causing an increase or decrease in disjoining pressure respectively. In chalks, the mineral-brine interface is positively charged since pH is $< 8.5 - 9$ in addition to a high Ca^{2+} concentration near the surface (Zhang and Austad, 2005). The brine-oil interface, however, is generally negatively charged, which is explained by dissociation of carboxylic acids at the interface (Buckley, Takamura, and Morrow, 1989). As a result, the two interfaces will attract each other and thin out the brine film in the middle, causing a decrease in the disjoining pressure. Ultimately the film collapses, which allows the oil phase to directly come in contact with the chalk surface, and the water-wetness decreases.

However, recent work by Shariatpanahi et al., (2016), has shown that cations also can have a large effect on the initial wetting of chalk. The research was designed to obtain the initial wetting state of Stevs Klint cores, by measuring the oil recovery by spontaneous imbibition with different imbibition fluids. The cores were saturated and imbibed with the same brine during the experiments. The tested brines that were used involves the following brines: $MgCl_2$, $CaCl_2$, $NaCl$, VB0S and DI-water. All cores were saturated with the same oil with $AN = 0.17$ mgKOH/g. Since neither of these brines contain a combination of SO_4^{2-} and Ca^{2+} , wettability alteration does not take place and the initial wetting can therefore be studied.

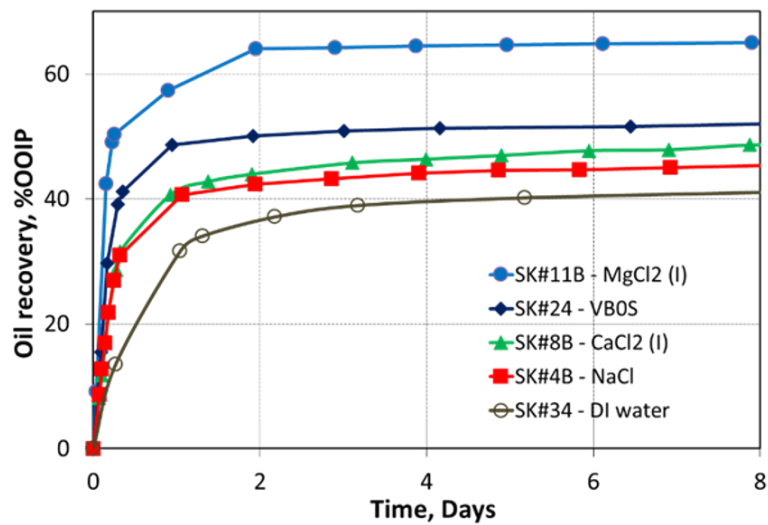


Figure 3.3: Effect of FW composition on the initial wetting state of Stevs Klint cores. $S_{wi}=10$ %, and $S_{oi}=90$ % of oil with $AN = 0.17$ mgKOH/g. The spontaneous imbibition was done at 23 °C. Figure by (Shariatpanahi et al., 2016).

According to the results, the core with $MgCl_2$ brine as formation water is of highest initial water-wetness, and it has a very high recovery of 65 % of OOIP. On the other side, the core of lowest initial water wetness, is the core containing DI-water, with only 40 % of OOIP. The low initial water wetness could be a result of increased accessibility for the carboxylic acids in the crude oil phase due to the lack of an ionic double layer. Furthermore, the study concluded that high concentration of Mg^{2+} occupies the mineral surface. The negatively charged carboxylic acids have less affinity to Mg^{2+} than Ca^{2+} resulting in less adsorption and a more water-wet system.

Standnes and Austad observed in 2000, that the number of carboxylic acid groups in the oil had a significant affect on the wettability. The carboxylic acid groups from the oil phase actively adsorb onto the reactive chalk surface and behave as anchor molecules for the oil phase. In figure (3.4) a clear correlation between AN-number of the oil and the wettability of chalk can be seen. The oil with AN = 0 has the highest recovery. While oils with increasing AN have correspondingly lower recoveries. Hence it appears that with increasing AN-numbers, there is an equivalent decrease in water-wetness.

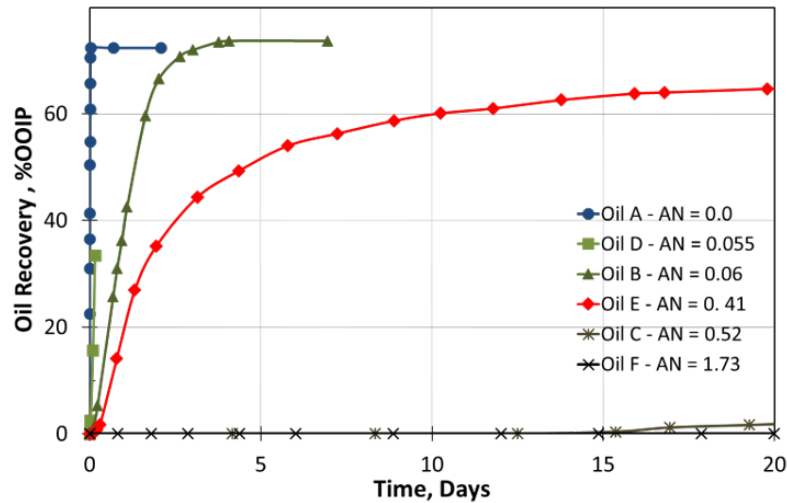


Figure 3.4: Oil production vs Time for oils with different AN-numbers by spontaneous imbibition. Oil recovery decreases as the AN-number increases (Standnes and Austad, 2000).

Initial sulphate is another parameter which plays a decisive role on the initial wettability of outcrop cores. In 2007, Puntervold et al., conducted spontaneous imbibition experiments on two outcrop rocks (Stevens Klint) to study the effect initial SO_4^{2-} had on wettability. One of the cores were pre-cleaned by flooding with DI water prior to oil aging in order to remove SO_4^{2-} . The second core was not cleaned, hence SO_4^{2-} present on the chalk surface was preserved. The results showed that the non-cleaned core had a recovery of 70 %, while the cleaned only had 30 % recovery. A chromatographic wettability test (see section 2.5.4), showed that the non-cleaned had a $WI = 0.84$ (very water-wet), while the cleaned had a $WI = 0.65$ (neutral/slightly water-wet). Hence, the non-cleaned appeared more water-wet than the cleaned. The results from Puntervold et al., were obtained based on spontaneous imbibition on outcrop cores. Consequently, these findings are only true for outcrop cores. Nevertheless, they show that initial sulphate can be a crucial parameter when potential reservoirs are evaluated for Smart Water EOR. For instance if a reservoir is evaluated for Smart Water, but has initial sulphate, it may already be relatively water-wet, hence wettability alteration will have no effect.

According to Rao (1996), there is a general agreement between researchers that

water-wetness increases with temperature. As the temperature increases, decarboxylation of acids initiates, hence the AN number of crude oil decreases (Shimoyama and Johns, 1971; Hamouda and Rezaei Gomari, 2006). However, in 2005, Zhang and Austad designed laboratory experiments that measured the effect temperature had on wettability, by isolating the effect of AN. Their study concluded that temperature only had a small effect on chalk wettability, and that AN was the main wetting parameter.

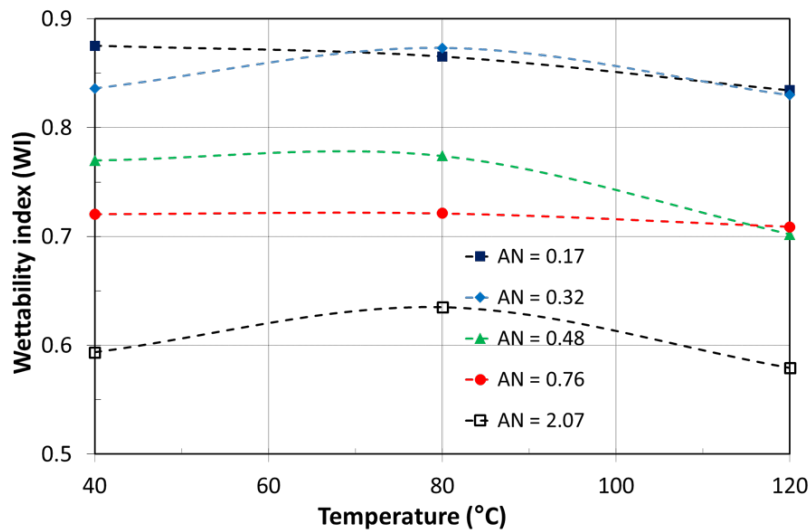


Figure 3.5: Effect of crude oil AN and aging temperature on water wet surface area. The temperature has only a minor effect on the wettability. Figure by (Zhang et al., 2006).

In addition, they concluded that the decarboxylation of acids was not due to high temperatures, but rather due to the presence of $\text{CaCO}_3(\text{s})$. The formation, which consists of $\text{CaCO}_3(\text{s})$, acts like a catalyst for the decomposition of carboxylic acids. Consequently, the role of temperature in relation to wettability is rather uncertain.

A recent study by Hopkins et al., in 2016, found that the quantity of oil a core is flooded with, has an affect on the initial wetting of the core. The experiment was performed by flooding the same oil with $\text{AN}=0.34 \text{ mgKOH/g}$, but in different amounts, into two similar very water-wet SK chalk cores with $S_{wi}=10 \%$ of formation water. One of the cores (core A) was flooded with 15 PV of oil at $50 \text{ }^\circ\text{C}$, while 5 PV was injected into the other core (core B) at the same temperature. The wetting state was then assessed by performing spontaneous- and forced imbibition and a chromatographic wettability test. The acid number in the effluent was measured during flooding of 15 PV, and the results are presented in the figure below, showing the measured AN of the oil versus PV flooded.

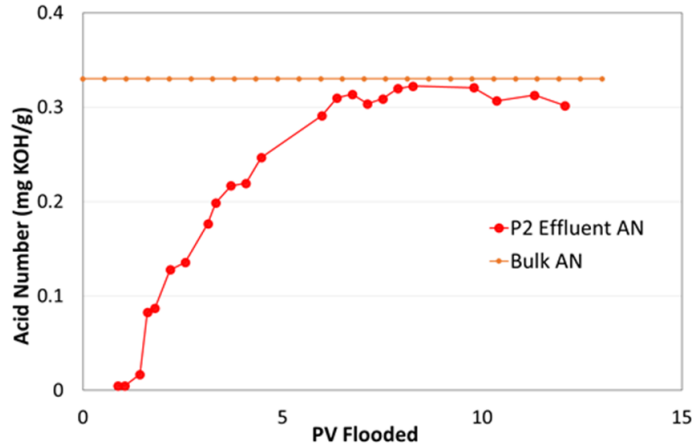


Figure 3.6: Acid number of effluent crude oil versus PV flooded. Oil was injected in one direction at a temperature of 50 °C at a rate of 0.1 ml/min. $S_{wi}=10\%$, oil with AN= 0.34 mgKOH/g (Hopkins, 2017).

In figure (3.6), the AN of the effluent increases from almost zero to AN = 0.34 mgKOH/g of the oil, in a time of 8-9 PV flooded. After this time, it reaches a plateau where an equilibrium is established between adsorbed carboxylic acids on the chalk and in the oil bulk phase. The physical explanation for this, is that sites on the chalk is gradually filled up by adsorbed carboxylic acids. Eventually all the sites are filled up, and the plateau is reached. Subsequently, the other core was flooded with 5 PV, which according to the first core, is not enough to reach equilibrium. The core flooded with 5 PV was therefore expected to be more water-wet, since there should be more available sorption sites on the chalk surface.

Spontaneous imbibition confirmed that core A flooded with 15 PV behaved less water-wet than core B flooded with 5 PV, both in terms of imbibition rate and ultimate recovery. The Amott water indexes were calculated to be 0.311 for core A, and 0.351 for core B, while the chromatographic wettability tests also confirmed that the core A flooded with 15 PV was less water-wet than core B, with WI=0.703 and WI=0.742, respectively. Consequently, the amount of oil a core is flooded with, has an effect on the wettability of the core. This is explained by the fact that it takes time to fill all the available sites on the chalk surface for the carboxylic acids.

3.3 Potential Determining Ions in Chalk

In 1990, Pierre et al. observed that H^+ and OH^- were not the only potential determining ions on chalk particles. By measuring the electro-kinetic mobility as a function of pH of dispersed calcite particles in NaCl solutions with added $CaCl_2$ and Na_2SO_4 , they found that both Ca^{2+} and SO_4^{2-} affected the surface charge. This was also confirmed by (Strand et al., 2006), and the effect of these potential determining ions can be seen in figure (3.7). The figure shows the measured zeta potential as a function of Ca^{2+} and SO_4^{2-} -concentration. The zeta potential measurements were conducted on a NaCl-brine containing 4 wt % milled chalk particles with varying amounts of Ca^{2+} and SO_4^{2-} in the brine.

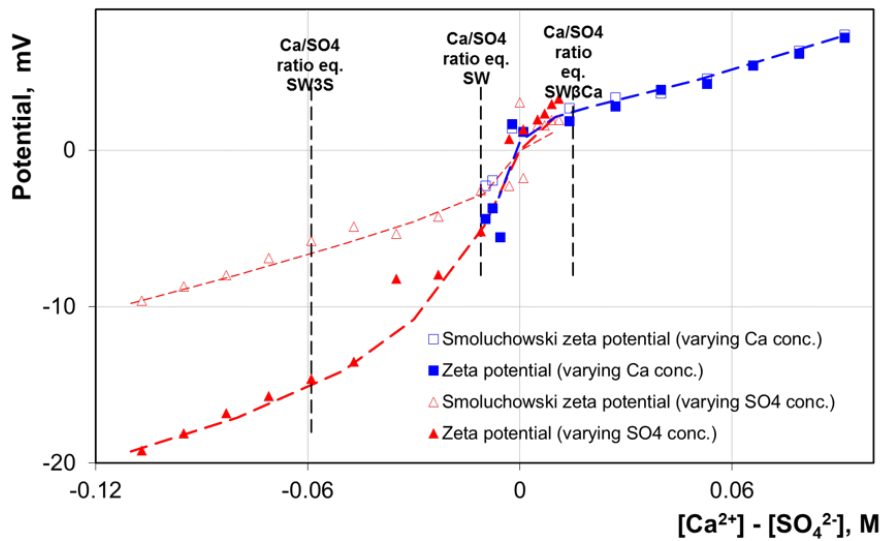


Figure 3.7: Zeta potential on Stevns Klint chalk as a function of Ca^{2+} and SO_4^{2-} -concentration at a pH 8.4 (Strand et al., 2006).

When the ratio of $Ca^{2+}/SO_4^{2-} < 0$, the zeta potential is negative, indicating that the suspended calcite particles have a negative surface charge. Whereas when the ratio $Ca^{2+}/SO_4^{2-} > 0$, the zeta potential becomes positive and the chalk particles acquire a positive surface charge. Consequently, the results from the study indicates that the surface charge of the chalk particles is governed by the relative concentration of these two potential determining ions.

To further study how these ions interact with each other, figure (3.8) is presented by (Strand et al., 2006), which shows the relative ion concentration of the effluent from a viscous flood on a Stevns Klint chalk core. The effluent concentration profile of SO_4^{2-} is retarded relative to the effluent concentration profile of the tracer SCN^- , and is delayed by approximately 0.1 PV injected. The figure clearly display the affinity SO_4^{2-} has towards the chalk surface, as it is clearly adsorbed onto the chalk, resulting in a delay in the effluent concentration profile.

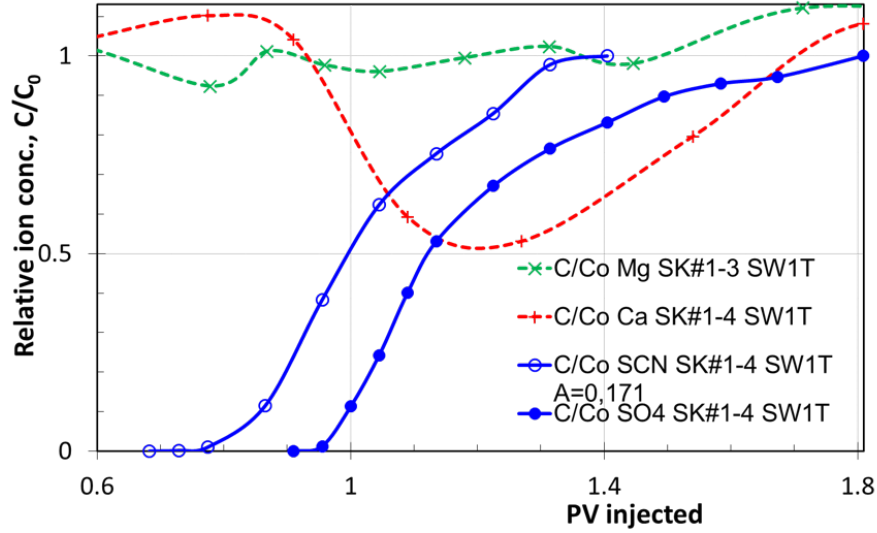


Figure 3.8: By plotting the relative ion concentration vs PV injected, the interaction of the divalent ions SO_4^{2-} , Ca^{2+} and Mg^{2+} is studied (Strand et al., 2006).

Between PV injected; 0.9-1.8, there is a significant decrease in the relative concentration of Ca^{2+} . According to Strand et al. (2006), this is due to co-adsorption of Ca^{2+} -ions onto the adsorbed SO_4^{2-} -ions. The effluent relative ion concentration profile for Mg^{2+} is stable, and no large fluctuations are observed. Hence, there appears to be a synergy between SO_4^{2-} and Ca^{2+} , that causes the wettability alteration. While the Mg^{2+} -ion does not have a direct role in the wettability alteration.

However, Zhang et al. (2006) found that Mg^{2+} could substitute Ca^{2+} on the surface of the chalk at temperatures above 70 °C. Hence, Mg^{2+} has an indirect role in wettability alteration at higher temperatures, since it allows for a higher Ca^{2+} -concentration in the brine. As a result through systematic research, three potential determining ions have been found important for the wettability alteration process: SO_4^{2-} is the absolute necessary ion since it adsorbs onto the positive chalk surface and lowers the surface charge. This allows Ca^{2+} to co-adsorb onto the SO_4^{2-} -ion, and carboxylic acid is then displaced from the surface (Zhang, 2006). The proposed mechanism for wettability alteration in chalks of low water-wetness, is given below.

3.4 Smart Water EOR Mechanism

When Smart Water is injected into a reservoir, the negatively charged SO_4^{2-} will adsorb onto the positively charged chalk surface. The SO_4^{2-} -ion is only active in the aqueous phase, and will only attach where water is in contact with the rock. As previously demonstrated by (Pierre et al, 1990), the SO_4^{2-} will act to lower the positive surface charge of the chalk surface. Due to the weakening of the electrostatic repulsive force, more Ca^{2+} ions are attracted towards the surface. The surplus of Ca^{2+} ions available near the surface can then react with the strongly adsorbed carboxylic acid (RCOO^-) and thereby release it from the surface (Strand et al., 2006). The mechanism can be expressed through the following reaction suggested by (Austad et al., 2009):



In the reaction above, SO_4^{2-} is the governing ion that ensures an increase of Ca^{2+} close to the surface, hence, it acts as a catalyst for the Smart Water effect. Experiments have been run with brines consisting of only SO_4^{2-} -ions, and they have confirmed that SO_4^{2-} alone cannot induced wettability alteration. The effect is rather a synergetic interplay between SO_4^{2-} , Ca^{2+} and the reactive and positively charged chalk surface (Strand et al., 2005; Zhang et al., 2006; Austad et al., 2009).

At higher temperatures, $T > 100^\circ$, experiments conducted by Zhang et al. (2006) showed that Mg^{2+} has the ability of substituting Ca^{2+} at the chalk surface. Austad et al. (2009) suggests Mg^{2+} is able to displace Ca^{2+} linked to the carboxylic material in the aqueous phase. As before, SO_4^{2-} adsorbs to the chalk surface and lowers the electrostatic repulsion, however now an excess of Mg^{2+} is at the surface, which causes an increase of Ca^{2+} in the brine. The reaction then becomes:



Spontaneous imbibition experiments conducted at 130° by Zhang et al., produced more oil when Mg^{2+} was in the brine compared to brine with Ca^{2+} . The reason for this is that Mg^{2+} -free reservoirs will precipitate $CaSO_4(s)$ at high temperatures as seen in figure (5.5). Consequently, the precipitation process makes Ca^{2+} less efficient at higher temperatures, which explains the results presented by Zhang et al., (2006).

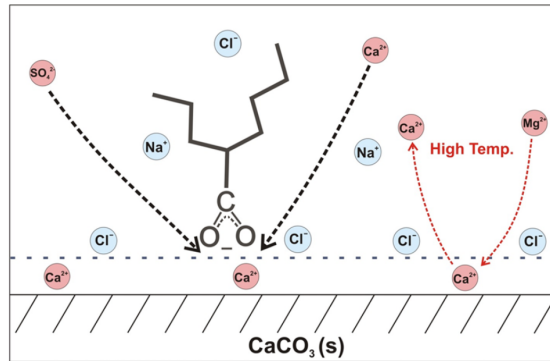
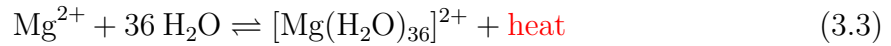


Figure 3.9: Illustration of the Smart Water mechanism showing how the determining ions interact with the chalk surface to release the carboxylic acids. Figure from the Smart Water EOR group at the University of Stavanger.

3.5 Temperature Effect on Wettability Alteration

Temperature is one of the most decisive parameters in terms of wettability alteration, because it will affect the reactivity of the potential determining ions. At lower temperatures, ions dissolved in water becomes surrounded by H₂O - molecules in a process known as hydration. The H₂O - molecules orient themselves such that the electrical charge of the ion is neutralized. Several water - molecules can cluster around an ion due to the ion-dipole force and create a rigid structure that reduces the reactivity of the ion significantly. Hydration reactions are always exothermic due to the strong ion-dipole attraction which is created with water, and are therefore controlled by temperature (Burton, 1988). For instance, when a Mg²⁺ - ion is hydrated, heat is released:



Hence, if temperature increases, the equilibrium will move toward the left according to Le Châtelier's principle, and Mg²⁺ becomes less hydrated. The effect temperature has on hydrated SO₄²⁻-ions, are displayed in figure (3.10), where the effluent concentration profiles for SO₄²⁻ are compared at different temperatures. As the temperature increases, the effluent concentration profiles becomes progressively more retarded, due to adsorption of SO₄²⁻-ion on the chalk surface. The increase in adsorption with temperature, is due to dehydration of the SO₄²⁻-ion, which makes the water structure around the ion break. The reactivity of the SO₄²⁻-ion becomes much higher as a result, and more ions adsorb onto the chalk surface. Since the water structure around ions begin breaking around 90 °C - 100 °C, wettability modification is hard to achieve at lower temperatures < 90 °C due to hydrated ions (Strand et al., 2008).

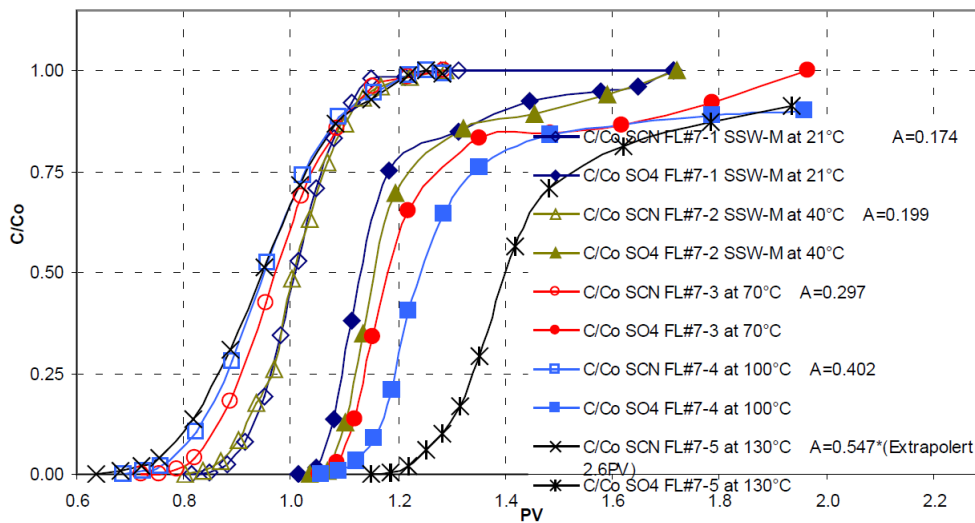


Figure 3.10: Adsorption of sulfate on chalk at different temperatures (Strand et al., 2006).

3.6 Modified Seawater for EOR

Injection of SW into chalk reservoirs can increase the water-wetness, causing a higher oil recovery. However, research by Fathi (2012) has shown that modifications of SW can make it even more efficient at altering the wetting state. The modifications that were proposed by Fathi et al., involves removal of NaCl from SW and also spiking the SW with additional SO_4^{2-} . Results from the research are shown in figure (3.11 a) and b)), at 70 °C and 90 °C, respectively.

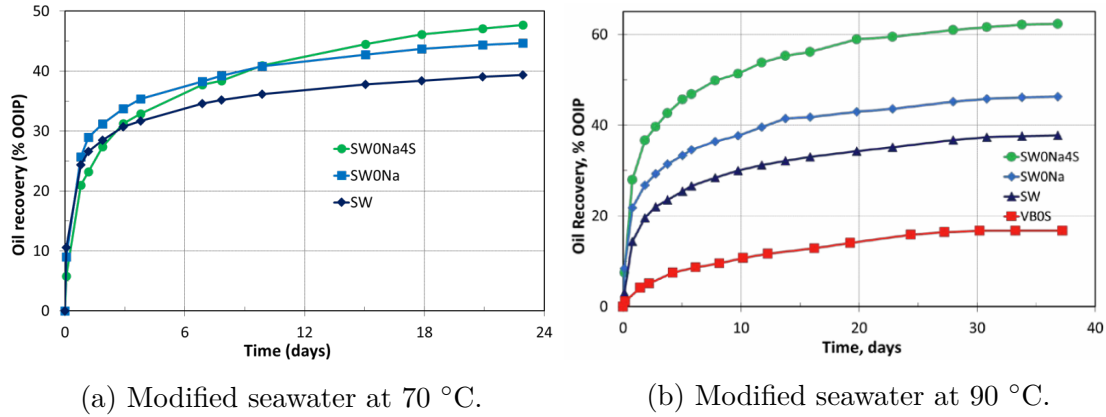


Figure 3.11: Comparison of modified SW at 70 °C and 90 °C. Normal seawater, SW, is compared to SW depleted in NaCl, SW0Na, and to SW depleted in NaCl and spiked with 4 times the SO_4^{2-} , SW0Na4S. Figures after (Fathi, 2012).

The effect of monovalent ions and SO_4^{2-} -concentration were studied by varying the amount of NaCl and SO_4^{2-} in SW. Hence, normal SW was compared to SW completely depleted of NaCl, termed as "SW0Na", in addition to a SW spiked with SO_4^{2-} and depleted in NaCl, called "SW0Na4S". Both at 70 °C and at 90 °C, there is a trend where SW depleted of NaCl has a higher oil recovery. The increase in oil recovery, is higher at 90 ° compared to 70 °C. The increase in oil recovery when NaCl is removed, is according to Fathi (2012) due to better access for the potential determining ions. Even though Na^+ and Cl^- are not potential determining ions and therefore not present in the Stern layer, they will be present in the double layer. The presence of Na^+ will then decrease the access of Ca^{2+} and Mg^{2+} . At the same time will Cl^- -ions reduce the accessibility of the SO_4^{2-} ions at the surface. Hence, when NaCl is removed from the SW, the access for the potential determining ions are improved, and both the imbibition rate and oil recovery increases.

When comparing SW0Na4S with SW at 70 °C, there is approximately 8-9 % higher oil recovery when the SW is spiked 4 times with SO_4^{2-} . At 90 °C, the oil recovery is significantly higher for SW0Na4S, with an ultimate recovery of over 60 % compared to SW with an oil recovery slightly under 40 %. The concentration of SO_4^{2-} in the brine has the largest effect on oil recovery. Therefore, it appears that adjustments

to the divalent composition of the SW is more important than removal of NaCl.

Punternvold et al. (2015) further built upon the results from (Fathi, 2012). The study looked into how much removal of NaCl and how much addition of SO_4^{2-} is enough to actually observe a significant increase in oil recovery. Oil recovery by spontaneous imbibition was then performed at 90 °C, with a backpressure of 10 bar (same set-up as shown in figure (4.4)). Modified SW with varying amount of NaCl from 0-100 % relative to SW, were imbibed at 90 °C with the results showing in figure (3.12 a)). Similarly, the amount of SO_4^{2-} was increased in SW0Na at factors 0-4, and oil recovery was measured by spontaneous imbibition. The oil recoveries from that test are shown in figure (3.12 b)). In both test series, a new core was prepared for each imbibition fluid.

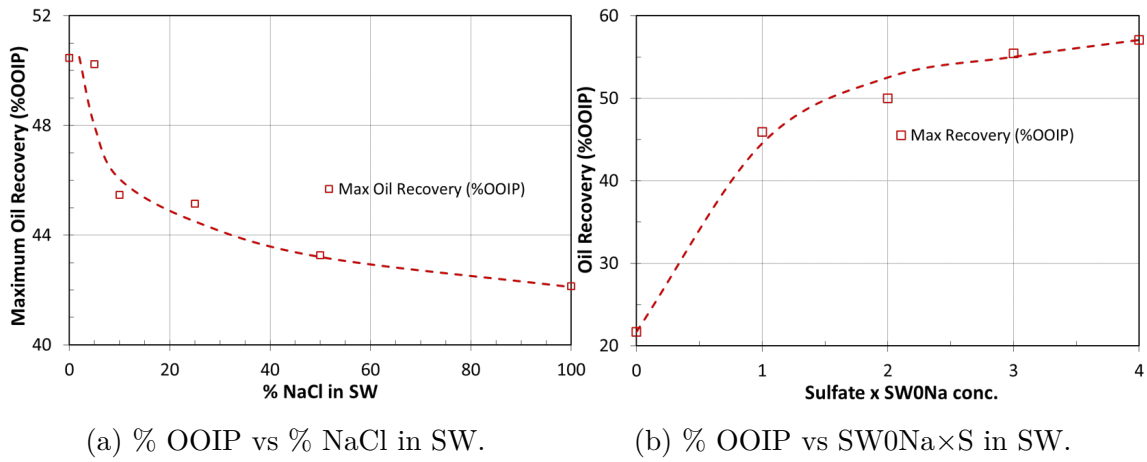


Figure 3.12: Oil Recovery as a function of SW composition at 90 °C. $S_{wi} = 10\%$, AN=0.5 mgKOH/g. In figure a) the maximum oil recovery is given as a function of % NaCl in SW. While figure b) show the maximum oil recovery as a function of times SO_4^{2-} that are in normal SW. For example will "2" on the x-axis correspond to two times the SO_4^{2-} -concentration that are in SW given in table (4.4). Figures from Punternvold et al. (2015).

The results from the study by Puntervold et al. (2015) show that a considerable amount of NaCl must be removed in order to see a significant effect in oil recovery. Between 50-100 % NaCl, the oil recovery decreases linearly with % NaCl in SW, and removal of NaCl in that range will only add to 2-3 extra % in oil recovery. However, when over 90 % NaCl has been removed, the slope increases greatly in figure a), and larger oil recoveries are observed.

In figure b), it is observed that the oil recovery is quite low when the content of SO_4^{2-} in SW is between a factor of 0-3 of the normal amount in SW. By comparing $4 \times \text{SO}_4^{2-}$, with $1 \times \text{SO}_4^{2-}$, there is an increase in oil recovery of 10 %. Consequently, only by spiking SW with 3-4 times the normal content of SO_4^{2-} , will there be a significant effect on the oil recovery.

3.7 Production of Smart Water

3.7.1 Smart Water Production by Membranes

When a fluid stream passes a filter and two or more components from the liquid are separated out, it is defined as a filtration process (Cheryan, 1998). Filtration, is usually expressed in terms of separation of immiscible solids from fluids. Whenever dissolved solutes need to be filtered out, membrane filters are required since they can filter out particles in the ionic range (1-10 Å). Membrane filters are selective barriers, hence they will permeate some components while others are retained.

Recently, Nair, (2019), studied the possibility of producing Smart Water from SW by use of nano-filtration membranes (NF). These filters are pressure-driven, where SW is forced through a semi-permeable membrane, which causes the SW to split into a retentate- and a permeate stream as shown in the figure below.

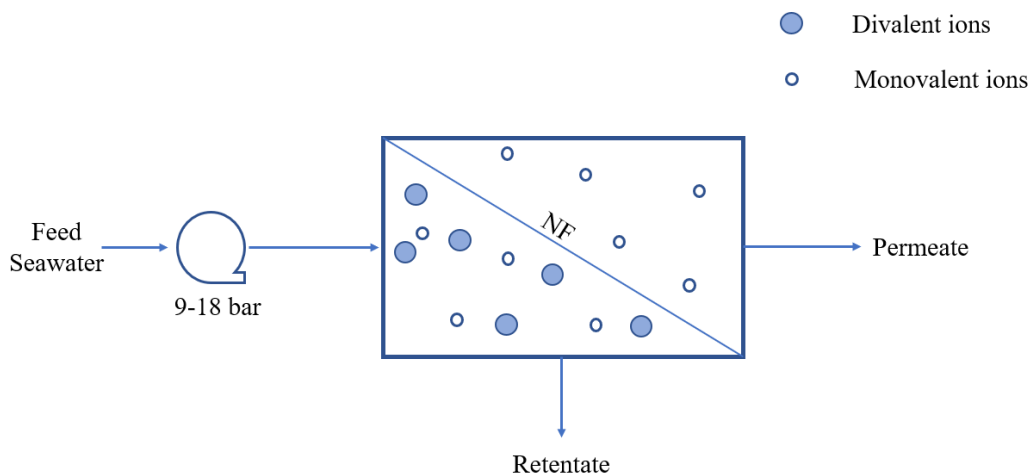


Figure 3.13: Illustration of Smart Water production from SW using NF membranes. SW is used as feed into the membrane, and the selective membrane allow some ions to permeate and some are retained in the retentate. Figure after (Nair, 2019).

When SW is forced through the membrane, ideally the retentate should be enriched in divalent ions and depleted of monovalent ions, whereas the permeate should have a low concentration of divalent ions. The retentate can then be used as Smart Water in carbonate reservoirs, while the permeate could be used in sandstone reservoirs. The results from the research show that there are two main concerns with the method. Most notably, is the fact that between 30 % - 45 % of the Ca^{2+} ions are permeated through the membrane. The ion rejection of several ions are displayed below:

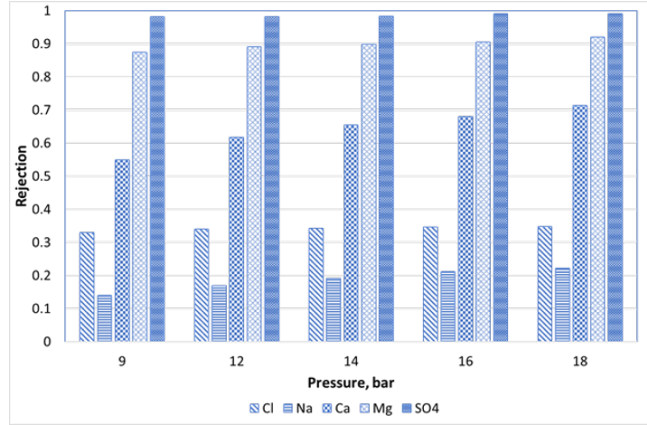


Figure 3.14: Distribution of ion rejection by the NF membrane. SO_4^{2-} and Mg^{2+} are rejected almost completely, while Ca^{2+} rejection is between 55 % - 70 %. Around 30 % of the Cl^- ions are rejected, whereas Na^+ is slightly less rejected, with 10 % - 20 % (Nair, 2019).

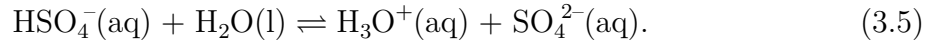
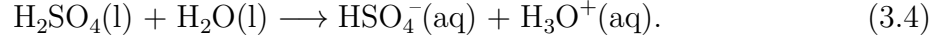
Since the Smart water effect is based on co-adsorption of Ca^{2+} onto the SO_4^{2-} -ion, it relies on an equal concentration of both ions. As only SO_4^{2-} is sufficiently retained and not Ca^{2+} , there is an imbalance in ion concentration of the two important divalent ions. The second concern is related to the concentration of monovalent ions in the retentate. Due to a high concentration of divalent ions in the retentate, monovalent ions are also present to maintain charge balance, which can be seen in table (3.1). The obtained composition of the retentate is therefore not optimal for carbonate reservoirs. In addition, the ionic composition of the SW feed is almost identical to the retentate. Hence improvements of the membrane technology must be implemented, or different technologies must be pursued in order to create a more efficient Smart Water than SW.

Table 3.1: NF 270 at 9 bar pressure, gave the best ionic composition out of all the tested membranes. Still, the composition is not ideal for wettability alteration in carbonates, since too much monovalent ions are held back, and too many Ca^{2+} -ions permeates through.

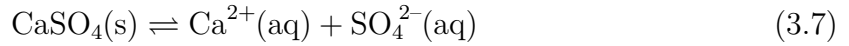
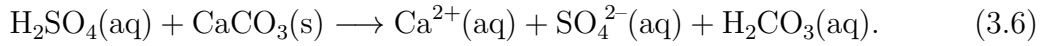
Ion	SW Feed mM	Retentate mM	Permeate mM
Na^+	479.3	477.9	417.6
Cl^-	555.9	553.4	503.6
Ca^{2+}	12.8	11.0	8.0
Mg^{2+}	53.8	56.1	33.0
SO_4^{2-}	29.9	32.4	0.1

3.7.2 Production of Smart Water by Sulphuric Acid

Production of Smart Water by injection of sulphuric acid (H_2SO_4) into the reservoir is based on two chemical processes; dissociation of an acid and dissolution of calcite rock. The acid solution is made by adding sulphuric acid from a 1M stock solution, to DI-water in a pre-determined concentration. When dissolved in water, it will dissociate in two stages since it is a diprotic acid, and add free SO_4^{2-} -ions to the brine:



The solution is then injected into the chalk outcrop cores. As the brine enters the porous medium of the chalk cores, dissolution of calcite takes place according to the following reaction:



Dissolution of calcite provides Ca^{2+} -ions to the brine, and the brine now contains SO_4^{2-} -ions and Ca^{2+} -ions in solution, and the production of Smart Water is complete.

In terms of equipment, this technology is dependent on sulphuric acid and fresh water. The sulphuric acid is readily available on the international market, and can be bought in large quantities, and is therefore cheap. While the fresh water can be made on-site by using reverse osmosis membranes to desalinate SW. RO-membranes systems are cost-effective, reliable and can be installed on the rigs.

4 | Experimental

4.1 Materials

4.1.1 The Outcrop Rock

In order to resemble the biogenic chalk reservoirs found at the Norwegian continental shelf, among them Ekofisk and Valhall, the outcrop Stevns Klint chalk close to København were used as analogue to the real reservoir rock. The carbonates have the same age as the upper Tor and lower Ekofisk formation, and are reported to be 98-99 % pure biogenic chalk (Frykman, 2001). The cores were drilled out from the same outcrop block that were 20-30 cm in height. They were then dried, and later cut to desired length and shaven to get a smooth surface. Properties of the core are summarized in the table below. In addition, Stevns Klint chalk is reported to have surface area of about 2.0 m²/g, however this was never measured, but read in literature (Frykman, 2001). The measured properties of the cores are summarized in the table below.

Table 4.1: Stevns Klint Cores used during this thesis with physical parameters. All cores have been cut out from the same outcrop block, and therefore have very similar properties, such as ϕ and k.

Core	L (cm)	D (cm)	V _b (cm ³)	ϕ (%)	k (mD)	PV (ml)
SK1	7.02	3.78	78.78	49	4.65	38.32
SK2	6.47	3.78	72.61	50	5.47	36.15
SK3	6.30	3.79	71.07	48	4.83	34.37
SK4	6.31	3.80	71.56	49	4.95	36.27
SK5	6.23	3.79	70.28	49	4.98	34.67
SK6	6.25	3.79	70.88	48	5.14	33.78
SKWW	7.07	3.79	79.80	49	4.64	39.20

4.1.2 Preparation of Oil

A general description of the process of modifying crude oil to different AN is given here. The crude oils that come directly from reservoirs have very high AN, and it is therefore necessary to modify the crude oil to AN-values.

RES-40 Preparation

RES-40 is the "high AN-oil" and was made by mixing crude oil from the Heidrun field with n-Heptane in a 60/40 ratio respectively. Subsequently, the oil was centrifuged and then filtered with a $5\mu\text{m}$ millipore filter. The acid and base number were then measured with a Mettler Toledo T50 auto-titrator. The measured values are shown in table (4.2).

RES-40-0 Preparation

The RES-40-0 has an $\text{AN} = 0$, and is made with RES-40 as the basis oil. The preparation of the oil begins by adding 20 wt% silica gel to the RES-40 oil, followed by 1 week of stirring at room temperature. The role of the silica gel, is to extract the polar oil components out of the oil, hence reducing the acid number of the oil. Then an additional 20 wt% silica gel is added to the oil, and put on stirring for an additional week. After a total of two weeks of stirring, precipitates have formed, which are due to adsorption of polar oil components into the silica gel. Next, the oil is centrifuged in order to separate the silica gel from the oil phase. Afterwards the oil was filtered with a $5\mu\text{m}$ millipore filter, and stored in a flask.

Oil A Preparation

Afterwards, the RES-40 and the RES-40-0 are mixed in different proportions to make oils of lower AN. By adding more and more RES-40-0 to the RES-40, the lower the AN becomes. The target AN can be calculated as follows:

$$\text{Target AN} = \text{AN}_{\text{RES-40}} \cdot \frac{V_{\text{RES-40}}}{V_{\text{RES-40+RES-40-0}}} + \text{AN}_{\text{RES-40-0}} \cdot \frac{V_{\text{RES-40-0}}}{V_{\text{RES-40+RES-40-0}}} \quad (4.1)$$

The final product of the mixing, gave an oil with AN=0.50 which was termed as "Oil A", and was used during this study to saturate the chalk cores. Properties of the oils are given in tables (4.2) and (4.3).

Synthetic Oil

The synthetic oil was used to saturate core SKWW. This oil has no polar oil components and is therefore not able to alter the wettability of the core. Consequently, by saturating core SKWW with this oil, the initial wettability is preserved. The synthetic oil was prepared by mixing 58 % Marcol with 42 % n-Heptane.

Table 4.2: The measured AN and BN numbers are given for the three oils. The AN and BN were reproduced three times for each oil with an uncertainty of ± 0.05 mgKOH/g.

Oil	ρ (g/cm ³)	AN (mgKOH/g)	BN (mgKOH/g)	$\mu_{25^\circ\text{C}}$ (mPas)
RES-40	-	2.40	0.90	-
RES-40-0	-	0.07	0.01	-
Oil A	0.8101	0.50	0.24	2.50
Synthetic Oil	-	-	-	2.70

Table 4.3: Interfacial tension of oil A in equilibrium with DI, FW, SW and Smart Water at 23 °C in addition to synthetic oil and DI-water.

σ at 23 °C	
Synth. Oil/DI-water	41 mN/m
Oil A/DI-water	18 mN/m
Oil A/Smart Water	14 mN/m
Oil A/FW	11 mN/m
Oil A/SW	10 mN/m

4.1.3 Brines

Valhall Formation Brine FW (VB0S)

Initial water saturation in the chalk cores was established with a brine termed as VB0S. This brine has a composition similar to the formation water in the chalk formation Valhall, situated in the North Sea, but does not contain SO_4^{2-} . It is important to avoid SO_4^{2-} in the initial saturation establishment, since SO_4^{2-} will most likely render the core water-wet (Punternvold et al., 2007), consequently no SO_4^{2-} -ions are added to the brine. The ionic composition of VB0S can be seen in table (4.4).

Seawater (SW)

SW contains both SO_4^{2-} -ions and Ca^{2+} -ions and is considered to be an excellent Smart Water in chalk (Austad et al., 2008). During the experiments, the SW served as a benchmark for the Smart Water performance.

Gypsum (Smart Water)

Gypsum ($\text{CaSO}_4 \cdot 2\text{H}_2\text{O}$) dissolved in DI-water is used as the Smart Water in this thesis, to represent the brine produced by acid flooding in chalk. The concentration of SO_4^{2-} -ions and Ca^{2+} -ions at 90 °C in the Smart Water was determined based on the bulk solution test presented in section (4.7).

Preparation of Brines

The brines were prepared by adding approximately 400 ml de-ionized water (DI) to a 1000 ml volumetric flask. Salts were then added to the volumetric flask according to the recipe given in the appendix (B.3). During mixing however, carbonate and sulphate salts were dissolved separately to avoid precipitation. After all salts had dissolved, the volumetric flask was filled up to the meniscus, and put on stirring at 23 °C for 24 hours. Afterwards the brines were filtered through a .22 μm Millipore-filter, and stored in a bottle.

Table 4.4: Composition of the formation water at Valhall (VB0S), seawater (SW) and Smart Water.

Ion	FW (VB0S) mM	SW mM	Smart Water mM
HCO₃⁻	9.0	2.0	0.00
Cl⁻	1066.0	525.0	0.00
Mg²⁺	8.0	45.0	0.00
Ca²⁺	29.0	13.0	13.0
Na⁺	997.0	450.0	0.00
K⁺	5.0	10.0	0.00
SO₄²⁻	0.0	24.0	13.0
Density g/cm ³	1.041	1.024	0.995
TDS g/L	62.83	33.39	1.770

4.2 Analyses

During the experimental work, several analyses were carried out. Hence a brief introduction of the equipment that were used for each analysis, is given in this section.

4.2.1 Viscosity Measurement

A rheometer by Anton Paar was used to measure the viscosities reported in this thesis. The model was a MCR 302, and a rotating cone-plate was used to measure the viscosity. The viscosity was measured between a shear rate of 50 (1/S) to 500 (1/s), with 5 measuring points. To ensure that the measured viscosity was the correct, three equal measurements were repeated for each fluid.

4.2.2 IFT Measurement

The interfacial tension (IFT) was measured with a manual force tensiometer, Kruss K6. The accuracy of the instrument is reported by the manufacturer to be ± 0.5 mN/m (KRUSS, 2019).

4.2.3 pH Measurements

To measure the pH of the effluent from the acid flooding, a pH meter known as SevenCompact from Mettler Toledo was used. The pH meter has a calibration program for quality assurance. Thus, each time the instrument was used, it was calibrated with buffer solutions of pH = 4, 7 and 10.

4.2.4 Density Measurements

The density of the formation water, oil and SW was measured with a 5-digit density meter called DMA-4500 from Anton Paar. Whenever a fluid is injected into the instrument, it enters a glass u-tube which allows the user to inspect the sample for any air bubbles that could deter the measurement.

4.2.5 Acid-Number (AN) and Base-Number (BN)

A Mettler Toledo T50 auto-titrator was used to quantify the amount of acids and bases in the crude oil. The instrument perform a potentiometric titration on the solution and then convert the electrical potential to the corresponding acid and base number, mgKOH/g. The measurement procedure follows the standard ASTM procedure, however, modifications proposed by Fan and Buckley (2006) were used.

Before the oil sample could be measured, a standard of potassium hydrogen phtalate (KHP) had to be run one time to determine the exact concentration of the titrant. The titrant is used to neutralize the acid or base content in the crude oil. Hence, to calculate the exact amount of acid and base content in the oil, it is important to know the titrant concentration and the precise volume of titrant added. Since the modification of Fan and Buckley (2006) served as a guideline, measurements were performed in the following sequence: First a blank with spiked solution (stearic acid) was run, then a spiked blank with 1 ml of the oil sample was measured, followed by a spiked blank again. Each time, the weight of the blank with spiking solution was measured, to ensure consistency in the measurements. The analysis were repeated until three close measurements had been obtained.

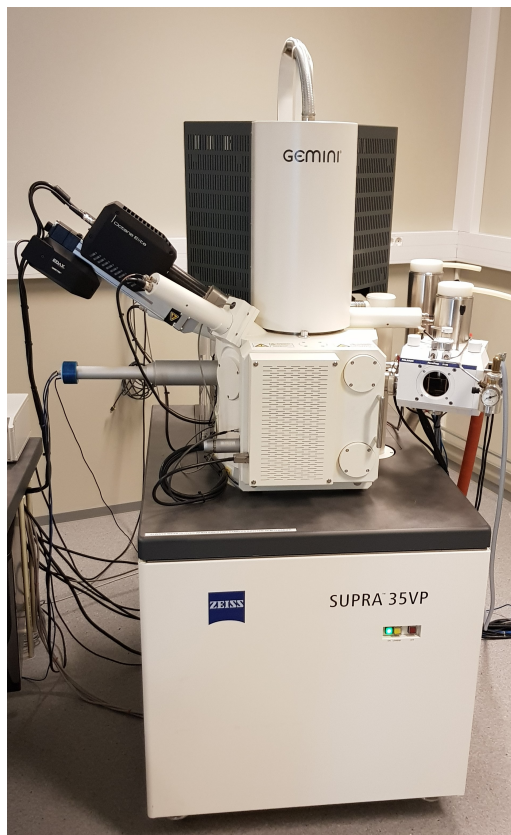
4.2.6 PHREEQC

PHREEQC was used to simulate precipitation of $\text{CaSO}_4(\text{s})$ at different temperatures. The database used during this simulation was phreeqc.dat.

4.2.7 Scanning Electron Microscope with EDX

A scanning electron microscope (SEM), known as ZEISS SUPRA 35VP, was used to investigate the chalk surface on a microscopic scale. The instrument is shown in figure 4.1 (a). The microscope obtains an image by scanning a focused electron beam onto a small part of the chalk surface, and then detects the signals transmitted back from the surface. The signals that are detected and used to generate an image are mainly: Secondary electrons, backscattered electrons and X-rays (NanoScience, 2019). Prior to the scanning, all samples were coated with Palladium (Pd) to increase the conductivity of the sample as shown in figure 4.1 (b). The coating is absolutely necessary for the electron scanning microscope, since it relies on electron flow on the surface.

The SEM-instrument also had energy dispersive X-ray detectors (EDX). The output data from the EDX-analysis were given as a spectrum of peaks for the individual elements. Each element was detected by the SEM-instrument, and the atomic % was computed automatically by the software.



(a) Scanning electron microscope.



(b) Palladium coating

Figure 4.1: Scanning electron microscope (SUPRA V35) and Palladium coating on chalk samples.

4.2.8 Ion Chromatography Analyses of Brines

To analyse the anionic and cationic composition of the effluent samples, an ion chromatograph known as DIONEX ICS-3000 was used. Prior to the analysis, the effluent samples were diluted 1000 times with a tritulation system by Gilson. The output data of the ionic composition from the ion chromatography (IC) are given as individual peaks for the different ions. The area under each peak is related to the concentration of the ion representing that peak. By using an external standard fluid, for example SW with known ionic composition, the area of each peak can be converted to concentration as follows:

$$\frac{C_{SW}}{A_{SW}} = \frac{C_{\text{SO}_4^{2-}}}{A_{\text{SO}_4^{2-}}} \longrightarrow C_{\text{SO}_4^{2-}} = \frac{C_{SW}}{A_{SW}} \cdot A_{\text{SO}_4^{2-}}. \quad (4.2)$$

Where C_{SW} is the concentration of SO_4^{2-} -ions in SW and is equal to 24 mM, while A_{SW} is the area under the SO_4^{2-} -peak from the SW-sample, which was computed by the IC. Analogously, $C_{\text{SO}_4^{2-}}$ is the concentration of SO_4^{2-} -ions in the effluent sample, and $A_{\text{SO}_4^{2-}}$ is the area under the SO_4^{2-} -peak from the effluent sample.

4.3 Methodology

In this section the methodology of the experimental part is presented. The Smart Water group at UIS have worked with Stevns Klint chalk for over 20 years, and have therefore established a set of steps on how the cores must be prepared to best represent a reservoir chalk core. A general methodology of how each core was prepared is given, along with a description of how the acid flooding, spontaneous imbibition and forced imbibition were conducted.

4.3.1 Chalk Core Cleaning

Since the Stevns Klint area is situated close to the sea, there is a high possibility that the cores contain SO_4^{2-} due to contact with SW. Therefore, all chalk cores, regardless of the type of experiment, had to be cleaned with DI-water. As previously discussed, even a small concentration of SO_4^{2-} present in the core can have a strong influence on the initial wetting, since the sulphate hinders the organic oil components to adsorb onto the mineral surface (Punternvold et al., 2007). It also serves to get rid of salts that are easily dissolvable.

The cleaning process was done as proposed by Punternvold et al., 2007, where it is suggested to flush the core with at least 4 PVs of a brine free of SO_4^{2-} and without negatively charged ions. Therefore all cores were cleaned by flooding over 4 PVs with DI-water at a rate of 0.1 ml/min at room temperature. As all the chalk cores were relatively fragile, the confining pressure was set at 20 bars, during flooding. Batch tests of the effluent were then taken and further mixed with Ba^{2+} to check if any precipitation of $\text{BaSO}_4(\text{s})$ took place. Consequently, if there are SO_4^{2-} , reaction (4.3) will take place, and the water will no longer be blank but rather look cloudy:



4.3.2 Permeability and Porosity Measurements

Permeability measurements were performed while the cores were flooded with DI-water during the cleaning process. The average pressure drop, ΔP , were measured at three different rates; 0.05 ml/min, 0.100 ml/min and 0.150 ml/min at room temperature 23 °C, with the set-up shown in figure (4.7). This sequence were the same for all cores. By plotting q vs ΔP , the slope was found and the permeability could be determined with Darcy's law (2.5). It is worth noting that Darcy's law is merely an approximation, and is only valid under certain conditions. For incompressible single phase fluid flow in the laminar flow regime in a uniform homogeneous rock that is 100 % saturated, the Darcy equation is valid. Since the Stevns Klint chalk is reported to be 98-99% pure chalk, and the flow rate during permeability measurements were low, the results in table (4.1) were assumed to be within reasoning.

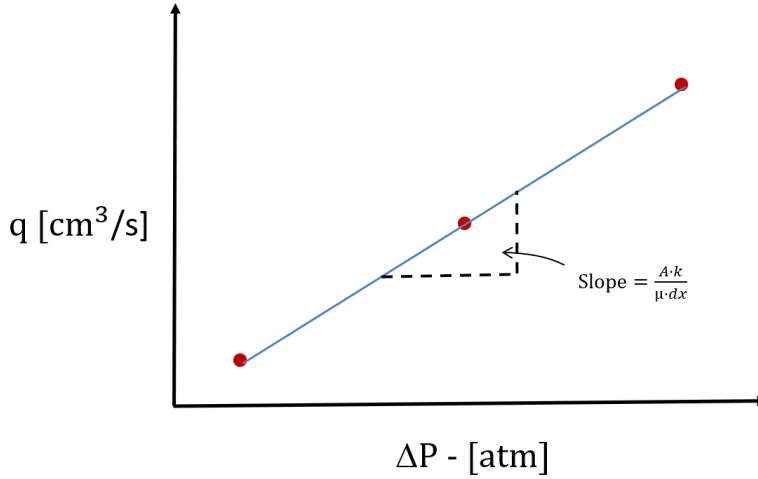


Figure 4.2: Determination of permeability. The pressure drop across the core were measured at three different rates; 0.05, 0.100 and 0.150 ml/min. Since the fluid was DI at ambient temperature, the viscosity, μ , was assumed to be ~ 1 mPas.

In order to calculate the porosity, ϕ , the bulk volume, V_b , had to be measured along with the dry and saturated weight of the cores. The bulk volume was found by measuring the length and diameter of the cores. Subsequently, the dry weight, W_{dry} , and the saturated weight, W_{sat} were measured. To ensure that the cores were fully saturated, they were put in vacuum before being saturated to remove air. Since the density of the DI-water, ρ_w was close to 1.00 g/cm³, V_p was found by taking the difference between W_{sat} and W_{dry} . The porosity could then be calculated as:

$$\phi = \frac{W_{sat} - W_{dry}}{\frac{\rho_w}{\frac{\pi d^2}{4} \cdot L}} = \frac{V_p}{V_b}. \quad (4.4)$$

4.4 Core Restoration for SI and FI Experiments

Before the spontaneous imbibition (SI) and forced imbibition (FI) experiments, the cores went through a restoration process to establish the formation water and oil saturation. The cores were saturated with $S_{wi}= 10$ % FW given in table (4.4) and $S_{oi}= 90$ % with oil A of AN = 0.50 mgKOH/g, with properties given in table (4.2).

4.4.1 Establishing Initial Water Saturation

In order to obtain 10 % initial water saturation, S_{wi} , the FW, was diluted 10 times. The core was then put into a desiccator under vacuum, and brine was slowly introduced to the core. The core was held under vacuum with diluted FW for 30 min to make sure that it was fully saturated. Then the saturated weight was measured before it was put into a desiccator with silica gel. It stayed in the desiccator to let the diluted brine evaporate until the target weight had been reached. The target weight, W_{target} is given by:

$$W_{target} = \text{Dry Weight} + PV \cdot 0.10 \cdot \rho_{FW}, \quad (4.5)$$

where PV is the pore volume, and ρ_{FW} is the density of the formation water (VB0S). Afterwards, the core was left for 3 days to ensure that the water had an even distribution inside the core.

4.4.2 Establishing Initial Oil Saturation

The chalk cores with 10 % FW saturation, were mounted in the set-up shown in figure (4.3), and the temperature was set at 50°C inside the heating chamber, to lower the differential pressure applied across the core. Before oil was injected into the core, it was put on vacuum to remove air, to ensure a fully saturated core. Then, oil was injected from both sides with 1 PV of oil. Subsequently, 70 ml of oil was flooded across the core in one direction, before the direction was switched once again and 70 ml was flooded through the other inlet. The reasoning behind this was to be sure that the oil had adsorbed evenly from both inlets through to the center of the core.

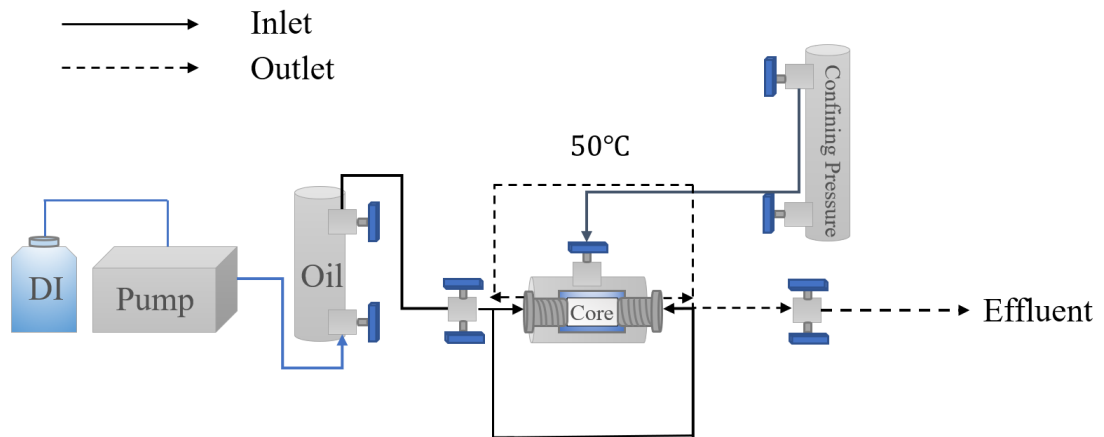


Figure 4.3: Set-up used for establishment of oil saturation. The set-up includes confining pressure of 20 bars, a heating chamber holding 50°C and two inlets and outlets.

4.4.3 Ageing

After the cores had been saturated, they were wrapped in teflon tape and put into an ageing cell. The cell was filled with oil, and that is also why teflon tape was put on to avoid unrepresentative adsorption of oil on the outer surface of the cores. Then they were put in a heating chamber which held 90°C, which is the same temperature the spontaneous imbibition experiments were executed at.

4.5 Oil Recovery by Spontaneous Imbibition

Following two weeks of ageing, the cores were placed inside imbibition steel cells, and further filled up with either SW, FW or Smart Water. Marbles were placed below the chalk cores to increase the available surface area for the imbibition fluid. The reference core, SK2, was filled up with FW, SK5 with SW and SK6 with Smart Water. The steel cells were put into heat chambers holding a temperature of 90°C for two of the cores, while the reference core SK2 was held at 70°C. Since the spontaneous imbibition experiments were performed at high temperatures, a piston cell providing 10 bars was connected to each steel cell to avoid evaporation. The piston cells were tested for leakages prior to the experiment. As a precaution, grease was applied on the o-rings to ensure that the cell was properly sealed. A burette was used to collect and measure the volume of produced oil. The set-up for the spontaneous imbibition experiment is displayed in figure (4.4), showing the aforementioned equipment.

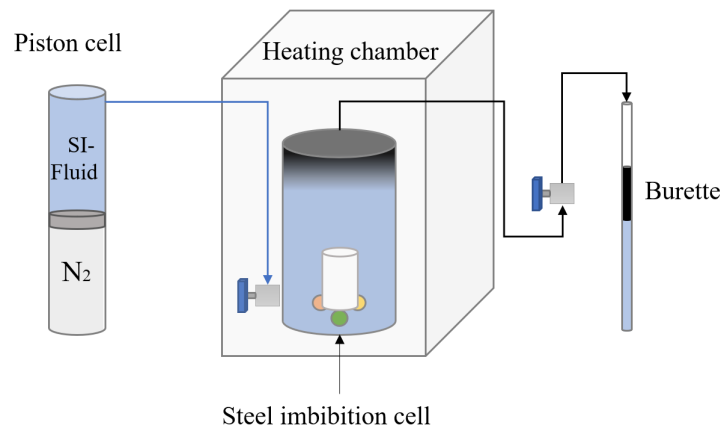


Figure 4.4: Experimental set-up of the spontaneous imbibition. Chalk core is resting on marbles so that the whole surface area is available for the brine.

4.6 Oil Recovery by Forced Imbibition

After oil production through spontaneous imbibition had reached a recovery plateau, the cores were subsequently put in a flooding set-up similar to that shown in (4.7). When brine is injected rather than spontaneously imbibed into the core, the viscous forces become more prominent. If enough pressure is applied, they could overrule capillary forces. Hence, an evaluation of the viscous forces of the different brines can therefore be compared. The flooding was conducted at the same temperature as the spontaneous imbibition, and the effluent/produced oil was still measured and collected with a burette. The injection rate was set to, 1 PV/day, and oil was then produced by forced displacement. The low injection rate is merely to avoid too high pressure drop in these low permeable chalk cores that can damage them.

4.7 Bulk Solution Test

A bulk solution test performed by Konstantina Nanidou, Aleksandar Mirkovic and the Smart Water EOR group (2019), is presented here. The test is the basis for the injected H_2SO_4 -concentrations during the acid flooding. Furthermore, it is used to determine the maximum amount of gypsum ($\text{CaSO}_4 \cdot 2\text{H}_2\text{O}$) that can be added to DI-water at $90\text{ }^\circ\text{C}$, without having precipitation of $\text{CaSO}_4(\text{s})$. Recall that the gypsum brine will represent the synthetic version of the H_2SO_4 based Smart Water, and is used as Smart Water during the spontaneous- and forced imbibition experiments. The gypsum brine is then an idealisation of the H_2SO_4 based Smart Water that ensures an equal proportion of SO_4^{2-} -ions and Ca^{2+} -ions, thereby simplifying the experimental testing conditions.

The bulk solution test was performed to obtain the solubility of $\text{CaSO}_4(\text{s})$ at different temperatures, and different H_2SO_4 -concentrations in equilibrium with $\text{CaCO}_3(\text{s})$. The experimental procedure was as follows: At temperatures of $50\text{ }^\circ\text{C}$, $70\text{ }^\circ\text{C}$, $100\text{ }^\circ\text{C}$ and $130\text{ }^\circ\text{C}$, 10g of CaCO_3 -powder was mixed in a 10 ml sample glass, subsequently various amounts of H_2SO_4 was added. Then the samples were stirred for 24 hours, before being centrifuged. The equilibrated fluid was then gathered and analysed for Ca^{2+} and SO_4^{2-} by the ion chromatograph. The results from the ion chromatography are shown in table (4.5) below. The bold numbers represents the solutions that precipitated $\text{CaSO}_4(\text{s})$.

Table 4.5: Bulk solution test: DI-water with H₂SO₄ equilibrated with CaCO₃. Numbers in bold indicates which samples that precipitates at a given concentration. All the numbers in this table are from the Ion Chromatography.

DI-water [H ₂ SO ₄] (mM)	Eq. at 50°C		Eq. at 70°C		Eq. at 100°C		Eq. at 130°C	
	SO ₄ ²⁻ (mM)	Ca ²⁺ (mM)	SO ₄ ²⁻ (mM)	Ca ²⁺ (mM)	SO ₄ ²⁻ (mM)	Ca ²⁺ (mM)	SO ₄ ²⁻ (mM)	Ca ²⁺ (mM)
4	4.2	4.9
6	7.0	9.6
8	8.0	9.3
10	9.4	6.3	8.5	4.8
12	12.1	11.5	9.2	7.3
16	.	.	15.7	18.2	13.4	11.9	.	.
18	19.4	17.1	14.9	11.8	13.4	11.9	.	.
20	20.2	20.5	14.4	14.8	12.7	13.0	.	.

Based on table (4.5), the injected concentrations of H₂SO₄ in DI-water at 70 °C were 12 mM, 15 mM and 18 mM, while at 130 °C the selected concentrations were 6 mM and 8 mM. The injected acid concentrations are given in table (4.6). Note that the values in the table deviate from the actual selected concentrations since they were measured by the ion chromatograph. Further on in the thesis, only values measured by the ion chromatograph are presented.

Table 4.6: pH and H₂SO₄ concentration of the injected acid solutions.

H ₂ SO ₄	pH
4.9 mM	2.24
8.5 mM	2.19
9.7 mM	2.16
13.3 mM	2.09
16.7 mM	2.05

4.7.1 Synthetic Production of H₂SO₄ Based Smart Water

The spontaneous imbibition and forced imbibition were run at 90 °C. Since the solubility of CaSO₄(s) not had been tested in the bulk test, a trend plot based on table (4.5) was made in order to determine the concentration of SO₄²⁻ and Ca²⁺ that could be added to DI-water at 90 °C. As a precaution, values slightly under the precipitation concentrations (bold numbers in table 4.5), were used in the trend plot, to be on the safe side in terms of precipitation of CaSO₄(s).

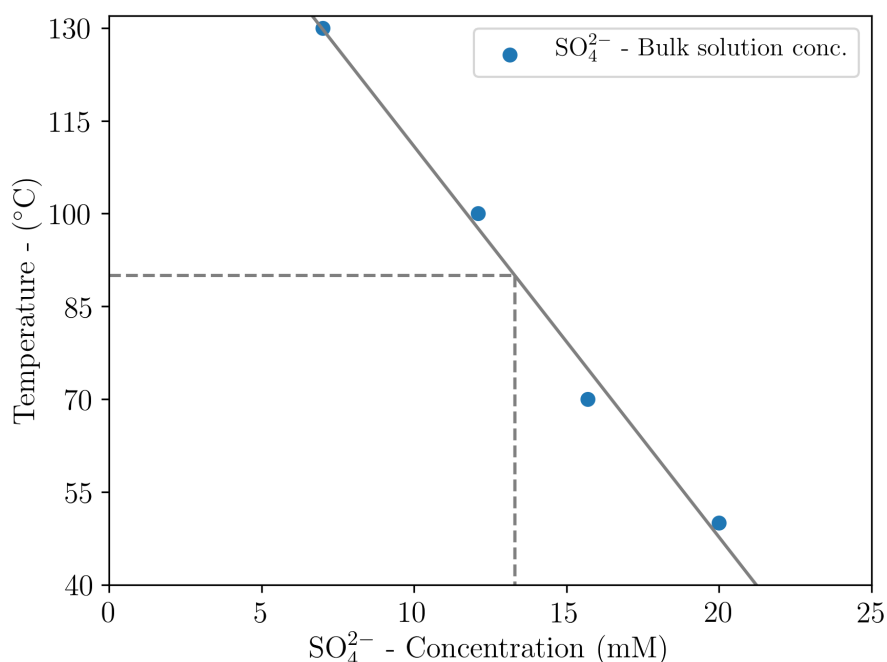


Figure 4.5: A trend plot showing the concentration of SO₄²⁻-ions at 90 °C that could be added to DI-water equilibrated with CaCO₃(s) and not yield precipitation of CaSO₄(s). The blue dots represents SO₄²⁻-values from table (4.5) and were used to find the concentration.

From the trend plot, the maximum SO₄²⁻-concentration at 90 °C was found to be close to 13 mM. With a molecular weight of 172.17 g/mol, a total of 2.238 g of gypsum was therefore added to 1 L of DI-water to make the Smart Water. The composition of the Smart Water is given in table (4.4). This Smart Water was then used in the spontaneous and forced imbibition experiments at 90 °C and in the parallel study at 70 °C.

4.8 Acid Flooding

Sulphuric acid, H_2SO_4 , is a strong acid which is readily soluble in water in an exothermic reaction. It is a highly corrosive liquid, clear in appearance without odor, and has a density of 1.8302 g/cm^3 (William, 2014). When dissolved in water, it will give two protons per molecule since it is a diprotic acid, which is shown in equations (3.4) and (3.5).

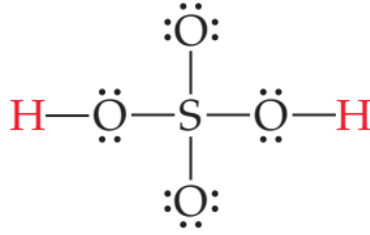


Figure 4.6: The chemical structure of sulphuric acid H_2SO_4 (Brown et al., 2000).

Since H_2SO_4 is a strong acid, it ionizes completely in the first reaction (3.4), and therefore the acid-dissociation constant is arbitrarily large, $K_a > 1$. HSO_4^- however, is a weak acid and will only partially dissociate, which is represented with the equilibrium arrows. The corresponding acid-dissociation constant is $K_{a2} = 1.2 \cdot 10^{-2}$ for reaction (3.5) (Brown et al., 2000).

The procedure of making the sulphuric acid solution has already been mentioned in section (3.7.2), however, a short guideline is given here. Around 400 ml of DI-water is added to a 1000 ml volumetric flask. Subsequently, various amounts of H_2SO_4 were added to DI-water. The injected concentrations are given in table (4.6), and were measured by an ion chromatograph. The H_2SO_4 was added to the volumetric flask from a 1M H_2SO_4 stock solution with an adjustable pipette. In order to calculate the volume needed from the 1M H_2SO_4 stock solution to make the desired concentrations, a simple dilution formula was used.

$$C_1 \cdot V_1 = C_2 \cdot V_2. \quad (4.6)$$

Where C_1 is the concentration of the stock solution, and V_1 is the volume needed from the stock solution. While C_2 is the concentration of the final solution and V_2 is the volume of the final solution.

An example calculation for a 4.9 mM H_2SO_4 solution is given below:

$$V_1 = \frac{4.9 \cdot 10^{-3} \text{ M} \cdot 1 \text{ L}}{1 \text{ M}} = 4.9 \cdot 10^{-3} \text{ L}. \quad (4.7)$$

Consequently, in order to make a 4.9 mM H_2SO_4 solution, 4.9 ml was withdrawn from the 1M H_2SO_4 stock solution with the pipette, and added to the 1L volumetric flask. The pipette was tested before use, by taking a volume of water with known density and then measuring that volume on a weighing scale to make sure it was accurate. Afterwards the volumetric flask with 4.9 ml of H_2SO_4 is filled up to the meniscus with DI-water. Subsequently, the solution was put on magnetic stirring for 24 hours at room temperature.

Production of Smart Water through acid flooding of the acid solutions given in table (4.6) was conducted with the set-up shown in figure (4.7). The acid flooding experiment looked into acid-dissociation and dissolution of chalk, therefore no restoration of initial water saturation, S_{wi} or oil saturation, S_{oi} , had to be established. Prior to the flooding, the core was cleaned by flooding the core with DI-water as explained in section (4.3.1).

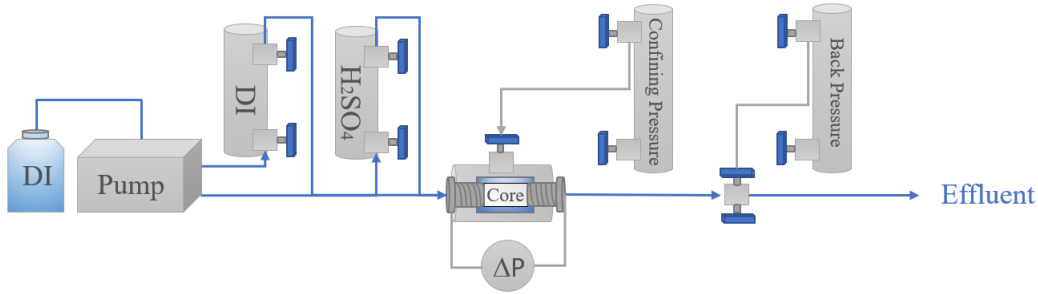


Figure 4.7: Illustration of the core flooding set-up used during acid flooding and also for the forced imbibition experiments during oil recovery. The Hassler core was mounted inside a heat oven, such that flooding could be done at different temperatures.

After each acid flooding, the core was cleaned before the next acid flooding in order to remove SO_4^{2-} from the core. This was accomplished by flooding with DI-water at the same rate and temperature as the acid flooding experiment had been run at. The rate was always at 0.32 ml/min (12 PV/d), and the temperatures were 70 °C and 130 °C respectively. The cleaning process usually lasted for approximately 36 hours, equivalent to flooding through almost 18 PV. To confirm the core was free of SO_4^{2-} , effluent was mixed with Ba^{2+} to check for any precipitation of $\text{BaSO}_4(\text{s})$. The acid flooding was performed at 70 °C with concentrations of 9.7, 13.3, and 16.7 mM H_2SO_4 . While at 130 °C, concentrations of 4.9 and 8.5 mM were injected. Effluent samples were collected with an auto-sampler from trilution. The samples were then pH-tested and analysed in the ion chromatography to check if the composition of the effluent obtained an equal proportion of SO_4^{2-} and Ca^{2+} , and whether or not the effluent could be a potential Smart Water.

5 | Results and Discussion

Results are discussed and presented in this section and related to theory introduced earlier in the thesis. The potential of Smart Water production through acid flooding is evaluated, where the effluent composition of the produced Smart Water is plotted versus pore volumes injected. The pH of the effluent from the acid flooding is also presented, as it tells something about the distribution of carbonate species in the solution and surface charge of the chalk surface. During the acid flooding, parameters such as temperature and concentration of the injected sulphuric acid are varied during the acid flooding, in order to obtain precipitation limits of Ca^{2+} and SO_4^{2-} . Even though precipitation limits were obtained in the bulk solution test, they also had to be tested during the flooding. When a solution is transported across a core, chemical reactions may not have time to fully take place, and therefore different precipitation limits can be observed. Subsequently, results from the SEM-analysis of the acid flooded core are given, to investigate if any dissolution effects can be detected and also to get a general characterization of the chalk outcrop core. Results from the spontaneous and forced imbibition experiments are then presented, where the oil recovery of the Smart Water produced through acid flooding is compared to SW and FW.

5.1 Acid Flooding

Based on the saturation concentrations from the bulk solution test in table (4.5), flooding experiments were conducted at 70 °C and 130 °C with the set-up in figure (4.7). DI-water with increasing concentration of H₂SO₄ was injected into a water-wet Stevns Klint core, saturated 100 % with DI-water. The injection rate was set at 12 PV/day (0.32 ml/min). The objective of the flooding experiment was for mainly two reasons. Most importantly, it was to verify if the production of Smart Water according to section (3.7.2) was achievable, with the proportions of Ca²⁺ and SO₄²⁻ in a 1:1 ratio, since the wettability alteration process relies on adsorption of SO₄²⁻ and subsequent co-adsorption of Ca²⁺. Secondly, the precipitation limits established in the bulk solution test were investigated, by injecting diluted sulphuric acid solutions in concentrations that were close to or at the precipitation limit into the chalk cores. The core used for this study was SK1, and the corresponding parameters for that core are given in table (4.1).

5.1.1 Acid Flooding at 70°

Ion Analysis of Effluent

In the figure below, the concentration of SO_4^{2-} and Ca^{2+} -ions from the ion chromatography analysis is plotted versus pore volume injected. Figure (5.1) show analysis of the effluent solution at 70 °C with injected DI-water with measured H_2SO_4 -concentrations of 9.7, 13.3 and 16.7 mM. The injected acid concentration is shown as a grey-staped line in the plots.

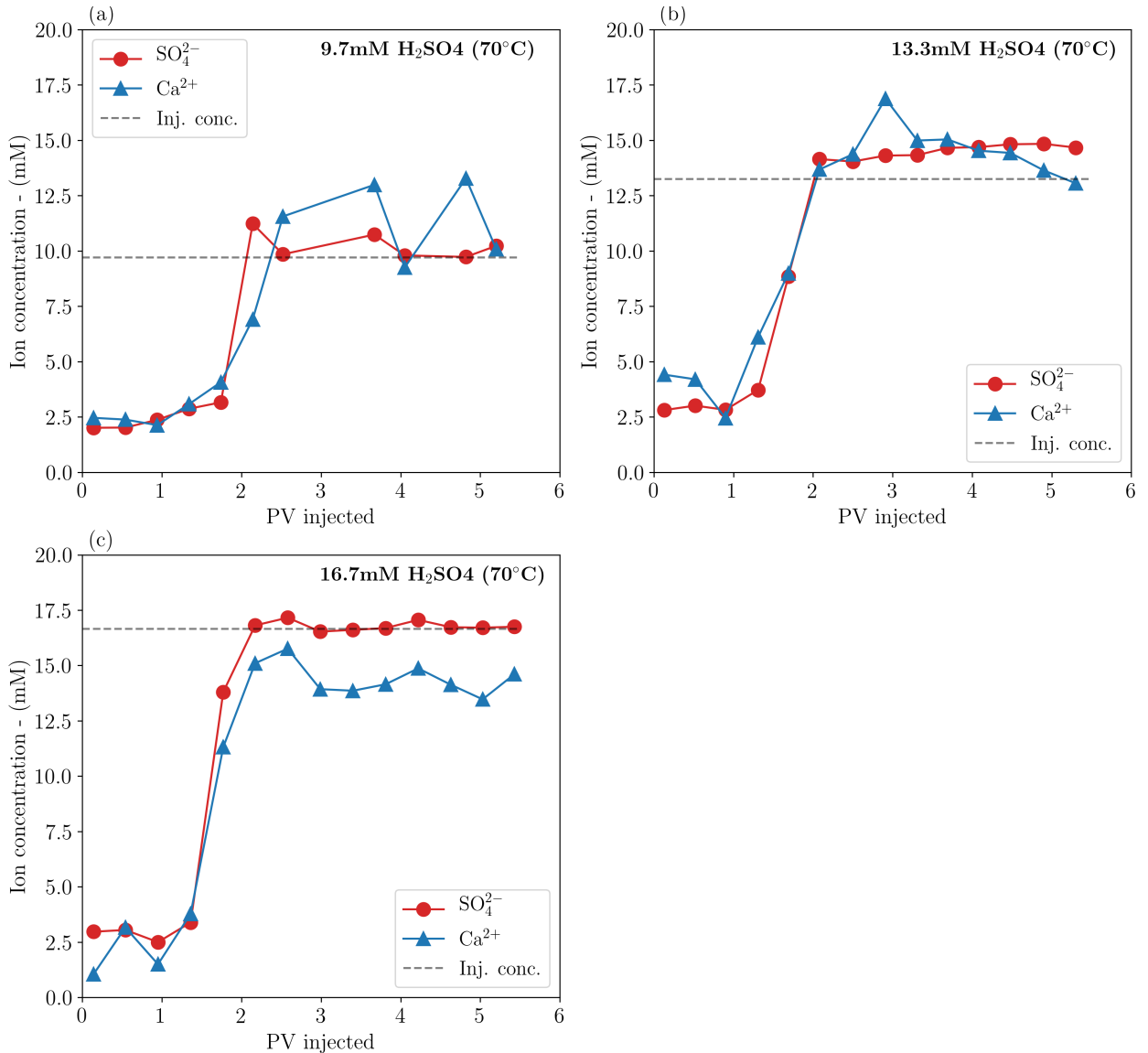


Figure 5.1: Injection of DI-water with increasing H_2SO_4 -concentration at 70 °C with a rate of 12 PV/d = 0.32 ml/min. In figure a) 9.7 mM H_2SO_4 was injected, in b) 13.3 mM H_2SO_4 and in c) 16.7 mM H_2SO_4 . The concentration of SO_4^{2-} and Ca^{2+} are based on analysis of effluent fluid by ion chromatography.

At 70 °C, no precipitation is observed at any of the concentrations. At almost all the injected concentrations of H_2SO_4 , the Ca^{2+} -concentration is following the SO_4^{2-} -concentration, which is in line with equation (3.6), presented in section (3.7.2). The only exception is when the 16.7 mM H_2SO_4 -solution is injected, then the Ca^{2+} -concentration is not reaching up to the SO_4^{2-} -concentration as shown in figure 5.1 (c).

The equilibrium at 9.7 mM, 13.3 mM and 16.7 mM are all stabilising after 2 pore volumes. It is also apparent that adsorption of SO_4^{2-} is taking place, which can be seen as a delay in the arrival of the effluent concentration profiles. If the SO_4^{2-} -ion had been non-reactive, the observed effluent curve would have been S-shaped. The effluent concentration profile should be close to half of the injected concentration after 1 PV injected. However, they are delayed and the effluent concentration profiles arrive after 1.5-1.8 PV. The initial effluent concentration of SO_4^{2-} in figure 5.1 (a), (b) and (c) begins at 2.5 mM. This indicates that the cleaning process mentioned in section (5.1) may not have been adequate enough.

Effluent pH Evaluation

The pH was measured on "fresh" effluent samples to ensure consistency in the measurements. It was observed that if the pH-measurement of the effluent sample was delayed by 1 day, the pH would decrease with 0.5 units. The decrease in pH is due to CO_2 in the atmosphere that can dissolve into the effluent samples and thereby lower the pH. As a result, all samples were measured within 6 hours after sampling. In figure (5.2), the effluent pH is plotted against PV injected for sulphuric acid solution 9.7 mM, 13.3 mM and 16.7 mM.

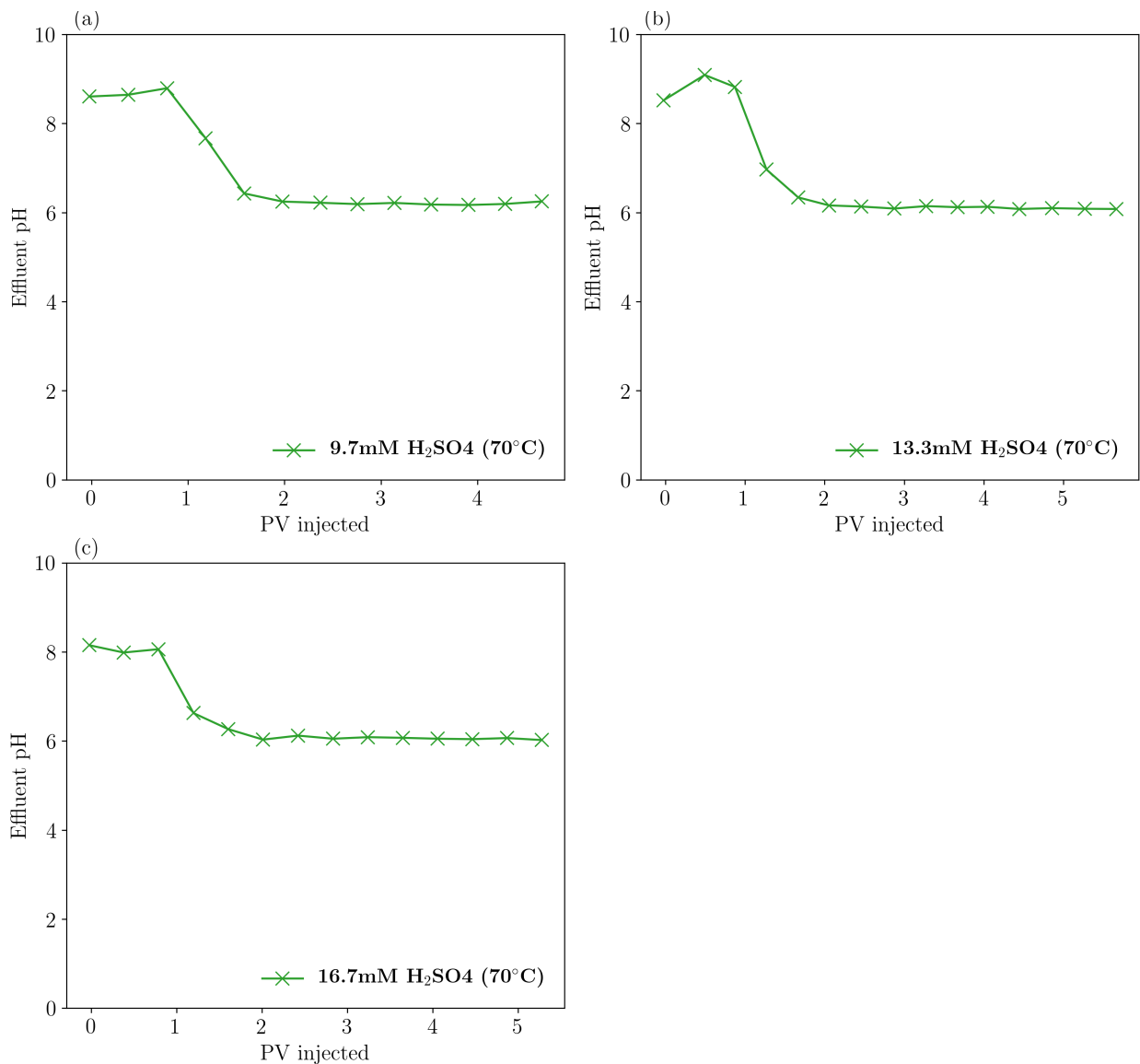


Figure 5.2: The effluent pH measured on fresh samples are shown in figure (a), (b) and (c) from the acid flooding conducted at 70 °C. In figure (a), the injected H_2SO_4 -concentration was 9.7 mM, in (b), 13.3 mM and in (c), 16.7 mM.

The trend is similar for all the input concentrations, where the pH for the first pore volume injected is on the alkaline side and close to 8, and then transitions toward an equilibrium pH equal to 6 when about 2 pore volumes have been injected. The equilibrium pH-trend corresponds to the time when the solution reaches chemical equilibrium with SO_4^{2-} and Ca^{2+} as shown in figure (5.1), which is after 2 pore volumes injected. The first three measurements are of the DI-water which originally saturated the core, hence the pH is higher initially. The combination of DI-water in equilibrium with $\text{CaCO}_3(\text{s})$ yields a system on the alkaline side due to free hydroxide ions (OH^-), according to the following reaction:



Prior to injection, the acid solution pH was measured to be ~ 2 (table 4.6), which equivalent to a free hydrogen concentration of 0.01 M. The equilibrium pH however is close to 6, hence the corresponding hydrogen concentration in solution is only $1 \cdot 10^{-6}$ M. The small concentration of free hydrogen ions in solution yields a slightly acidic environment, and also indicates that dissolution of calcite rock is constrained due to the common ion effect of Ca^{2+} , since not enough carbonate ions (CO_3^{2-}) are available to neutralise the hydrogen ions.

5.1.2 Acid Flooding at 130°

Ion Analysis of Effluent

In figure (5.3), the ion chromatographic analysis of the effluent brine from the acid flooding at 130 °C is given. The ion concentration of Ca^{2+} and SO_4^{2-} is plotted versus PV injected for the 4.9 mM solution in (a), and 8.5 mM in (b).

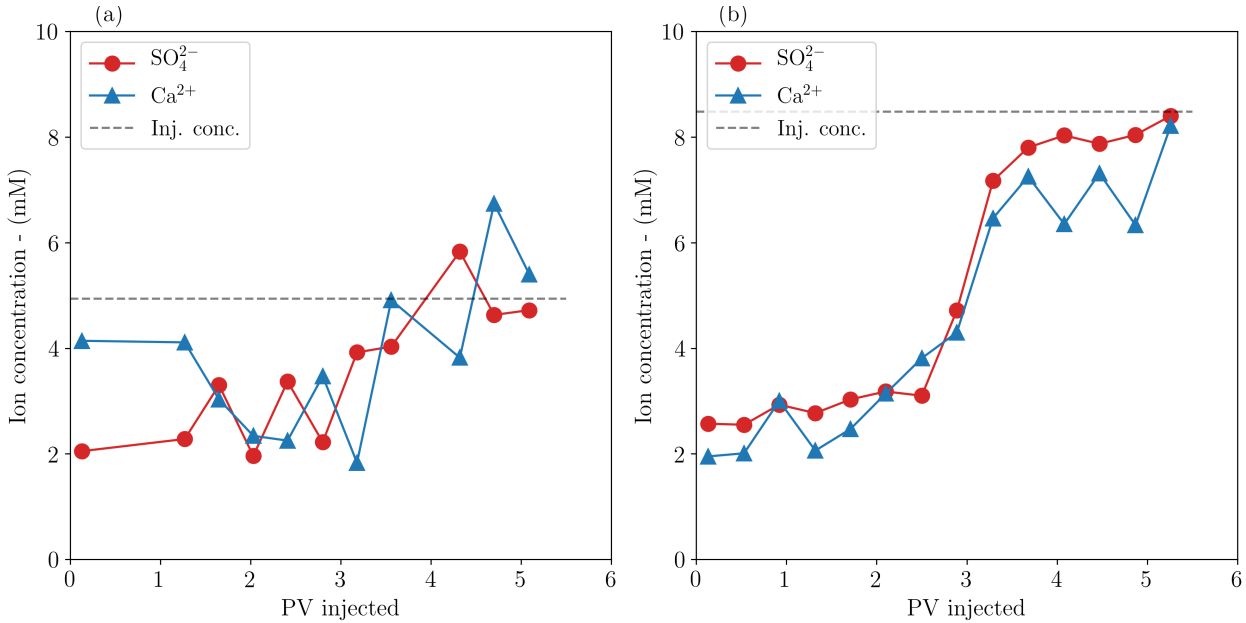


Figure 5.3: Injection of DI-water with increasing H_2SO_4 -concentration at 130 °C with a rate of 12 PV/d = 0.32 ml/min. In figure a) 4.9 mM H_2SO_4 was injected while in figure b) 8.5 mM was injected. The effluent fluid was analysed by an ion chromatography.

Since the solubility of $\text{CaSO}_4(\text{s})$ decreases with increasing temperature, the injected concentrations at 130 °C are significantly lower than at 70 °C. Based on table (4.5), the solution with 8.5 mM H_2SO_4 should precipitate and yield $\text{CaSO}_4(\text{s})$. However, during flooding no precipitation was observed, and the effluent concentration of Ca^{2+} and SO_4^{2-} reaches the input concentration. Since no precipitation occurs, it could mean that it is possible to transport a supersaturated solution across the core. Another reason, might be that the injection rate (12 PV/d) was too high. At lower rates the solution has more time to react with the chalk and precipitation and dissolution processes are expected to be more prominent. A noticeable difference between flooding at 70 °C and 130 °C is that equilibrium is established at a slower rate at 130 °C. Both at 4.9 mM and 8.5 mM the equilibrium establishes after approximately 3.5 pore volumes, compared to 2 pore volumes at 70 °C.

Effluent pH Evaluation

Figure (5.4) show the effluent pH of the brines from the acid flooding at 130 °C versus PV injected. In figure 5.4 (a), the injected concentration was 4.9 mM H₂SO₄, while in 5.4 (b) the injected concentration was 8.5 mM.

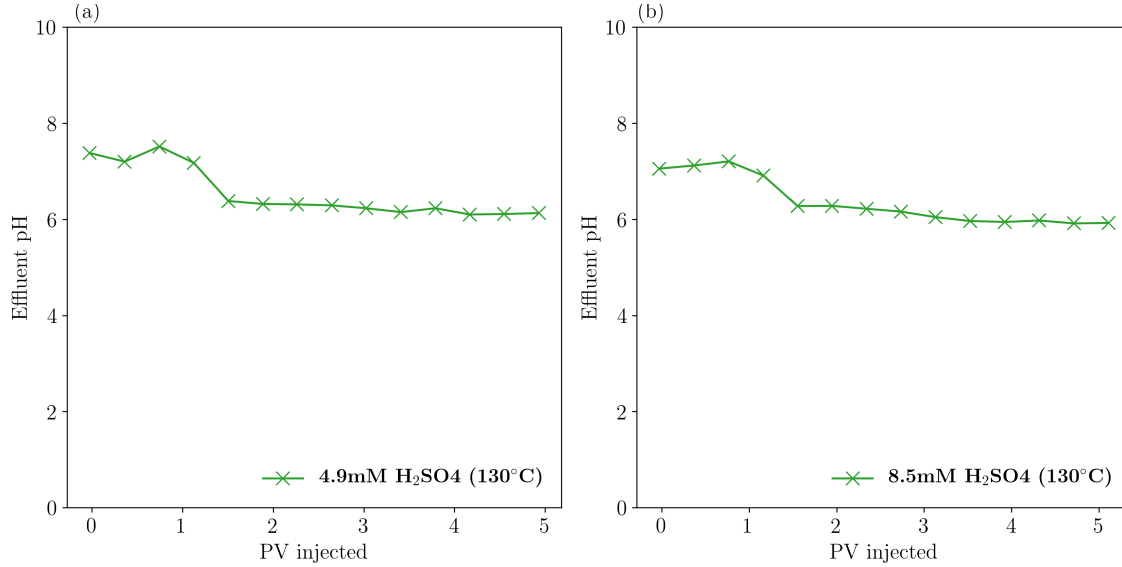


Figure 5.4: Effluent pH measured on fresh samples of the brines flooded at 130 °C. Figure (a) show the effluent from acid flooding of 4.9 mM H₂SO₄, and (b) 8.5 mM H₂SO₄.

At 130 °C, the pH of the first three effluent samples are ~ 7.5 . Thus, the initial pH is slightly lower than at 70 °C, where the three first measurements for all input concentrations were ~ 8.7 . When liquid water molecules dissociates into hydrogen and hydroxide ions, the reaction absorbs heat, shown in the equation below:



Hence, when the temperature increases, according to Le Châtelier's principle, the forward reaction is favoured and more liquid molecules will dissociate. Consequently the equilibrium constant, K_w , increases and the pH decreases correspondingly. Even though the measured pH is lower, the concentration of H⁺ and OH⁻ are still the same, so the acidity itself is not lower than at 70 °C.

The equilibrium-pH is established at around 3 pore volumes injected, which is equivalent to the chemical equilibrium of Ca²⁺ and SO₄²⁻ at 130 °C. At equilibrium the pH is averaging at 6, which is slightly lower than the equilibrium pH seen at 70 °C. This difference can also be explained to be mainly due to reaction (5.2).

5.1.3 Summary of Acid Flooding

In this section the most important observations during the acid flooding is summarised and discussed. The average ion concentration of Ca^{2+} and SO_4^{2-} in the effluent brines, along with pH for the different injected sulphuric acid solutions are given in table (5.1).

The process which adds Ca^{2+} -ions to the solution is a dissolution process of the chalk surface. When the acid comes in contact with the rock, the solid surface consisting mainly of $\text{CaCO}_3(\text{s})$ dissolves according to the following mechanistic model:



The effluent concentration of Ca^{2+} is close to or equal to the SO_4^{2-} -concentration in the effluent brines from the acid flooding, as observed in figure 5.1 (a) and (b), and in figure 5.3 (a) and (b). However, when 16.7 mM H_2SO_4 was injected at 70 °C, the ion analysis in figure 5.1 (c), shows that the Ca^{2+} -concentration is about 2.4 mM below the SO_4^{2-} -concentration. Hence, almost all effluent brines acquires an optimal composition, with just one exception. Since the Ca^{2+} -ions co-adsorb onto the SO_4^{2-} -ions, it is necessary to have equal concentrations to avoid having a limiting reactant that would prohibit the full potential of the Smart Water brine. The effluent samples which were analysed in the ion chromatograph, confirm that the Smart Water acquires a favourable composition, which is a brine of low salinity with the right proportions of Ca^{2+} and SO_4^{2-} through dissociation of H_2SO_4 and dissolution of $\text{CaCO}_3(\text{s})$. Recall from figure (1.2) that SW depleted in NaCl already has shown to be more efficient in the wettability alteration process than normal SW.

At 70 °C the brines reaches equilibrium in the ion concentration after 2 pore volumes injected. While at 130 °C the brines reaches equilibrium after 3 pore volumes. At 130 °C, the reactivity of the SO_4^{2-} is higher than it is at 70 °C, as earlier explained in section (3.5). The increase in ion activity results in more adsorption of SO_4^{2-} onto the chalk surface, hence a larger delay in the effluent concentration profile is observed.

As for the 16.7 mM H_2SO_4 -solution, the difference between SO_4^{2-} - and Ca^{2+} -concentration, may be an indication that the maximum possible Ca^{2+} -concentration in the brine has been reached. Consequently, there might be a limit as to how much of the $\text{CaCO}_3(\text{s})$ that can actually be dissolved by acid flooding. According to the Bjerrum plot (2.8), the relative concentration of the CO_3^{2-} -ion is equal to zero at a pH of 6. Considering that all the effluent brines in the acid flooding had a pH of ~ 6.1 as shown in table (5.1), it appears as if no more of the chalk surface can be dissolved. Had there been more CO_3^{2-} -ions present, they would have reacted with the H^+ -ions, and thereby raised the pH of the system. When the chalk surface dissolves, Ca^{2+} -ions in the brine effectively controls the dissolution process by the common ion effect, causing reaction (5.3) to shift toward the left due to Le Châteliers principle. This chemical principle could be the underlying reason for why the Ca^{2+} concentration in figure 5.1 (c) is not able to reach the SO_4^{2-} -concentration. The highest Ca^{2+} -concentration observed during the acid flooding, was equal to 14.7 mM, which is close to the concentration of Ca^{2+} in SW which has 13 mM. Consequently, even though the injected concentration of SO_4^{2-} -ions is higher, there might be a limit on the Ca^{2+} -concentration. This could effectively inhibit the potential of the Smart Water, since the mechanism is based on an equal proportion of the two ions.

Furthermore, no precipitation is taking place in any of the solutions that were injected into the chalk core, as all effluent concentrations reaches the injected in figures (5.1) and (5.3). In addition based on the flooding experiments, it appears to be possible to transport solutions in a supersaturated state, with 8.5 mM at 130 °C as evidence. The equilibrium pH is on the acidic side and stabilizes just above 6 for all the brines tested. This is good regarding the surface charge of the chalk, which is positive for $\text{pH} < 8$. The Smart Water mechanism rely on a positive surface charge, where SO_4^{2-} adsorb due to charge difference with the surface. It also indicates that there exists free H^+ ions in the solution, that causes an acidic environment.

Initially the effluent solution, which is the dead volume with DI-water, has a pH over 8 as seen in figure (5.2). The corresponding carbonate distribution displayed in the Bjerrum plot (2.8), show that there is mostly HCO_3^- -ions and a small concentration of CO_3^{2-} -ions at that pH. However, when the diluted acid solution front reaches the outlet of the core, the average pH is at ~ 6.1 . The subsequent carbonate distribution according to the Bjerrum plot, is equal to 0 % carbonate, CO_3^{2-} , 50 % bicarbonate, HCO_3^- , and 50 % carbonic acid H_2CO_3^* at this pH. To explain this new distribution of carbonic species, equation (2.39) from section (2.7.1) is utilized. The addition of protons in the core, shifts reaction (2.39) toward the left, and H_2CO_3^* is formed as a result. Hence, when the strong sulphuric acid is injected into the core, a buffer solution is created consisting of the weak carbonic acid and the weak bicarbonate base. As previously discussed, this reaction has a $\text{pKa} = 6.3$. According to the Henderson-Hasselbach equation (2.45), the $\text{pH} = \text{pKa}$, when the concentration of the weak acid and weak base is equal. Considering that there is an equal amount of HCO_3^- and H_2CO_3^* , the equilibrium pH during the acid flooding is therefore close to the pKa of the buffer solution.

Table 5.1: Summary of the effluent ion concentration of Ca^{2+} and SO_4^{2-} and pH from the acid flooding for the different injected diluted acid solutions. The values presented in the table, were calculated as an average of the equilibrium values.

DI-water [H_2SO_4] (mM)	Effluent Ion Conc.		Average Effluent pH (-)
	Ca^{2+} (mM)	SO_4^{2-} (mM)	
4.9	5.1	5.2	6.16
8.5	7.07	8.1	5.96
9.7	11.5	10.2	6.20
13.3	14.2	14.7	6.11
16.7	16.8	14.4	6.06

5.1.4 PHREEQC Simulation - Improvements to Smart Water

The solubility of anhydrite, $\text{CaSO}_4(\text{s})$, controls the amount of sulphuric acid which can be added to DI-water, and therefore the concentration of free Ca^{2+} and SO_4^{2-} that can take part in the wettability alteration. The solubility of $\text{CaSO}_4(\text{s})$ in pure water at 25 °C is governed by the solubility product, K_{sp} .



Hence, in pure water at room temperature, the product of $[\text{Ca}^{2+}]$ and $[\text{SO}_4^{2-}]$ in water cannot be larger than $K_{sp} = 2.4 \cdot 10^{-5}$. If higher concentrations are added to the water of these ions, reaction (5.4) will shift towards the left and solid $\text{CaSO}_4(\text{s})$ will be formed. Since the dissolution reaction of $\text{CaSO}_4(\text{s})$ releases heat (exothermic), the solubility will decrease when the temperature increases. To study how temperature and SO_4^{2-} -concentration affects solubility of $\text{CaSO}_4(\text{s})$, simulations were run in PHREEQC. In the input file in PHREEQC, $\text{CaCO}_3(\text{s})$ was put as equilibrium phase, while SO_4^{2-} was added to the solution in different concentrations. PHREEQC then calculate the amount of precipitation of $\text{CaSO}_4(\text{s})$ at thermodynamic equilibrium. Results from the simulation are shown in figure (5.5) below:

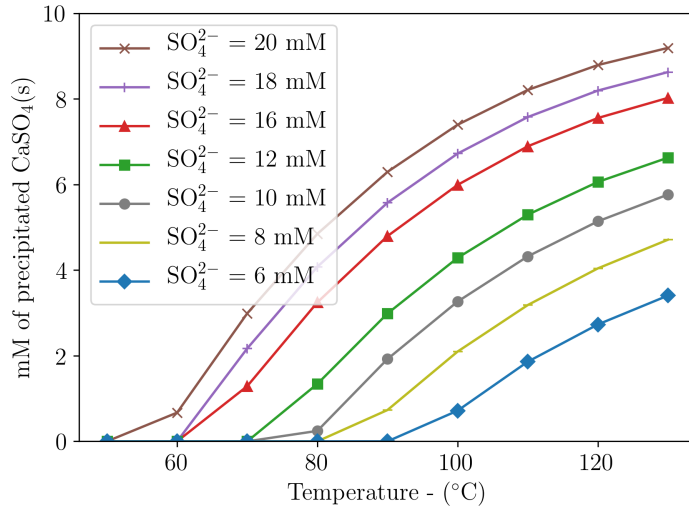
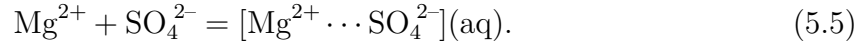


Figure 5.5: Simulation of Precipitation of Anhydrite in DI-water performed in PHREEQC with $\text{CaCO}_3(\text{s})$ as equilibrium phase.

When the temperature in figure (5.5) increases, the concentration of SO_4^{2-} -ions that yield precipitation, is correspondingly lower. At a temperature of 90°, only the solution with 6 mM of SO_4^{2-} -ions is not precipitating any $\text{CaSO}_4(\text{s})$.

However, improvements can be performed to allow for a higher concentration of SO_4^{2-} in the solution. For instance, Mg^{2+} -ions can be added to the brine, which will form complexes with SO_4^{2-} -ions accordingly:



As previously discussed in section (2.7), the formation of MgSO_4 -complexes increases the solubility of anhydrite, since less free SO_4^{2-} -ions are in the solution. Hence, when Mg^{2+} was added in solution in equal amounts as SO_4^{2-} in PHREEQC, precipitation was taking place a lot less frequently than shown in figure (5.6). Now, a concentration of 12 mM of SO_4^{2-} could potentially be used at 90°C , in contrast to 6 mM, which is a doubling in the SO_4^{2-} concentration.

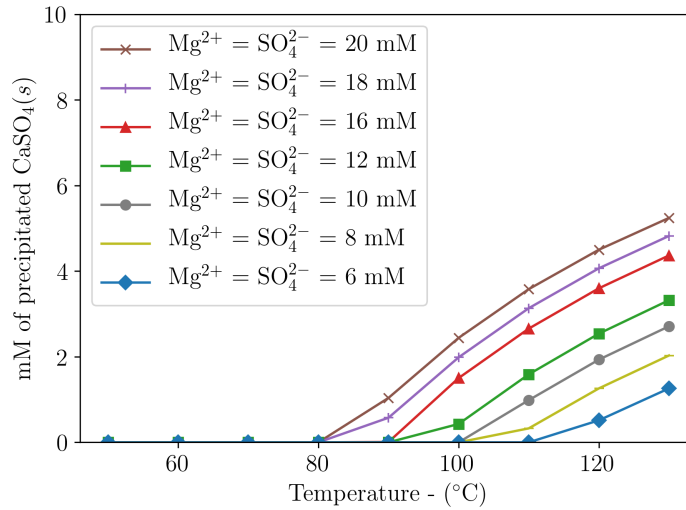


Figure 5.6: Simulation of Precipitation of Anhydrite in DI-water with $\text{CaCO}_3(\text{s})$ as equilibrium phase performed in PHREEQC. Here Mg^{2+} -ions have been added in equal concentration as SO_4^{2-} .

Consequently, an improved Smart Water could be made by adding Mg^{2+} to the brine. However, this was not investigated further in this thesis, and the focus was rather to obtain the performance of the Smart Water without any additives.

5.2 Scanning Electron Microscope Analysis

5.2.1 Chalk Characterization

Figure (5.7) shows the surface of core SK1 magnified 1000 times, which was flooded with sulphuric acid. The surface appears homogeneous, with biogenic material and pore throats (dark spots) distributed evenly.

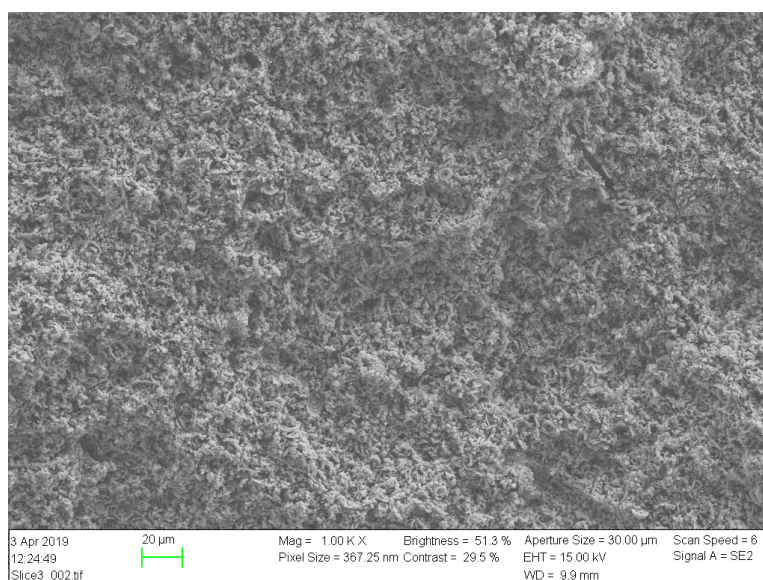


Figure 5.7: Microscopic image of the chalk surface of core SK1, magnified 1000 times.

An EDX-analysis was run on the same surface, and the results are given in table (5.2) below:

Table 5.2: EDX-analysis on a chalk piece from a Stevns Klint core which comes straight from an outcrop block.

Element	Weight %	Atomic %
Mg	0.04	0.07
Al	0.06	0.09
Si	0.42	0.60
S	0.33	0.42
Ca	99.14	98.83

The elemental composition of the rock, can give an indication of how pure the rock is. For instance, the atomic % of Ca is related to the amount of calcite the chalk consists of. Since the atomic % is 98.83, the surface in the figure above is almost pure calcite. The amount of sulfur, S, can be linked to the abundance of SO_4^{2-} -ions. The small content of S present (0.42 atomic %), is most likely a small amount of SO_4^{2-} -ions which are left in the core after acid flooding with H_2SO_4 . Recall that the initial effluent SO_4^{2-} -concentration began at 2.5 mM in figures (5.1) and (5.3). It could also be sulphur detected from anhydrite minerals ($\text{CaSO}_4(\text{s})$). The element Mg is linked to the content of MgCO_3 , however a combination of Mg, Al and Si might indicate that there is clay present. Considering the small amount of Mg and Al (0.07 % and 0.09 %), there is not much clay present in this chalk core. Figure (5.8) below, shows the chalk surface presented in figure (5.7) further zoomed in to a magnification of 10 000.

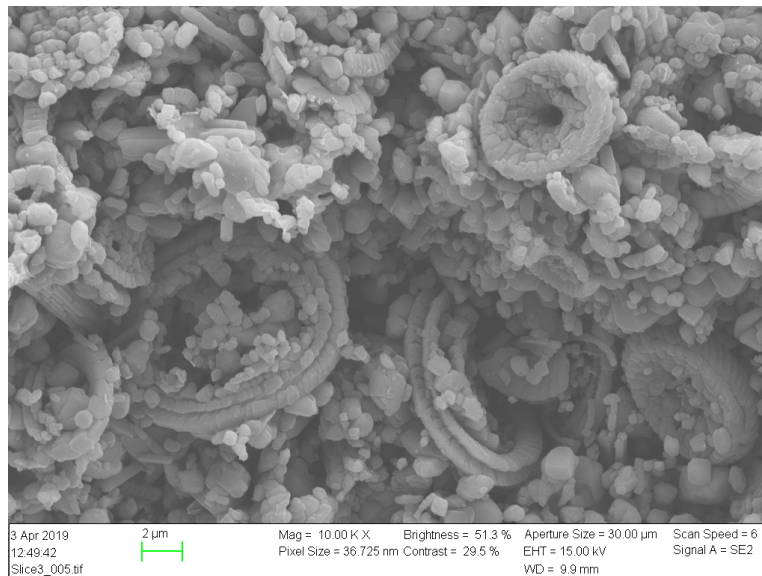


Figure 5.8: SEM-image of the chalk surface magnified 10 000 of a Stevns Klint Core. Several visible coccolith rings are seen in the picture. The dark spots are the pore throats.

Now the chalk surface looks more heterogeneous, with a mixture of small grains in combination with larger intact coccoliths. The dark spots represents the pore volume where fluids are stored in the rock. In this figure, the pore throat size ranges from $0.5\mu\text{m}$ - $3\mu\text{m}$. A lot of small pores can be observed along with some larger pores, together they yield a very porous chalk. All the cores which were used in this thesis, had porosities in the range 48-49 %. High chalk porosities are also seen in the chalk reservoirs at Valhall and Ekofisk where $\phi \sim 40 - 50\%$. Due to the small pores, the permeability in chalks is very low, and the range for the cores used in this study was between 4.65-5.14 mD.

5.2.2 Investigation of Acid-Dissolution

During the acid flooding experiment, the core was removed from the Hassler core holder to see if any dissolution effects could be seen. In figure 5.9 (a), the inlet of the chalk core is shown, while figure 5.9 (b) shows the outlet of the core.



(a) Inlet of the chalk core.

(b) Outlet of the chalk core.

Figure 5.9: Comparison of dissolution between inlet and outlet of a chalk core flooded with acid. The inlet has clear signs of dissolution compared to the outlet.

Dissolution effects at the inlet (a) can clearly be seen by the imprint from the injection device, while the outlet (b) shows no sign of dissolution. To further study the core for any dissolution effects, a slice from the inlet of the core was cut, and a slice from the outlet was cut. Afterwards, the slices were broken up in pieces such that the inner surfaces of the core were exposed. The pieces were subsequently studied at magnifications of 100, 1000, 2000, 5000, 10 000, 20 000 and 30 000 in the scanning electron microscope, to check for any apparent effects from the acid-flooding would show across the core.

A comparison of the chalk at a magnification of 10 000 at the inlet in figure (5.10) and the outlet in figure (5.11) are shown below along with the EDX-analysis for inlet in table (5.3) and outlet in table (5.4):

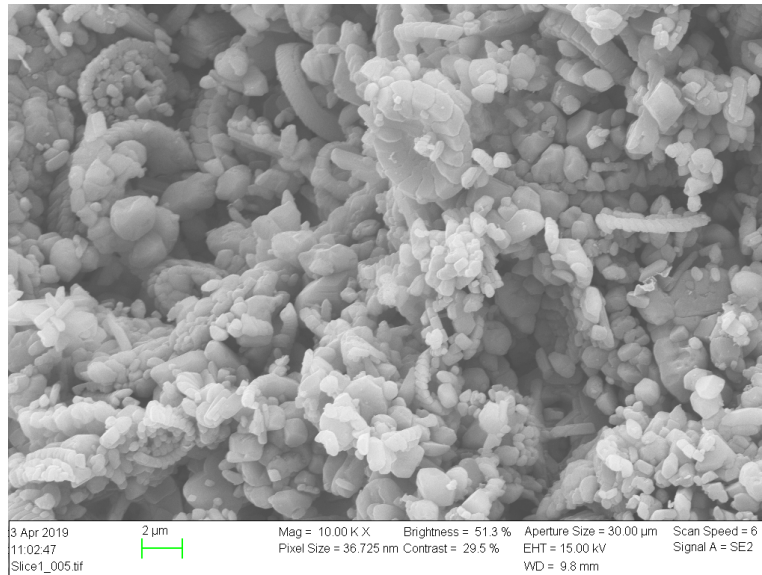


Figure 5.10: SEM-image of the inlet of chalk core flooded with acid at a magnification of 10 000.

Table 5.3: EDX-analysis on chalk piece from the inlet slice post acid-flooding.

Element	Weight %	Atomic %
Mg	0.21	0.34
Al	0.33	0.49
Si	0.62	0.88
S	0.25	0.31
Ca	98.60	97.99

The SEM-image of the inlet show no clear sign of dissolution effects after acid flooding. The grains do not look damaged or rounded by the acid, and intact coccoliths are also seen. In addition the EDX-analysis of the inlet piece, exhibits a rather pure calcite rock, with possibly a tiny amount of clay, represented by Mg, Al and Si.

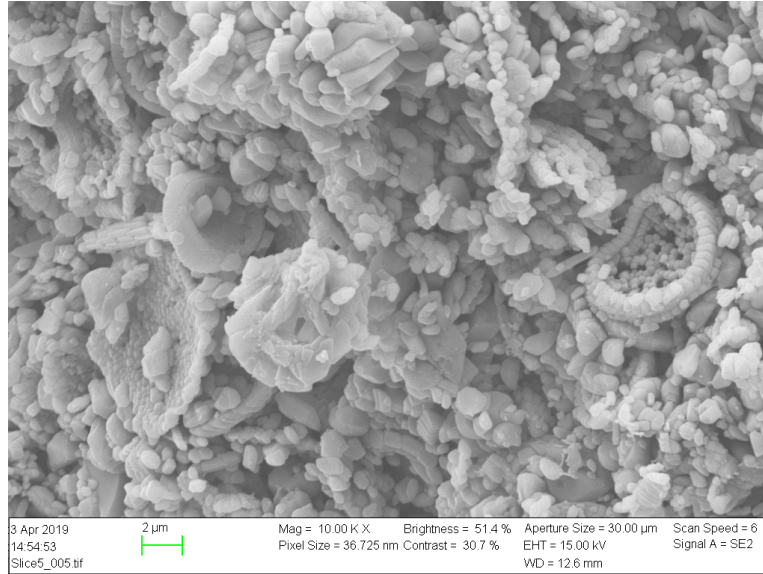


Figure 5.11: SEM-image of the outlet of chalk core flooded with acid at a magnification of 10 000. The chalk surface appears to be unaffected by the acid flooding.

Table 5.4: EDX-analysis on chalk piece from the outlet slice post acid-flooding.

Element	Weight %	Atomic %
Mg	0.00	0.00
Al	0.03	0.04
Si	0.26	0.37
S	0.24	0.30
Ca	99.48	99.30

The SEM-image of the outlet piece is similar to the inlet image. Where no difference in the grain texture is observed. The EDX-analysis show that there is possibly less clay at the outlet than at the inlet. The amount of sulphur, which is linked to the SO_4^{2-} -ion, is the same in the outlet and the inlet. Prior to the scanning electron microscope, there was an expectation that the grains possibly could be rounded due to acid-dissolution. However, no rounding of grains are shown in neither of the microscope-images. The SEM-engineer suggested that there could be a higher concentration of intact coccoliths in the outlet than in the inlet due to dissolution, however this was not observed. Consequently, it appears as if the only visible dissolution that takes place, is at the outer surface of the inlet as shown in figure (5.9 a)). This might be due to the subsequent release of Ca^{2+} into the solution after dissolution at the outer surface, which effectively negates further dissolution of the rock due to the common ion effect described in section (2.7).

5.3 Smart Water EOR in Chalk

All cores used in this thesis were saturated with $S_{wi}= 10$ % FW (VB0S) and $S_{oi}= 90$ % oil with AN = 0.5 mgKOH/g. The amount of polar oil components is therefore high, and the cores are expected to be of a less water-wet state due to adsorption of polar oil components. When the Smart Water is injected into the cores, the wetting state is expected to become more water-wet. The SO_4^{2-} -ions adsorb onto the chalk surface which allows Ca^{2+} to co-adsorb, and polar oil components are then displaced from the surface as described in section (3.4) (Zhang, 2006). As a result the core becomes more water-wet, and water will imbibe into the matrix yielding a larger oil recovery, causing the microscopic sweep efficiency to increase. The full Smart Water mechanism is explained more thoroughly in section (3.4).

In order to evaluate how good the Smart Water is at altering the wettability of the mixed-wet chalk cores, oil recovery by spontaneous and forced imbibition is performed. The Smart Water is compared relative to SW which already is known to be an excellent wettability modifier (Austad et al., 2008). To establish a baseline where absolutely no wettability alteration is taking place, a third core is imbibed with FW. As a result, three different fluids are imbibed in order to evaluate the performance of the brines. The preparation along with the ionic composition of these brines are given in section (4.1.3). In addition a completely water-wet core is also introduced, to have a reference where the capillary forces are at their strongest. The core was prepared as part of another experimental master's thesis conducted in the same laboratory (Wathne, 2019). Nonetheless, since the core comes from the same outcrop block, the oil recovery by spontaneous imbibition is presented in figure (5.12) and compared to the cores used in this study. It was decided to test the Smart Water at 90 °C, as wettability alteration is expected at this temperature based on several experimental studies (Zhang, 2006; Puntervold, 2008; Fathi, 2012). If the temperature is too low, the reactivity of the SO_4^{2-} becomes so small that no wettability alteration will take place as discussed in section (3.5). Hence, spontaneous imbibition experiments were conducted with both Smart Water and SW at 90 °C.

A parallel study was performed by Andreassen (2019) at 70 °C with the exact same fluids, to test the temperature effect mentioned above. At lower temperatures (< 90 °C) the reactivity of ions are greatly reduced due to hydration of ions, which was demonstrated in section (3.5). It is therefore expected that less wettability alteration will take place in the parallel study, and hence also less oil recovered. It was decided to share a reference core between these two studies, where FW, was used as imbibition fluid. Therefore, spontaneous and forced imbibition of the reference core, SK2, were performed at 70 °C with FW.

5.3.1 Initial Wetting of the SK Cores

The original initial wetting of the Stevns Klint cores from the outcrop block used in this experimental study, is investigated in this section. In order to preserve the initial wetting of core SKWW, it was saturated with 80 % synthetic oil (table 4.2) and 20 % DI-water. The synthetic oil does not contain any polar oil components, consequently the oil phase cannot adsorb onto the chalk surface, and the original wetting state is therefore preserved. Subsequently, oil recovery by spontaneous imbibition at 25 °C was performed to study the wetting state of SKWW. The results are shown in figure (5.12).

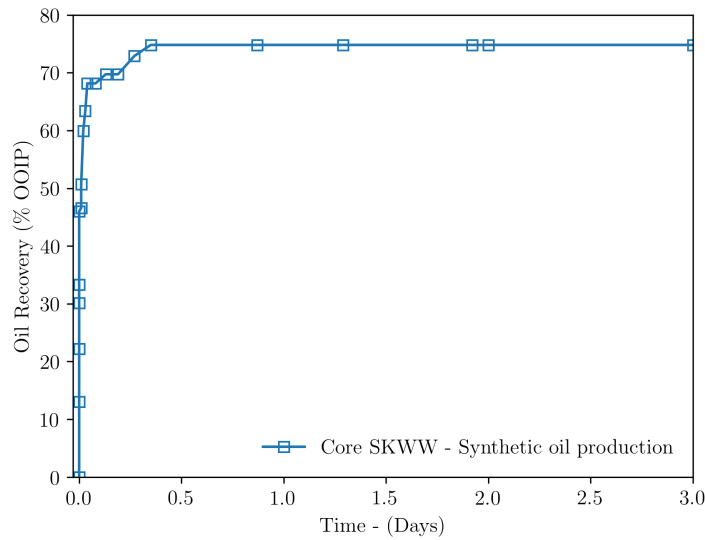


Figure 5.12: Spontaneous imbibition at 25 °C with DI for core SKWW. Core saturation $S_{oi}= 80$ % with synthetic oil and $S_{wi}= 20$ % DI-water.

It is evident from figure (5.12), that core SKWW is strongly water-wet. Recall from section (2.5.5), that the imbibition rate and ultimate oil recovery will indicate how water-wet a core is. Here, strong capillary forces are acting which is displayed in the figure by a steep oil recovery gradient, which means that the imbibition rate is fast. The oil recovery is also very high, with the ultimate oil recovery ending at 75 % OOIP. The high oil recovery, means that the core is capable of imbibing a lot of fluid due to strong capillary forces. Almost 70 % oil recovery is obtained after just 1 hour, while the recovery plateau is reached after 8 hours. Afterwards the core was subjected to forced imbibition, however no additional oil was produced. The core therefore appears to be completely water-wet according to the Amott water index equation (2.16), and hence the original wetting state of the cores used in this study are in the strongly water-wet category. Since the core is strongly water-wet, it is used as the reference core during calculation of the modified Amott water index, I_{W-SI}^* , in equation (2.21). Hence, $SI_{WWC}= 0.75$ is used as value when calculating the modified Amott water index for cores, SK2-SK6.

5.3.2 Initial Wetting State of the Restored SK Cores

In section (4.4), the restoration process of establishing the saturation of the cores (SK2-SK6) with 10 % FW and 90 % oil A with AN = 0.50 mgKOH/g was given. Through this restoration process, they are exposed to an oil with polar oil components that can adsorb onto the chalk surface and thereby alter the wettability, in contrast to the completely water-wet core SKWW. To investigate how oil A in table (4.2) affects the initially water-wet cores, spontaneous imbibition of core SK2 with FW was performed. Since FW does not contain the potential determining ion, SO_4^{2-} , it will not be able to alter the wettability of core SK2. Results from the spontaneous imbibition experiment of core SK2 with the formation brine FW at 70 °C, is given in figure (5.13). Considering, that all cores have gone through the same restoration process described in section (4.4), with equal saturation and in addition are from the same outcrop block, they are expected to have similar initial wetting as core SK2.

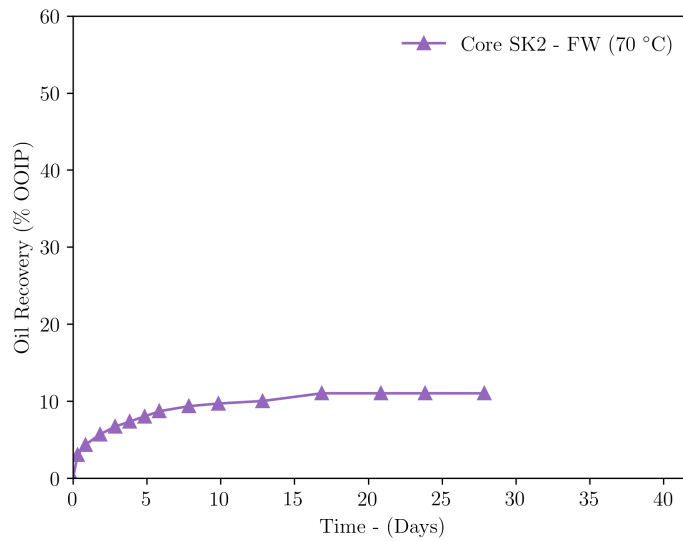


Figure 5.13: Spontaneous imbibition experiment at 70 °C, showing the oil recovery with FW as imbibition fluid versus time for core SK2. $S_{wi}=10$ % with FW, and 90 % oil with AN=0.5 mgKOH/g.

The oil recovery for FW reaches a plateau after 17 days at 10 % of OOIP, with no additional oil production. Compared to the water-wet core presented above, core SK2 has a lower imbibition rate, shown in figure (5.16) as a less steep oil recovery gradient. The ultimate oil recovery is substantially lower than SKWW, with only 10 % OOIP recovered. The combination of low recovery of oil through spontaneous imbibition of core SK2 and low imbibition rate, indicates that the core is of low water-wetness compared to the completely water-wet core in figure (5.12). The

modified Amott water index further confirms that it is of low water wetness.

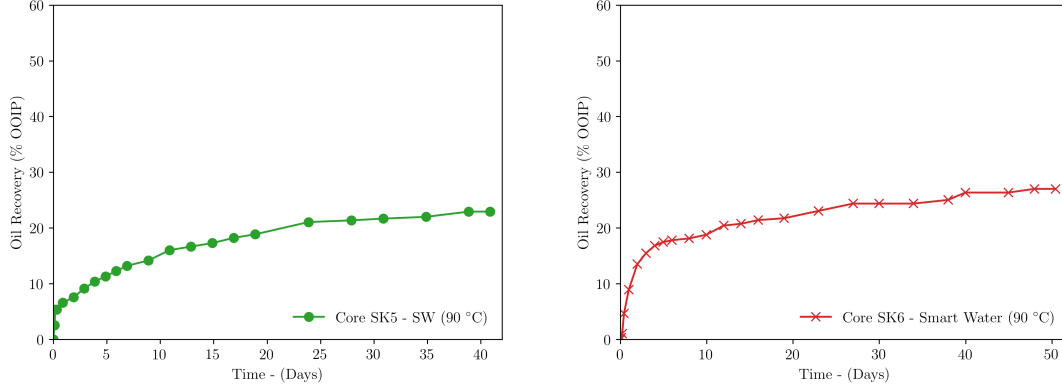
$$I_{W-SI}^* = \frac{0.10}{0.75} = 0.13. \quad (5.6)$$

Performance of FW on Spontaneous Imbibition at 90 °C

As previously mentioned, core SK2 was shared between this study and the parallel study at 70 °C. Therefore the oil recovery by spontaneous imbibition is performed at 20 °C below SK5 and SK6 at 90 °C. However, considering that the compressibility of oil is $\sim C_t=10^{-3}/^{\circ}\text{C}$, an increase in temperature of 20 °C, would only yield an extra 2 % in oil recovery. Consequently, the expected oil recovery for FW at 90 °C, would have been 12 % due to thermal expansion (Piñerez Torrijos et al., 2019).

5.3.3 Comparison of SW and Smart Water

Oil recovery by spontaneous imbibition at 90 °C is given for SW in figure 5.14 (a), and for Smart Water in figure 5.14 (b).



(a) SI of core SK5 with SW.

(b) SI of core SK6 with Smart Water.

Figure 5.14: Oil recovery by spontaneous imbibition at 90 °C. Both cores with $S_{wi}=10$ % with FW, and $S_{oi}=90$ % oil with AN=0.5 mgKOH/g.

The oil recovery with SW for core SK5 reaches a recovery plateau at approximately 23 % OOIP after 39 days, as shown in figure 5.14 (a). Consequently, the oil recovery is 12 % OOIP more than FW. The time it takes to reach the plateau is considerably longer for SW, and oil production does not cease before after 39 days of the experiment. The modified Amott water index for core SK5 is,

$$I_{W-SI}^* = \frac{0.23}{0.75} = 0.31. \quad (5.7)$$

The oil recovery with Smart Water at 90 °C is close to 27 % OOIP for core SK6 in figure 5.14 (b). It reaches a recovery plateau after 50 days, which is 10 days later than SW at the same temperature. A noticeable difference between SW in figure and Smart Water, is that the initial imbibition rate is higher for Smart Water. The ultimate oil recovery of the Smart Water is slightly higher than SW, with 4 % additional oil recovery. The modified Amott water index for core SK6 is,

$$I_{W-SI}^* = \frac{0.27}{0.75} = 0.36. \quad (5.8)$$

Hence, based on a faster imbibition rate, higher oil recovery and the modified Amott water index, core SK6 imbibed with the Smart Water is more water-wet than the core imbibed with SW. An explanation to the experimental results are given below.

5.3.4 Spontaneous Imbibition - Discussion

The results from the spontaneous imbibition experiments are summarized in figure (5.15). While showing the performance of the SW and Smart Water in terms of wettability alteration, the figure also displays the change in behaviour of the SK cores prior to and after the core restoration process in section (4.4). Where SKWW represents the behaviour prior to core restoration, while cores SK2, SK5 and SK6 represents the behaviour after core restoration.

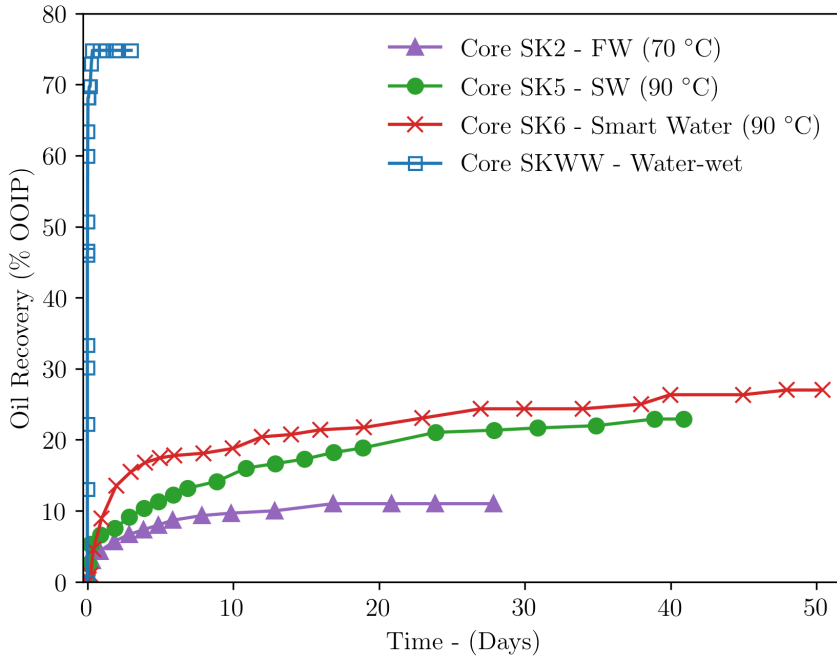


Figure 5.15: Comparison of SW, FW and Smart Water on spontaneous imbibition performance. In addition the oil recovery for the completely water-wet core (SKWW) is shown. Imbibition of SW and Smart Water for core SK5 and SK6 respectively, were performed at 90 °C, while FW for core SK2 was imbibed at 70 °C.

The original wetting state of the SK cores are strongly water-wet as shown by the fast imbibition rate and high oil recovery of core SKWW. However, when the cores are exposed to oil A containing polar oil components, the behaviour of the chalk cores changes radically, which is captured by core SK2, in terms of a lower imbibition rate and lower oil recovery. Nevertheless, it is worth noting that the interfacial tension of the synthetic oil is $\sigma = 41$ mN/m in equilibrium with DI-water, which is higher than oil A in equilibrium with FW, SW and Smart Water as seen in table (4.3). The modified Amott wettability index for core SK2 is $I_{W-SI}^* = 0.13$, and the change in wettability from core SKWW to core SK2 is therefore substantial according to the modified Amott water index. Hence, it shows how effective the polar oil components in oil A are able to alter the wettability of the cores.

Core SK2 imbibed with FW has the lowest recovery with 10 %, and is the baseline fluid where no wettability alteration is taking place. Capillary forces on the core restored with crude oil A are therefore weak and only some water imbibes into the rock, yielding a low recovery. A small FW imbibition confirms the core is slightly water-wet.

Higher recoveries are seen with SW and Smart Water with oil recoveries of 23 % and 27 %, respectively. Both SW and Smart Water have the necessary potential determining ions Ca^{2+} and SO_4^{2-} , and can therefore alter the wettability towards a more water-wet state. This is also confirmed by calculating the modified Amott water index for SW and Smart Water. For SW and Smart Water the $I_{W-SI}^* = 0.31$ and 0.36 , respectively. Hence, they have clearly increased the water wetness, compared to FW with $I_{W-SI}^* = 0.13$. When the water-wetness increases, the wetting angle, θ , decreases due to water spreading at the rock surface. As a result, the capillary pressure, P_c given in equation (2.13) increases. Recall from figure (2.5), that a positive P_c is required for water to spontaneously imbibe, indicated by the number 2, in the same figure. Consequently, the oil recovery is between 13 % - 17 % higher for SW and Smart Water than for FW due to stronger capillary forces induced by an increase in the water wetness.

Oil recovery with Smart Water is slightly higher than the SW recovery with 4 % additional production. Smart Water contains 13 mM of SO_4^{2-} and Ca^{2+} , which is half the SO_4^{2-} -concentration in SW. Hence, it performs better than SW, while still having a lower amount of SO_4^{2-} . This could be due to low salinity as discussed in section (3.6). Smart Water has total dissolved salts (TDS) equal to 1.770 g/L, compared to SW which has a TDS of 33.390 g/L, also given in table (4.4). In addition, the Smart Water does not contain any monovalent ions, such as Na^+ and Cl^- , which are present in SW. These monovalent ions are situated in the double layer and can effectively restrict the access for Ca^{2+} and Mg^{2+} toward the positively charged chalk surface. As a result, less carboxylic acids are released from the surface, and therefore less wettability alteration takes place. Recall from section (3.6), where research by Puntervold et al. (2015) showed that about 90 % of the salt in SW had to be removed in order to have a significant effect on oil recovery by spontaneous imbibition. Considering, that the Smart Water has zero salt added, there appears to be a salinity effect which is making it slightly more efficient at altering the wettability of the chalk than SW. Summary of the key numbers mentioned in this section and from the figures are given in the table below.

Table 5.5: Oil recovery by spontaneous imbibition comparison of FW, SW and Smart Water in addition to the completely water-wet core SKWW.

Core nr.:	Imbibition Fluid	TDS (g/L)	$\text{Ca}^{2+}/\text{SO}_4^{2-}$ (mM)	OOIP %	I_{W-SI}^*
Core SK2	FW	62.83	29.0/0.0	10.0	0.13
Core SK5	SW	33.39	13.0/24.0	22.9	0.31
Core SK6	Smart Water	1.77	13.0/13.0	27.0	0.36
Core SKWW	DI	0.00	0.0/0.0	74.8	1.00

After oil recovery by spontaneous imbibition of FW had ended at 10 % OOIP, the core SK2 was put into a Hassler core holder at 70 °C, and oil recovery was continued with forced imbibition of FW at an injection rate of 1 PV/d. Oil recovery for core SK2 is shown in figure (5.16).

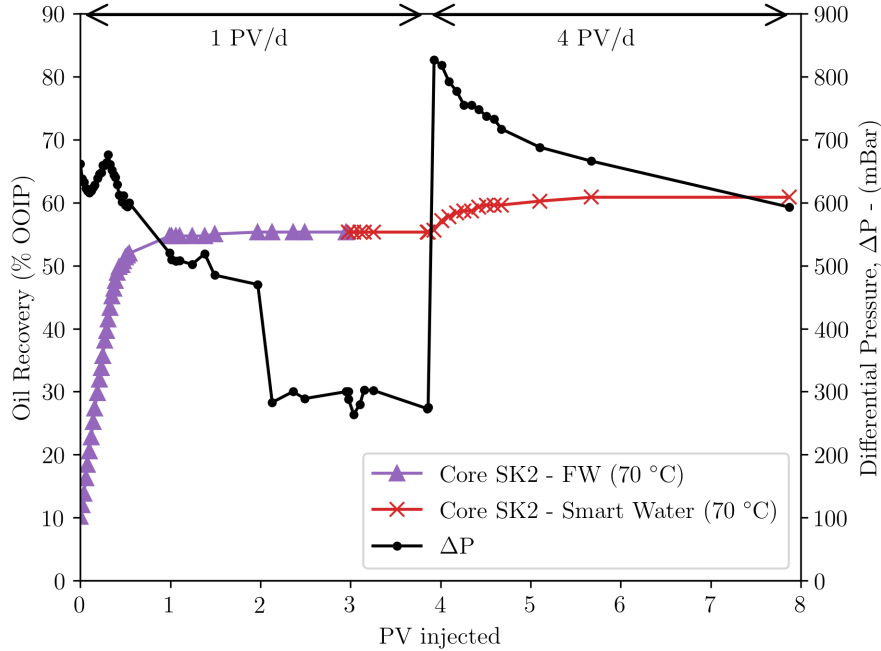


Figure 5.16: Oil recovery by forced imbibition of FW and Smart Water at 70 °C for core SK2. The oil recovery begins at 10 % of the OOIP, which is the recovered oil by SI.

The oil recovery reached a plateau after 2 PV injected, and was then at 55 % OOIP, as seen in figure (5.16). After 3 pore volumes of FW had been injected, the fluid was changed to Smart Water, however no additional oil was produced. Subsequently, the rate was increased to 4 PV/d. The increase in viscous forces gave an additional 6 % of oil recovered, yielding an ultimate oil recovery of 61 % of OOIP. The sudden pressure drop at 2 pore volumes injected, was due to a mistake during the experiment which led to pressure loss, and it is expected that it otherwise would slowly decline as observed in figures (5.17) and (5.18). Since oil had been recovered with both SI and FI, the Amott water index, I_W introduced in section (2.5.2), was used to assess the wettability of the core SK2. Recalling equation (2.17), the Amott water, I_W , becomes:

$$I_W = \frac{0.10}{0.10 + 0.45} = 0.18. \quad (5.9)$$

Considering that $I_W=1$ corresponds to a completely water-wet system, core SK2 can be characterized as being of rather low water-wetness. The low water-wetness can be linked to the discussion presented in section (5.3.4), where it was concluded that FW does not have the ability of altering the wettability of the core, due to lack of SO_4^{2-} -ions in the brine.

When production of oil had ended with spontaneous imbibition of SW at 90 °C for core SK5, it was further subjected to forced imbibition at the same temperature. Results are presented in figure (5.17).

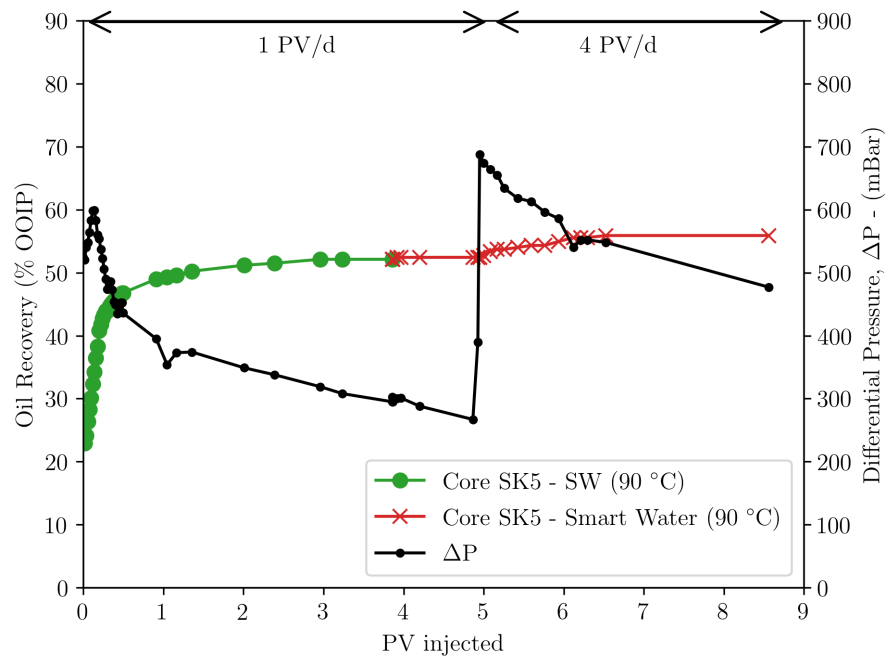


Figure 5.17: Oil recovery by forced imbibition of SW and Smart Water at 90 °C of core SK5.

The oil recovery reaches a production plateau at 3 pore volumes injected, at 52 % OOIP. At the oil recovery plateau the brine was switched from SW to Smart Water at 4 pore volumes injected. A slight pressure increase was observed followed by an increase in oil production of 0.31 %. Afterwards, the rate was set to 4 PV/d, and an additional 3.5 % of OOIP was produced. The Amott water index is calculated below:

$$I_W = \frac{0.23}{0.23 + 0.29} = 0.44. \quad (5.10)$$

The I_W is therefore twice as high for SK5 imbided with SW, compared to SK2 imbided with FW. Core SK5 therefore appear to be more water-wet than SK2 imbided with FW, thus confirming SW's ability of increasing the water-wetness.

Spontaneous imbibition of the Smart Water ended at an oil recovery of 27 %. Oil recovery was subsequently continued by forced imbibition, which reached a plateau after 3 PV injected at 55 % OOIP as shown in figure (5.18). Thus, by applying a pressure gradient across the core, the additional recovery increased by 28 % OOIP. The injection rate was further increased to 4 PV/d after 4 PV injected, and the oil recovery increased by 3 % OOIP.

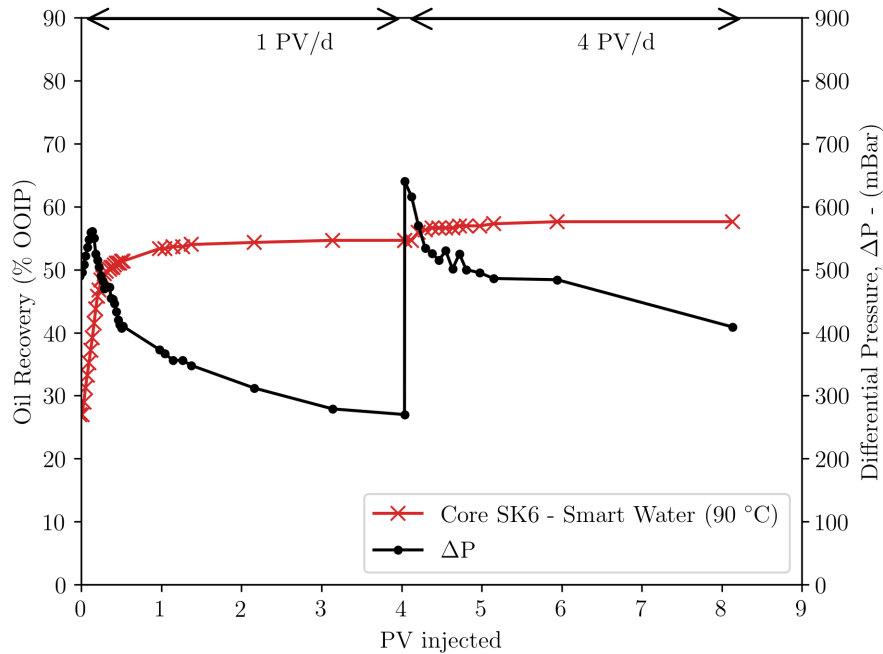


Figure 5.18: Oil recovery by forced imbibition of Smart Water at 90 °C for core SK6.

$$I_W = \frac{0.27}{0.27 + 0.28} = 0.49. \quad (5.11)$$

The I_W for core SK6 is slightly higher than it is for SK5. Hence, the Amott water indexes indicates that core SK6 imbibed with Smart Water has become slightly more water-wet than SK5 which is exposed to SW.

5.3.5 Forced Imbibition - Discussion

The results from the forced imbibition experiments are summarized in table (5.6).

Table 5.6: Results from oil recovery by forced imbibition experiments with SW, FW and Smart Water. The % OOIP from spontaneous imbibition (SI) is also shown along with ultimate oil recoveries from the two injection rates that were used.

Core	Imbibition Fluid	% OOIP (After SI)	% OOIP (1 PV/d)	% OOIP (4 PV/d)	I_w
SK2	FW	10	55	61	0.18
SK5	SW	23	52	56	0.44
SK6	Smart Water	27	55	58	0.49

The performance of the fluids in terms of wettability alteration, indicated by the Amott water wettability index, can be ranked from best to poorest as follows: Smart Water > SW > FW. Smart Water is therefore more efficient in increasing the water wetness than SW at 90 °C. The ultimate oil recovery at 1 PV/d is 55 % for Smart Water and 52 % for SW. Recall from section (3.1), that carbonate reservoirs generally have a low oil recovery factor ~ 30 % (Zhang and Austad, 2005). In addition, carbonate reservoirs hold almost 60 % of the world's oil (Montaron, 2008). Consequently, it can be of great economic benefit to inject Smart Water, even though the recovery increases by only 3 % OOIP compared to SW. Although it is more expensive to inject diluted sulphuric acid solutions than SW, the profit gained from the improved oil recovery could be enough to defend the cost linked to sulphuric acid and reversed osmosis membranes.

The oil recovery by forced imbibition is very efficient, and a piston like displacement is observed in all cores, as evident from the steep slope in the beginning of the oil recovery in the figures shown above. SW and the Smart Water reaches a recovery plateau after 3 PV injected, while FW reaches the plateau after just 2 PV injected. The relative fast oil production observed with FW, is closely related to the saturation distribution after spontaneous imbibition. The core imbibed with FW, began the forced imbibition after 10 % of oil had been recovered, which is between 12-16 % OOIP less than for SW and Smart Water. Consequently, the oil phase is more connected when the forced imbibition begins for FW, in contrast to SW and Smart Water, which have a lower oil saturation which could cause the oil phase to become discontinuous, and hence more difficult to produce.

During the forced imbibition experiments, the viscous forces are the dominating forces. However, in the beginning of the viscous floods in figure (5.16), (5.17) and (5.18), the differential pressure, ΔP , between 0 to 0.6 PV's, builds up slowly, instead of reaching a peak straight away as observed when the rate is switched to 4 PV/d.

The slow build-up in the ΔP , is an indication of the capillary forces working. When water enter the core, it imbibes into the narrow pores which mitigates a rapid pressure build-up. Spontaneous imbibition is therefore taking place when the injection rate is low 1 PV/d, and the oil recovery is a combined result of capillary and viscous forces. When the rate is increased to 4 PV/d, the pressure build-up is instant, and no dampening effect of the ΔP is observed. Recall equation (2.4), which expresses the pressure drop a fluid experience due to viscous forces. When the injection rate is increased, the ΔP also increases since it is proportional to velocity. Consequently, the higher injection rate of 4 PV/d yield stronger viscous forces that overrule the capillary forces. Therefore no dampening effect on the pressure build-up is observed, and the pressure rapidly increases from 270 mBar to 820 mBar.

Since ΔP is proportional to the rate q in Darcy's law (2.5), the observed pressure should increase with a factor of 4 when the rate was changed from 1 PV/d to 4 PV/d. This was however not seen in any of the flooding experiments. For the viscous flood of FW the pressure increases with a factor of 3, for SW a factor of 2.6 and for Smart Water with a factor of 2.4, hence the pressure response cannot be explained by Darcy's law. Considering that Darcy's law assumes single phase fluid flow, it is not valid in the flooding experiments, since there are two phases in the core, with an oil phase and the water phase present.

5.4 Temperature Effect on Wettability Alteration

5.4.1 Temperature Effect - Spontaneous Imbibition

Temperature has a large effect on wettability alteration, since it governs the activity of the potential determining ions. To investigate the temperature effect, spontaneous imbibition with SW was compared at 70 °C and 90 °C in figure 5.19 (a), and Smart Water was compared at 70 °C and 90 °C as shown in figure 5.19 (b).

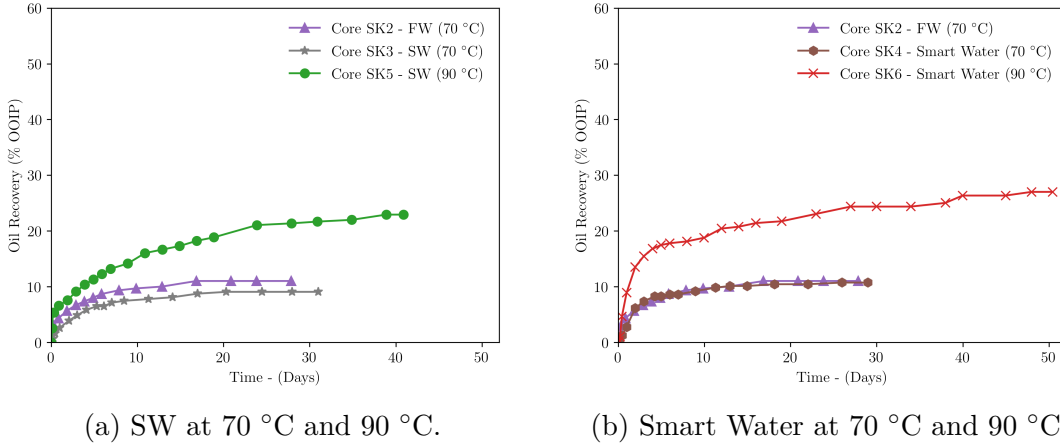


Figure 5.19: Comparison of SW and Smart Water by spontaneous imbibition at 70 °C and 90 °C. All cores with $S_{wi}=10$ % with FW, and $S_{oi}=90$ % oil with AN=0.5 mgKOH/g.

The average oil recovery for SW at 70 °C is 9 % OOIP with $I_{W-SI}^*=0.12$, while at 90 °C it is about 23 % OOIP and a $I_{W-SI}^*=0.31$. Hence, by increasing the temperature with 20 °C, there is a significant increase in oil recovery 15 % OOIP. At 70 °C, the oil recovery with Smart Water reaches a plateau at 11 % OOIP with $I_{W-SI}^*=0.15$ and is following the trend of FW, which is the baseline for no wettability alteration. When the temperature is at 90 °C, the recovery is 27 % OOIP and $I_{W-SI}^*=0.36$. Hence, the Smart Water at 70 °C, is not able to induce any change in wettability based on the low oil recovery and the modified Amott water index. The reason for the increase in oil recovery with temperature, is that the SO_4^{2-} , Ca^{2+} and Mg^{2+} -ions are strongly hydrated at lower temperatures, which were previously discussed in section (3.5) (Strand et al., 2008). The low reactivity of the ions are therefore negating any interaction with the chalk surface, and little or no carboxylic acids are therefore released from the surface. At higher temperatures, the ions begin to dehydrate and become more reactive. This temperature effect is closely related to the fact that all hydration reactions are exothermic (Burton, 1988). Recall equation (3.3) from section (3.5), where an increase in temperature shifted the reaction towards left, causing dehydration of the Mg^{2+} -ion. The increased reactivity causes more SO_4^{2-} -ions to adsorb onto the chalk surface. This further allows Ca^{2+} -ions to co-adsorb due

to less electrostatic repulsion (Austad et al., 2009). A higher number of carboxylic acids are therefore released from the surface, and the wettability is altered to a more water-wet state. The capillary forces are stronger at 90 °C than at 70 °C as a result, allowing more water to spontaneously imbibe into the smaller pores of the chalk.

Table 5.7: Summary of oil recoveries by spontaneous imbibition conducted at temperatures of 70 °C and 90 °C for SW and Smart Water.

Core	Fluid	Temp. (°C)	% OOIP	I_{W-SI}^*
SK3	SW	70	9	0.12
SK4	Smart Water	70	11	0.15
SK5	SW	90	23	0.31
SK6	Smart Water	90	27	0.36

5.4.2 Temperature Effect - Forced Imbibition

In section (5.4), the temperature had a large impact on the oil recovery by spontaneous imbibition. However, it is not reasonable to look for temperature effects during the forced imbibition experiments, since the cores will not have the same saturation distribution after spontaneous imbibition. For instance, core SK6 imbibed with Smart Water has produced 27 % OOIP by SI, while SK4 imbibed with the same fluid has produced only 11 % OOIP. Consequently, it would be wrong to compare these, since the oil phase in core SK4 will have a larger relative permeability than core SK6 due to a higher oil saturation. The same case is also for core SK3 and SK5 which were imbibed with SW at 70 °C and 90 °C, respectively. Therefore, results from forced imbibition performed in the parallel study at 70 °C are not presented.

6 | Conclusions and Future Work

6.1 Conclusions

- Acid flooding experiments on a Stevns Klint core were successfully performed at 70 °C and 130 °C. The effluent brines analysed by the ion chromatograph, confirms that the produced brines in the core obtain an equal proportion of SO_4^{2-} -ions and Ca^{2+} -ions, which is in line with the bulk solution test and equation (3.6). One exception was observed however when the injected acid concentration was 16.7 mM. The Ca^{2+} -concentration was then significantly lower than the SO_4^{2-} -concentration.
- The average pH of the effluent brines was ~ 6.1 . According to the Bjerrum plot, CO_3^{2-} -ions are not present at this pH. Free Ca^{2+} -ions in the brine are therefore effectively controlling the amount of $\text{CaCO}_3(\text{s})$ that can be dissolved by the common ion effect. Recall that the effluent brines from acid injection of 13.3 mM and 16.7 mM of H_2SO_4 had the same concentration of Ca^{2+} . Hence, there are indications that the supply of Ca^{2+} from dissolution is the limiting factor for acidic $\text{CaCO}_3(\text{s})$ dissolution.
- The wettability alteration efficiency of SW and the Smart Water was evaluated at 90 °C by spontaneous imbibition experiments. The initial imbibition rate was faster for Smart Water than for SW. In addition was the ultimate oil recovery 4 % OOIP higher for Smart Water. The modified Amott water index for core SK5 imbibed with SW, was equal to $I_{W-SI}^* = 0.31$, while for core SK6 imbibed with Smart Water, $I_{W-SI}^* = 0.36$. The imbibition rate, ultimate recovery of the spontaneous imbibition experiments at 90 °C and the modified Amott water index, indicates that Smart Water is more efficient at increasing the water wetness of SK chalk outcrop cores than SW.
- The modified Amott water index for core SK2, imbibed with FW at 70 °C, was $I_{W-SI}^* = 0.13$. Hence, both SW and Smart Water have increased the water wetness significantly compared to FW.
- The temperature had a significant effect on oil recovery by spontaneous imbibition. At 70 °C, SW and the Smart Water produced between 9 % and 11 % of OOIP, while at 90 °C, the production was 23 % and 27 % of OOIP, respectively. At higher temperatures, the reactivity of the ions increases, and more SO_4^{2-} -ions adsorb onto the chalk surface with subsequent co-adsorption of Ca^{2+} -ions.

- Oil recovery by forced imbibition was very efficient with steep oil recovery gradients associated with piston-like displacement for all imbibed fluids. The oil recovery plateau was reached after 2-3 PV injected. By applying a pressure gradient across the core, 29 % additional oil was recovered for SW, while it gave 28 % additional production for the Smart Water at an injection rate of 1 PV/d. Hence, no difference in performance was observed between SW and Smart Water during the forced imbibition, only through spontaneous imbibition.
- Modelling in PHREEQC show that Mg^{2+} -ions added to the brine allows for a higher concentration of SO_4^{2-} in the injected brine. The Mg^{2+} -ions form complexes with SO_4^{2-} -ions, which causes the solubility of $\text{CaSO}_4(\text{s})$ to increase.

6.2 Future Work

Based on the results from the experimental work performed in this thesis, some suggestions are given here that is worth investigating further.

- Repeat the acid flooding conducted in this experimental work, to further confirm that the production method works. In addition, a special focus should be held at injection concentrations of 16.7 mM at 70 °C and 8.5 mM at 130 °C H_2SO_4 . By running the experiment at 16.7 mM again, one can confirm/disapprove if the maximum Ca^{2+} -concentration was obtained during the 16.7 mM injection of H_2SO_4 or not. The 8.5 mM H_2SO_4 -injection should be repeated at a lower rate of 1 PV/d, instead of the faster rate, 12 PV/d. In the bulk solution test, the 8.5 mM acid solution precipitated $\text{CaSO}_4(\text{s})$. By lowering the injection rate, the solution has more time to react with the chalk surface, and precipitation of $\text{CaSO}_4(\text{s})$ is more likely to take place.
- Conduct an additional acid flooding, but add Mg^{2+} -ions to the fresh water. PHREEQC modelling showed that addition of Mg^{2+} -ions to the fresh water allow for a higher injected SO_4^{2-} -concentration. Recall that SW depleted in NaCl spiked with 4 times SO_4^{2-} is the most efficient SW. Thus it is of great interest to investigate this matter further.
- Perform acid flooding with higher acid concentrations, and test more temperatures, such as 80, 90 and 100 °C. Precipitation limits of $\text{CaSO}_4(\text{s})$ can then be more thoroughly examined. In addition it would be interesting to see whether or not the Ca^{2+} -concentration will be able to follow the SO_4^{2-} -concentration as the injected concentration of sulphuric acid increases.
- Compare the effluent brine from the acid flooding with the synthetically made Smart Water by measuring the oil recovery through spontaneous imbibition at 90 °C. Then the actual Smart Water produced by acid flooding can be tested, instead of using an idealised Smart Water made by gypsum in DI-water.

- Perform acid flooding experiments with actual reservoir cores from Ekofisk and Valhall. The Stevns Klint outcrop cores are merely an approximation of the real reservoir cores. Hence, before the production technology is recommended for use in chalk reservoirs, reproducible results should be obtained first.
- Conduct experiments on cores that are slightly more water-wet to evaluate if the wettability alteration process with Smart Water is wetting dependent.

Bibliography

- [1] Alibaba. *H₂SO₄ 98 % industrial sulphuric acid*. May 2019. URL: https://www.alibaba.com/product-detail/high-quality-industrial-grade-h2so4-98_60469405273.html.
- [2] Anderson, William. “Wettability Literature Survey- Part 2: Wettability Measurement”. In: *Journal of Petroleum Technology* 38.11 (Nov. 1986), pp. 1246–1262. ISSN: 0149-2136. URL: <https://doi.org/10.2118/13933-PA>.
- [3] Anderson, William G. “Wettability Literature Survey- Part 1: Rock/Oil/Brine Interactions and the Effects of Core Handling on Wettability”. In: *Journal of Petroleum Technology* 38.10 (Oct. 1986), pp. 1125–1144. ISSN: 0149-2136. URL: <https://doi.org/10.2118/13932-PA>.
- [4] Andreassen, Erlend. “Production of Smart Water by Acid Flooding in Chalk: Temperature Limitation at Slightly Water-Wet Conditions”. MA thesis. University of Stavanger, 2019.
- [5] Appelo, Tony and Postma, D. “Geochemistry, Ground Water and Pollution”. In: *Geochemistry, Groundwater and Pollution, Second Edition* (Jan. 2005), p. 536. DOI: <https://doi.org/10.1002/esp.3290200510>.
- [6] Austad, T. and Milner, J. *Spontaneous Imbibition of Water Into Low Permeable Chalk at Different Wettabilities Using Surfactants*. Houston, Texas, Jan. 1997. URL: <https://doi.org/10.2118/37236-MS>.
- [7] Austad, Tor, Strand, Skule, Madland, Merete V., Puntervold, Tina, and Korsnes, Reidar I. “Seawater in Chalk: An EOR and Compaction Fluid”. In: *SPE Reservoir Evaluation & Engineering* 11.04 (Aug. 2008), pp. 648–654. ISSN: 1094-6470. URL: <https://doi.org/10.2118/118431-PA>.
- [8] Austad, Tor, Strand, Skule, and Puntervold, Tina. “Fundamental Mechanisms for Smart Water in Sandstones and Carbonate”. In: Force Seminar, NPD., Feb. 2017.
- [9] Bissell, Harold J. and Chilingar, George V. “Chapter 4 Classification of Sedimentary Carbonate Rocks”. In: *Carbonate Rocks Origin, Occurrence and Classification*. Ed. by George V. Chilingar, Harold J. Bissell, and Rhodes W. Fairbridge. Vol. 9. Developments in Sedimentology. Elsevier, 1967, pp. 87–168. URL: [https://doi.org/10.1016/S0070-4571\(08\)71112-9](https://doi.org/10.1016/S0070-4571(08)71112-9).

- [10] Bjørlykke, Knut. *Petroleum Geoscience : From Sedimentary Environments to Rock Physics*. eng. 2nd ed. Berlin, Heidelberg: Springer, 2015. ISBN: 3-642-34132-2. URL: <https://doi.org/10.1007/978-3-642-02332-3>.
- [11] BP. *BP starts-up Clair Ridge production*. English. May 2019. URL: <https://www.bp.com/en/global/corporate/news-and-insights/press-releases/bp-starts-up-clair-ridge-production.html>.
- [12] Brown, Robert J. S. and Fatt, Irving. *Measurements Of Fractional Wettability Of Oil Fields' Rocks By The Nuclear Magnetic Relaxation Method*. Los Angeles, California, Jan. 1956. URL: <https://doi.org/10.2118/743-G>.
- [13] Brown, Theodore, LeMay, H. Eugene, Bursten, Bruce E., Murphy, Catherine, Woodward, Patrick, and Stoltzfuz, Matthew E. *Chemistry: The Central Science, 8th Edition*. Vol. 77. 9. Pearson, Sept. 2000. URL: <https://doi.org/10.1021/ed077p1126.2>.
- [14] Buckley, J. S., Takamura, K., and Morrow, N. R. "Influence of Electrical Surface Charges on the Wetting Properties of Crude Oils". In: *SPE Reservoir Engineering* 4.03 (Aug. 1989), pp. 332–340. ISSN: 0885-9248. URL: <https://doi.org/10.2118/16964-PA>.
- [15] Burton, George. *Chemical Ideas*. Vol. 4. Heinemann Educational Publishers, 1988.
- [16] Chang, Raymond and Goldsby, Ken. *General Chemistry*. 7th ed. McGraw-Hill, 2014. ISBN: 978-1-259-06042-7.
- [17] Cheryan, Munir. *Ultrafiltration and Microfiltration Handbook*. CRC Press, Jan. 1998. DOI: 10.1201/9781482278743.
- [18] Chilingar, George V. and Yen, T. F. "Some Notes on Wettability and Relative Permeabilities of Carbonate Reservoir Rocks, II". In: *Energy Sources* 7.1 (1983), pp. 67–75. URL: <https://doi.org/10.1080/00908318308908076>.
- [19] Craig, Forrest F. *The reservoir engineering aspects of waterflooding*. eng. Vol. 3. Henry L. Doherty series. New York: Henry L. Doherty Memorial Fund of AIME, 1971. ISBN: 0895202026.
- [20] Cuiec, L. *Rock/Crude-Oil Interactions and Wettability: An Attempt To Understand Their Interrelation*. Houston, Texas, Jan. 1984. URL: <https://doi.org/10.2118/13211-MS>.
- [21] Dake, L.P. *Fundamentals of Reservoir Engineering*. Developments in petroleum science. Elsevier Scientific Publishing Company, 1978. ISBN: 9780444418302. URL: <https://www.elsevier.com/books/fundamentals-of-reservoir-engineering/dake/978-0-444-41830-2>.
- [22] Denekas, M. O., Mattax, C. C., and Davis, G. T. *Effects of Crude Oil Components on Rock Wettability*. Jan. 1959. DOI: SPE-1276-G.

- [23] Derjaguin, B. V., Churaev, N. V., and Muller, V. M. “The Derjaguin—Landau—Verwey—Overbeek (DLVO) Theory of Stability of Lyophobic Colloids”. In: *Surface Forces*. Boston, MA: Springer US, 1987, pp. 293–310. ISBN: 978-1-4757-6639-4. URL: https://doi.org/10.1007/978-1-4757-6639-4_8.
- [24] Donaldson, Erle C. and Alam, Waqi. “CHAPTER 2 - Surface Forces”. In: *Wettability*. Ed. by Erle C. Donaldson and Waqi Alam. Gulf Publishing Company, 2008, pp. 57–119. ISBN: 978-1-933762-29-6. URL: <https://doi.org/10.1016/B978-1-933762-29-6.50008-9>.
- [25] Donaldson, Erle C., Thomas, Rex D., and Lorenz, Philip B. “Wettability Determination and Its Effect on Recovery Efficiency”. In: *Society of Petroleum Engineers Journal* 9.01 (Mar. 1969), pp. 13–20. ISSN: 0197-7520. URL: <https://doi.org/10.2118/2338-PA>.
- [26] Dubey, S. T. and Doe, P. H. “Base Number and Wetting Properties of Crude Oils”. In: *SPE Reservoir Engineering* 8.03 (Aug. 1993), pp. 195–200. ISSN: 0885-9248. URL: <https://doi.org/10.2118/22598-PA>.
- [27] Fairbridge, Rhodes W., Chilingar, George V., and Bissell, Harold J. “Chapter 1 Introduction”. In: *Carbonate Rocks Origin, Occurrence and Classification*. Ed. by George V. Chilingar, Harold J. Bissell, and Rhodes W. Fairbridge. Vol. 9. Developments in Sedimentology. Elsevier, 1967, pp. 1–28. URL: [https://doi.org/10.1016/S0070-4571\(08\)71109-9](https://doi.org/10.1016/S0070-4571(08)71109-9).
- [28] Fan, Tianguang and Buckley, Jill S. *Acid Number Measurements Revisited*. Tulsa, Oklahoma, USA, Jan. 2006. URL: <https://doi.org/10.2118/99884-MS>.
- [29] Fathi, Jafar. “Water-Based Enhanced Oil Recovery (EOR) in Carbonate Reservoirs - Initial Wetting Condition and Wettability Alteration by Smart Water”. PhD thesis. University of Stavanger, 2012.
- [30] Friedman, Gerald M. “Chapter 8 Chalk Reservoirs”. In: *Carbonate Reservoir Characterization: A Geologic - Engineering Analysis*. Ed. by G.V. Chilingarian, S.J. Mazzullo, and H.H. Rieke. Vol. 44. Developments in Petroleum Science. Elsevier, 1996, pp. 773–795. URL: [https://doi.org/10.1016/S0376-7361\(96\)80030-6](https://doi.org/10.1016/S0376-7361(96)80030-6).
- [31] Frykman, Peter. “Spatial variability in petrophysical properties in Upper Maastichtian chalk outcrops at Stevns Klint, Denmark”. In: *Marine and Petroleum Geology* 18.10 (2001), pp. 1041–1062. ISSN: 0264-8172. URL: [https://doi.org/10.1016/S0264-8172\(01\)00043-5](https://doi.org/10.1016/S0264-8172(01)00043-5).
- [32] Graue, A., Nesse, K., Baldwin, B.A, Spinler, E., and Tobola, D.P. “Impact of Fracture Permeability on Oil Recovery in Moderately Water-Wet Fractured Chalk Reservoirs”. In: *Society of Petroleum Engineers, SPE 75165* (Apr. 2002), p. 8. ISSN: 978-1-55563-951-8. URL: <https://doi.org/10.2118/75165-MS>.

- [33] Green and Willhite. *Enhanced oil recovery*. eng. Vol. 6. SPE textbook series. Richardson, Tex: Henry L. Doherty Memorial Fund of AIME, Society of Petroleum Engineers, 1998. ISBN: 1555630774.
- [34] Hall. “Analysis of gravity drainage”. In: *AIME: Journal of Petroleum Technology* 13.09 (1961), pp. 927–936. URL: <https://doi.org/10.2118/1517-G-PA>.
- [35] Hamouda, Aly Anis and Rezaei Gomari, Karam Ali. *Influence of Temperature on Wettability Alteration of Carbonate Reservoirs*. Tulsa, Oklahoma, USA, Jan. 2006. URL: <https://doi.org/10.2118/99848-MS>.
- [36] Hopkins, P. A., Omland, I., Layti, F., Strand, S., Puntervold, T., and Austad, Tor. “Crude Oil Quantity and Its Effect on Chalk Surface Wetting”. In: *Energy Fuels* 31.5 (May 2017), pp. 4663–4669. ISSN: 0887-0624. URL: <https://doi.org/10.1021/acs.energyfuels.6b02914>.
- [37] Hopkins, Paul Andrew. “Water-Based EOR and Initial Wettability in Carbonates”. PhD thesis. University of Stavanger, 2017.
- [38] KRUSS. *Force Tensiometer - K6*. English. KRUSS. 2019. URL: <https://www.kruss-scientific.com/products/tensiometers/force-tensiometer-k6/>.
- [39] Lucia F, jerry. *Carbonate Reservoir Characterization: An Integrated Approach*. Jan. 2007. ISBN: 978-3-540-72740-8. DOI: 10.1007/978-3-540-72742-2.
- [40] Montaron, Bernard. “Confronting Carbonates”. In: *Oil Review Middle East*. 4. ADIPEC. Schlumberger, 2008, pp. 132–135. URL: https://www.slb.com/~media/Files/industry_challenges/carbonates/industry_articles/200811_orme_confronting_carbonates.pdf.
- [41] Muskat, M. *Physical principles of oil production*. English. New York: McGraw-Hill Book Co., 1949.
- [42] Nair, Remya Ravindran. “Smart Water for Enhanced Oil Recovery from Seawater and Produced Water by Membranes”. PhD thesis. University of Stavanger, Mar. 2019.
- [43] NanoScience. *Scanning Electron Microscopy*. nanoScience Instruments. Apr. 2019. URL: <https://www.nanoscience.com/techniques/scanning-electron-microscopy/#electrons>.
- [44] Pierre, A., Lamarche, J.M., Mercier, R., Foissy, A., and Persello, J. “Calcium as Potential Determining Ion in Aqueous Calcite Suspensions”. In: *Journal of Dispersion Science and Technology* 11.6 (1990), pp. 611–635. URL: <https://doi.org/10.1080/01932699008943286>.
- [45] Piñerez Torrijos, I.D, Sæby, K.G, Strand, Skule, and Puntervold, T. “Impact of Temperature on Wettability Alteration by Smart Water in Chalk”. In: 2019.
- [46] Puntervold, Tina. “Waterflooding of carbonate reservoirs: EOR by wettability alteration”. PhD thesis. University of Stavanger, 2008.

- [47] Puntervold, Tina, Strand, Skule, and Austad, Tor. “New Method To Prepare Outcrop Chalk Cores for Wettability and Oil Recovery Studies at Low Initial Water Saturation”. In: *Energy Fuels* 21.6 (Nov. 2007), pp. 3425–3430. ISSN: 0887-0624. URL: <https://doi.org/10.1021/ef700323c>.
- [48] Puntervold, Tina, Strand, Skule, Ellouz, Raed, and Austad, Tor. “Modified seawater as a smart EOR fluid in chalk”. In: *Journal of Petroleum Science and Engineering* 133 (2015), pp. 440–443. ISSN: 0920-4105. URL: <https://doi.org/10.1016/j.petrol.2015.06.034>.
- [49] Rao, Dandina N. *Wettability Effects in Thermal Recovery Operations*. Tulsa, Oklahoma, Jan. 1996. URL: <https://doi.org/10.2118/35462-MS>.
- [50] Salathiel, R. A. “Oil Recovery by Surface Film Drainage In Mixed-Wettability Rocks”. In: *SPE-AIME: 4104-PA* (1973).
- [51] Shariatpanahi, S. F., Hopkins, P., Aksulu, H., Strand, S., Puntervold, T., and Austad, T. “Water Based EOR by Wettability Alteration in Dolomite”. In: *Energy Fuels* 30.1 (Jan. 2016), pp. 180–187. ISSN: 0887-0624. URL: <https://doi.org/10.1021/acs.energyfuels.5b02239>.
- [52] Shell. *Hydrocarbon Recovery Optimisation*. May 2019. URL: https://www.shell.com/energy-and-innovation/overcoming-technology-challenges/making-the-most-of-our-resources/_jcr_content/par/textimage.stream/1462800199005/79f4638ac5b75bdbd4c04c0b4dd2668051648ecb/eor-brochure-2016.pdf.
- [53] Shimoyama and Johns. “Catalytic Conversion of Fatty Acids to Petroleum-like Paraffins and their Maturation”. In: *Nature Physical Science* 232 (Aug. 1971), p. 140. URL: <https://doi.org/10.1038/physci232140a0>.
- [54] Standnes, Dag C and Austad, Tor. “Wettability alteration in chalk: 1. Preparation of core material and oil properties”. In: *Journal of Petroleum Science and Engineering* 28.3 (2000), pp. 111–121. ISSN: 0920-4105. URL: [https://doi.org/10.1016/S0920-4105\(00\)00083-8](https://doi.org/10.1016/S0920-4105(00)00083-8).
- [55] Strand, S., Standnes, D. C., and Austad, T. “New wettability test for chalk based on chromatographic separation of SCN- and SO₄²⁻”. In: *Journal of Petroleum Science and Engineering* 52.1 (June 2006), pp. 187–197. ISSN: 0920-4105. URL: <http://www.sciencedirect.com/science/article/pii/S0920410506000660>.
- [56] Strand, Skule, Høgenesen, Eli J., and Austad, Tor. “Wettability alteration of carbonates—Effects of potential determining ions (Ca²⁺ and SO₄²⁻) and temperature”. In: *Colloids and Surfaces A: Physicochemical and Engineering Aspects* 275.1 (2006), pp. 1–10. ISSN: 0927-7757. URL: <https://doi.org/10.1016/j.colsurfa.2005.10.061>.

- [57] Strand, Skule, Puntervold, Tina, and Austad, Tor. “Effect of Temperature on Enhanced Oil Recovery from Mixed-Wet Chalk Cores by Spontaneous Imbibition and Forced Displacement Using Seawater”. In: *Energy Fuels* 22.5 (Sept. 2008), pp. 3222–3225. ISSN: 0887-0624. URL: <https://doi.org/10.1021/ef800244v>.
- [58] Vo, Loan T., Gupta, Robin, and Hehmeyer, Owen J. *Ion Chromatography Analysis of Advanced Ion Management Carbonate Coreflood Experiments*. Abu Dhabi, UAE, Jan. 2012. URL: <https://doi.org/10.2118/161821-MS>.
- [59] Wathne, Agnes K. “Effect of Wettability on Waterflooding and Relative Permeability at Slightly Water-Wet Conditions”. MA thesis. University of Stavanger, 2019.
- [60] William, Haynes. *Handbook of Chemistry and Physics*. 95th ed. CRC, 2014. ISBN: 1482208687.
- [61] Wilson, James L. “Principles of Carbonate Sedimentation”. In: *Carbonate Facies in Geologic History*. New York, NY: Springer New York, 1975, pp. 1–19. URL: https://doi.org/10.1007/978-1-4612-6383-8_1.
- [62] Zhang, P. and Austad, T. *The Relative Effects of Acid Number and Temperature on Chalk Wettability*. The Woodlands, Texas, Jan. 2005. URL: <https://doi.org/10.2118/92999-MS>.
- [63] Zhang, Peimao. “Water-based EOR in Fractured Chalk - Wettability and Chemical Additives”. PhD thesis. University of Stavanger, 2006.
- [64] Zolotukhin, Anatolij B. *Introduction to petroleum reservoir engineering*. eng. Kristiansand, 2000.

Appendix

A		Poster
B		Chemicals and Brine Recipes
C		Imbibition Data
D		PHREEQC Data

A | Poster

The poster was made for the graduation ceremony for the Petroleum Engineering class, and was presented for students, teachers and people from the petroleum industry.

Introduction

Smart Water is a brine with a specific ionic composition that can change the wettability of the rock surface from mixed-wet toward a more water-wet state. The wettability process consists of a symbiotic effect between the potential determining ions SO_4^{2-} , Ca^{2+} and Mg^{2+} . The change in wettability induces positive capillary forces, P_c , that allow water to spontaneously imbibe into the smaller pores in the chalk leading to an increase in the microscopic sweep efficiency.

Considering that most carbonates are of low water wetness, it is of great interest to inject a brine that can alter the wettability toward a more water-wet state. Injection of SW has already proven to be a great success at the chalk reservoirs Ekofisk and Valhall. However, research by Puntervold et al. (2015) has shown that SW depleted of NaCl is even more efficient than SW at wettability alteration as seen in figure 1.

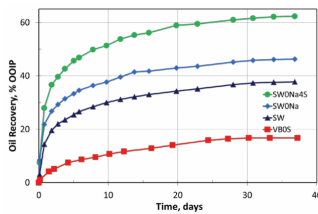
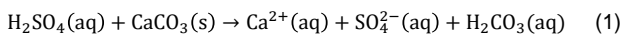


Figure 1: By lowering the amount of NaCl in SW, a higher oil recovery is observed.

Objectives

- Produce a Smart Water brine by injecting sulphuric acid $\text{H}_2\text{SO}_4(\text{aq})$ dissolved in fresh water into Stevns Klint chalk outcrop cores. Acid dissociation of $\text{H}_2\text{SO}_4(\text{aq})$ will provide SO_4^{2-} ions to the solution, and dissociation of the chalk surface, $\text{CaCO}_3(\text{s})$, will provide Ca^{2+} ions to solution according to the following reaction:



- Perform oil recovery by spontaneous imbibition at 90 °C to evaluate the performance of the Smart Water brine produced by acid flooding, compared to SW which already is an excellent wettability modifier in chalk. Gypsum dissolved in DI-water is used to synthetically produce the Smart Water to simplify the experimental test.

Methods

Acid flooding was performed on a Stevns Klint chalk outcrop core saturated with 100 % deionized (DI) water at 70 °C and 130 °C with the set-up shown in figure 2. The effluent brine was sampled and analysed with an ion chromatograph to evaluate if a 1:1 ratio between Ca^{2+} and SO_4^{2-} was obtained in line with equation (1).

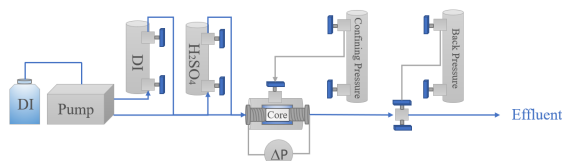


Figure 2: Set-up used during the acid flooding experiment. A confining pressure of 20 bar was used with a backpressure of 10 bar to.

The SI-experiment at 90 °C was performed with a backpressure of 10 bar to avoid any evaporation. Oil produced from the core was collected in a burette and the oil recovery was noted.

Results

Figure 3 presents the effluent concentration of SO_4^{2-} and Ca^{2+} when a 13.3 mM solution of $\text{H}_2\text{SO}_4(\text{aq})$ has been injected into a chalk core saturated with 100 % DI-water. Figure 4 shows the measured pH of the effluent samples.

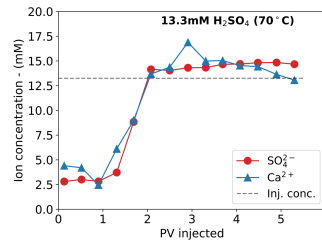


Figure 3: Effluent concentration of Ca^{2+} and SO_4^{2-} at 13.3 mM injected H_2SO_4

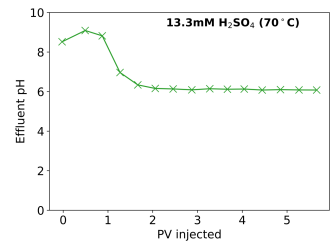


Figure 4: Effluent pH at 13.3mM injected H_2SO_4

The effluent concentration of SO_4^{2-} and Ca^{2+} is of equal proportion in line with equation 1. The produced brine by acid flooding has the necessary ions for wettability alteration in chalk, and is also of low salinity (< 2000 ppm) compared to SW (33 390 ppm). Recall that SW depleted in NaCl is more efficient at altering the wettability than SW. The initial effluent pH is on the alkaline side and transitions towards an equilibrium at pH ~ 6.

Figure 5 shows the oil recovery by spontaneous imbibition, with three imbibition fluids; FW, SW and Smart Water. The highest oil recovery is obtained with Smart Water with 27 % OOIP, then SW with 23 % OOIP and FW with 10 % OOIP. If wettability alteration is based on the oil recovery, then Smart Water is more efficient than SW at altering the wettability towards a more water-wet state.

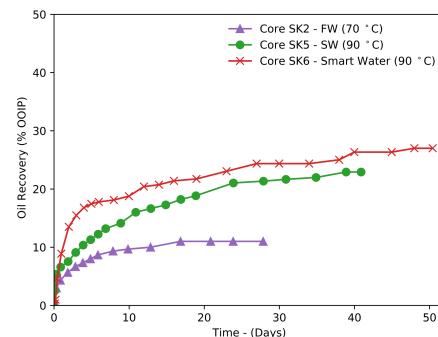


Figure 5: Oil recovery by spontaneous imbibition with imbibition fluids FW, SW and Smart Water.

Conclusions

The spontaneous imbibition experiment indicates that there is a potential benefit of producing Smart Water by acid flooding in chalk reservoirs. The Smart Water yields a higher oil recovery than SW, with 4 % OOIP more by spontaneous imbibition. Only a small increase in recovery can have huge economical profits.

In terms of practicality, fresh water can be produced on the rig by desalinating seawater through reverse osmosis membranes, while H_2SO_4 is readily available on the international market and can be bought in large quantities very cheap.

Future Work

Perform acid flooding with higher acid concentrations to verify if dissolution of CaCO_3 is constrained. In addition, Mg^{2+} ions can be added to the injected solution. Complexes such as $[\text{Mg}^{2+} \dots \text{SO}_4^{2-}](\text{aq})$ form as a result, allowing a higher injected concentration of $\text{H}_2\text{SO}_4(\text{aq})$.

Acknowledgement

All students and staff who participated in this experimental work. A special thanks to Erlend Andreassen.

Contact information

Markus Lindanger
+47 458 72 815
markus.lindanger@gmail.com

B | Chemicals and Brine Recipes

B.1 Acid Number Solutions

Table B.1: Chemicals for acid number measurements

Solution	Chemicals	Formula	Description
Titrant	KOH (> 85%) 2-propanol	KOH $\text{CH}_3\text{CHOHCH}_3$	2.8 g KOH (> 85%) dilute to 1000 ml with 2-propanol ($\text{CH}_3\text{CHOHCH}_3$)
Spiking solution	Stearic acid Acid titration solvent	$\text{CH}_3(\text{CH}_2)_{16}\text{COOH}$	0.5g Stearic Acid - ($\text{CH}_3(\text{CH}_2)_{16}\text{COOH}$) dilute to 100 ml with Acid titration solvent
Standard solution	Potassium Hydrogen Phtalate, KHP DI water	$\text{HOOC}_6\text{H}_4\text{COOK}$	0.2 g Potassium Hydrogen Phtalate, KHP diluted to 500 ml with DI water
Titration solvent	DI water 2-propanol Toluene	$\text{CH}_3\text{CHOHCH}_3$ $\text{C}_6\text{H}_5\text{CH}_3$	6 ml DI water dilute with 494 ml 2-propanol and with 500 ml Toluene
Electrode/ Electrolyte	Potassium chloride DI water	KCl	Mettler DG-114 Electrode 3 M KCl in DI water

B.2 Base Number Solutions

Table B.2: Chemicals for base number measurements

Solution	Chemicals	Formula	Description
Titrant	Perchloric Acid (70%) Acetic Anhydride Acetic Acid	HClO_4 (70%) $(\text{CH}_3\text{CO})_2\text{O}$ CH_3COOH	5 ml 70% Perchloric Acid (HClO_4) 15 ml Acetic Anhydride ($(\text{CH}_3\text{CO})_2\text{O}$) dilute to 1000 ml with Acetic Acid (CH_3COOH)
Spiking solution	Quinoline Decane	$\text{C}_9\text{H}_7\text{N}$ $\text{CH}_3(\text{CH}_2)_8\text{CH}_3$	0.5 g Quinoline ($\text{C}_9\text{H}_7\text{N}$) dilute to 100 ml with Decane ($\text{CH}_3(\text{CH}_2)_8\text{CH}_3$)
Standard solution	Potassium Hydrogen Phtalate, KHP Acetic Acid	$\text{HOOC}_6\text{H}_4\text{COOK}$ CH_3COOH	0.2 g Potassium Hydrogen Phtalate, KHP diluted to 250 ml with Acetic Acid (CH_3COOH)
Titration solvent	Methyl Isobutyl Ketone, MIKB	$(\text{CH}_3)_2\text{CHCH}_2\text{COCH}_3$	Methyl Isobutyl Ketone ($(\text{CH}_3)_2\text{CHCH}_2\text{COCH}_3$)
Electrode/ Electrolyte	Sodium Perchlorate, (solid) 2-propanol	$\text{NaClO}_4(\text{s})$ $\text{CH}_3\text{CHOHCH}_3$	Mettler DG-113 Electrode Electrolyte: Saturated Sodium Perchloride, ($\text{NaClO}_4(\text{s})$), in 2-propanol

B.3 Brine Recipes

Table B.3: Composition of the formation water at Valhall without sulphate, VB0S, synthetic seawater SW and Smart Water.

Salt	SSW g/l	VB0S g/l	Smart Water g/l
NaCl	23.38	57.70	0.00
Na ₂ SO ₄	3.41	0.00	0.00
KSCN	0.00	0.00	0.00
NaHCO ₃	0.17	0.781	0.00
KCl	0.75	0.395	0.00
MgCl ₂ × 6 H ₂ O	9.05	1.58	0.00
CaCl ₂ × 2 H ₂ O	1.91	4.26	0.00
BaCl ₂ × 2 H ₂ O	0.00	0.00	0.00
SrCl ₂ × 6 H ₂ O	0.00	0.00	0.00
CaSO ₄ × 2 H ₂ O	0.00	0.00	2.24
Density g/cm ³	1.024	1.041	0.995
TDS g/L	33.39	62.83	1.77

C | Imbibition Data

C.1 Imbibition Data for SK5

C.1.1 Spontaneous Imbibition Data - SK5

Table C.1: Data from spontaneous imbibition of SK5 with SSW. The OOIP is 31.85 ml.

Time (Days)	Volume Oil (ml)	% OOIP
0.00	0.00	0.00
0.10	0.80	2.51
0.20	1.70	5.34
0.31	1.70	5.34
0.88	2.10	6.59
1.88	2.40	7.54
2.88	2.90	9.10
3.88	3.30	10.36
4.88	3.60	11.30
5.88	3.90	12.24
6.88	4.20	13.19
8.88	4.50	14.13
10.88	5.10	16.01
12.88	5.30	16.64
14.88	5.50	17.27
16.88	5.80	18.21
18.88	6.00	18.84
23.88	6.70	21.04
27.88	6.80	21.35
30.88	6.90	21.66
34.88	7.00	21.98
38.88	7.30	22.92
40.88	7.30	22.92

C.1.2 Forced Imbibition Data - SK5

Table C.2: Forced imbibition data of SK5 with SSW initially and then later switched to Smart Water. The injection rate was set to 1 PV/day = 0.025 ml/min.

Fluid	PV injected	Volume (ml)	% OOIP	ΔP (mbar)	q (ml/min)
SSW	-0.09	7.30	22.92	100	0.025
SSW	-0.07	7.30	22.92	598	0.025
SSW	-0.01	7.30	22.92	530	0.025
SSW	0.00	7.30	22.92	524	0.025
SSW	0.02	7.30	22.92	520	0.025
SSW	0.04	7.70	24.18	540	0.025
SSW	0.06	8.40	26.37	548	0.025
SSW	0.08	9.00	28.26	564	0.025
SSW	0.10	9.60	30.14	583	0.025
SSW	0.12	10.30	32.34	598	0.025
SSW	0.15	10.90	34.22	599	0.025
SSW	0.17	11.60	36.42	583	0.025
SSW	0.19	12.20	38.30	560	0.025
SSW	0.21	13.00	40.82	554	0.025
SSW	0.23	13.30	41.76	537	0.025
SSW	0.25	13.60	42.70	523	0.025
SSW	0.27	13.80	43.33	506	0.025
SSW	0.29	14.00	43.95	490	0.025
SSW	0.32	14.00	43.95	474	0.025
SSW	0.34	14.20	44.58	482	0.025
SSW	0.36	14.30	44.90	486	0.025
SSW	0.38	14.40	45.21	473	0.025
SSW	0.40	14.50	45.52	454	0.025
SSW	0.42	14.60	45.84	449	0.025
SSW	0.44	14.70	46.15	435	0.025
SSW	0.46	14.80	46.47	436	0.025
SSW	0.49	14.80	46.47	452	0.025
SSW	0.51	14.90	46.78	452	0.025
SSW	0.52	14.90	46.78	436	0.025

Table B.2: Forced imbibition data of SK5 with Smart Water continued.

Fluid	PV injected	Volume (ml)	% OOIP	ΔP (mbar)	q (ml/min)
SSW	0.95	15.60	48.98	395	0.025
SSW	1.09	15.70	49.29	354	0.025
SSW	1.22	15.80	49.61	373	0.025
SSW	1.42	16.00	50.23	374	0.025
SSW	2.09	16.30	51.18	349	0.025
SSW	2.49	16.40	51.49	338	0.025
SSW	3.08	16.60	52.12	319	0.025
SSW	3.37	16.60	52.12	308	0.025
SSW	4.02	16.60	52.12	295	0.025
Smart Water	4.03	16.60	52.12	295	0.025
Smart Water	4.03	16.60	52.12	303	0.025
Smart Water	4.09	16.70	52.43	300	0.025
Smart Water	4.14	16.70	52.43	301	0.025
Smart Water	4.38	16.70	52.43	288	0.025
Smart Water	5.08	16.70	52.43	267	0.025
Smart Water	5.14	16.70	52.43	390	0.100
Smart Water	5.16	16.70	52.43	688	0.100
Smart Water	5.21	16.80	52.75	674	0.100
Smart Water	5.30	17.00	53.37	664	0.100
Smart Water	5.38	17.10	53.69	655	0.100
Smart Water	5.47	17.10	53.69	634	0.100
Smart Water	5.64	17.20	54.00	618	0.100
Smart Water	5.80	17.30	54.32	613	0.100
Smart Water	5.97	17.30	54.32	596	0.100
Smart Water	6.14	17.50	54.94	586	0.100
Smart Water	6.33	17.70	55.57	540	0.100
Smart Water	6.42	17.70	55.57	552	0.100
Smart Water	6.51	17.70	55.57	552	0.100
Smart Water	6.74	17.80	55.89	548	0.100
Smart Water	8.77	17.80	55.89	477	0.100

C.2 Imbibition Data for SK6

C.2.1 Spontaneous Imbibition Data - SK6

Table C.3: Data from spontaneous imbibition of SK6 with Smart Water. The OOIP is 30.38 ml.

Time (Days)	Volume Oil (ml)	% OOIP
0.00	0.00	0.00
0.10	0.10	0.33
0.21	0.30	0.99
0.42	1.40	4.61
0.97	2.70	8.89
1.97	4.10	13.50
2.97	4.70	15.47
3.97	5.10	16.79
4.97	5.30	17.45
5.97	5.40	17.78
7.97	5.50	18.11
9.97	5.70	18.77
11.97	6.20	20.41
13.97	6.30	20.74
15.97	6.50	21.40
18.97	6.60	21.73
22.97	7.00	23.05
26.97	7.30	24.03
29.97	7.40	24.36
33.97	7.40	24.36
37.97	7.60	25.02
39.97	8.00	26.34
44.97	8.00	26.34
47.97	8.20	27.00
50.42	8.20	27.00

C.2.2 Forced Imbibition Data - SK6

Table C.4: Forced imbibition data of SK6 with Smart Water. The injection rate was set to 1 PV/day = 0.023 ml/min.

Fluid	PV injected	Volume (ml)	% OOIP	ΔP (mbar)	q (ml/min)
Smart Water	-0.09	8.20	27.00	150.00	0.024
Smart Water	-0.07	8.20	27.00	488.00	0.024
Smart Water	-0.02	8.20	27.00	490.00	0.024
Smart Water	0.01	8.20	27.00	496.00	0.024
Smart Water	0.03	8.80	28.97	508.00	0.024
Smart Water	0.05	9.50	31.28	522.00	0.024
Smart Water	0.07	10.10	33.25	536.00	0.024
Smart Water	0.09	10.70	35.23	548.00	0.024
Smart Water	0.12	11.30	37.20	559.00	0.024
Smart Water	0.14	11.90	39.18	561.00	0.024
Smart Water	0.16	12.60	41.48	550.00	0.024
Smart Water	0.18	13.30	43.79	525.00	0.024
Smart Water	0.20	13.90	45.76	515.00	0.024
Smart Water	0.22	14.20	46.75	504.00	0.024
Smart Water	0.24	14.70	48.40	490.00	0.024
Smart Water	0.27	14.80	48.72	482.00	0.024
Smart Water	0.29	15.00	49.38	470.00	0.024
Smart Water	0.31	15.10	49.71	474.00	0.024
Smart Water	0.35	15.20	50.04	472.00	0.024
Smart Water	0.37	15.30	50.37	455.00	0.024
Smart Water	0.39	15.30	50.37	453.00	0.024
Smart Water	0.41	15.40	50.70	446.00	0.024
Smart Water	0.44	15.50	51.03	433.00	0.024
Smart Water	0.46	15.50	51.03	420.00	0.024

Forced imbibition data of SK6 with Smart Water continued.

Fluid	PV injected	Volume (ml)	% OOIP	ΔP (mbar)	q (ml/min)
Smart Water	0.48	15.50	51.03	413.00	0.024
Smart Water	0.50	15.60	51.36	407.00	0.024
Smart Water	0.52	15.60	51.36	410.00	0.024
Smart Water	0.98	16.20	53.33	373.00	0.024
Smart Water	1.04	16.20	53.33	367.00	0.024
Smart Water	1.15	16.30	53.66	356.00	0.024
Smart Water	1.26	16.30	53.66	356.00	0.024
Smart Water	1.37	16.40	53.99	348.00	0.024
Smart Water	2.16	16.50	54.32	312.00	0.024
Smart Water	3.14	16.60	54.65	279.00	0.024
Smart Water	4.04	16.60	54.65	270.00	0.024
Smart Water	4.04	16.60	54.65	640.00	0.096
Smart Water	4.12	16.60	54.65	616.00	0.096
Smart Water	4.21	17.00	55.97	570.00	0.096
Smart Water	4.30	17.10	56.30	534.00	0.096
Smart Water	4.38	17.20	56.63	526.00	0.096
Smart Water	4.47	17.20	56.63	515.00	0.096
Smart Water	4.55	17.20	56.63	530.00	0.096
Smart Water	4.64	17.20	56.63	501.00	0.096
Smart Water	4.72	17.30	56.95	525.00	0.096
Smart Water	4.81	17.30	56.95	500.00	0.096
Smart Water	4.98	17.30	56.95	495.00	0.096
Smart Water	5.15	17.40	57.28	486.00	0.096
Smart Water	5.94	17.50	57.61	484.00	0.096
Smart Water	8.14	17.50	57.61	409.00	0.096

C.3 Imbibition Data for SK2

C.3.1 Spontaneous Imbibition Data - SK2

Table C.5: Data from spontaneous imbibition of SK2 with FW (VB0S). The OOIP is 32.54 ml.

Time (Days)	Volume Oil (ml)	% OOIP
0.00	0.00	0.00
0.32	0.90	2.77
0.85	1.30	4.00
1.83	1.70	5.23
2.85	2.00	6.15
3.85	2.20	6.76
4.85	2.40	7.38
6.18	2.60	7.99
7.89	2.80	8.61
9.85	2.90	8.91
13.01	3.00	9.22
16.85	3.30	10.14
20.85	3.30	10.14
23.85	3.30	10.14
27.85	3.30	10.14

C.3.2 Forced Imbibition Data - SK2

Table C.6: Forced imbibition data of SK2 with FW (VB0S) and later switched to CaSO₄. The injection rate was set to 1 PV/day = 0.025 ml/min.

Fluid	PV injected	Volume (ml)	% OOIP	ΔP (mbar)	q (ml/min)
VB0S	-0.09	3.30	10.14	100.00	0.025
VB0S	-0.06	3.30	10.14	737.00	0.025
VB0S	-0.01	3.30	10.14	673.00	0.025
VB0S	0.00	3.30	10.14	662.00	0.025
VB0S	0.02	3.90	11.99	638.00	0.025
VB0S	0.04	4.50	13.83	633.00	0.025
VB0S	0.06	5.30	16.29	623.00	0.025
VB0S	0.08	6.00	18.44	619.00	0.025
VB0S	0.10	6.70	20.59	616.00	0.025
VB0S	0.12	7.40	22.74	619.00	0.025
VB0S	0.14	8.20	25.20	624.00	0.025
VB0S	0.16	8.90	27.36	628.00	0.025
VB0S	0.19	9.70	29.81	639.00	0.025
VB0S	0.21	10.40	31.97	646.00	0.025
VB0S	0.23	11.00	33.81	648.00	0.025
VB0S	0.25	11.60	35.65	659.00	0.025
VB0S	0.27	12.40	38.11	659.00	0.025
VB0S	0.29	12.90	39.65	664.00	0.025
VB0S	0.31	13.50	41.49	676.00	0.025
VB0S	0.33	14.10	43.34	661.00	0.025
VB0S	0.35	14.70	45.18	652.00	0.025
VB0S	0.37	15.10	46.41	644.00	0.025
VB0S	0.39	15.50	47.64	640.00	0.025
VB0S	0.41	15.90	48.87	629.00	0.025
VB0S	0.43	16.20	49.79	612.00	0.025
VB0S	0.46	16.30	50.10	601.00	0.025
VB0S	0.48	16.50	50.71	611.00	0.025
VB0S	0.50	16.70	51.33	596.00	0.025
VB0S	0.52	16.80	51.64	594.00	0.025
VB0S	0.54	16.90	51.94	600.00	0.025
VB0S	0.99	17.80	54.71	520.00	0.025
VB0S	1.01	17.80	54.71	510.00	0.025

Table B.6: Forced imbibition data of SK2 with Smart Water continued.

Fluid	PV injected	Volume (ml)	% OOIP	ΔP (mbar)	q (ml/min)
VB0S	1.06	17.80	54.71	507.00	0.025
VB0S	1.10	17.80	54.71	508.00	0.025
VB0S	1.24	17.80	54.71	502.00	0.025
VB0S	1.38	17.80	54.71	519.00	0.025
VB0S	1.49	17.90	55.02	485.00	0.025
VB0S	1.97	18.00	55.33	470.00	0.025
VB0S	2.13	18.00	55.33	283.00	0.025
VB0S	2.36	18.00	55.33	300.00	0.025
VB0S	2.49	18.00	55.33	289.00	0.025
VB0S	2.95	18.00	55.33	300.00	0.025
VB0S	2.98	18.00	55.33	125.00	0.025
VB0S	2.98	18.00	55.33	288.00	0.025
Smart Water	3.03	18.00	55.33	264.00	0.025
Smart Water	3.10	18.00	55.33	280.00	0.025
Smart Water	3.15	18.00	55.33	303.00	0.025
Smart Water	3.25	18.00	55.33	302.00	0.025
Smart Water	3.85	18.00	55.33	273.00	0.025
Smart Water	3.86	18.00	55.33	275.00	0.025
Smart Water	3.93	18.10	55.63	827.00	0.100
Smart Water	4.01	18.60	57.17	818.00	0.100
Smart Water	4.09	18.80	57.78	792.00	0.100
Smart Water	4.18	19.00	58.40	777.00	0.100
Smart Water	4.26	19.10	58.71	755.00	0.100
Smart Water	4.34	19.10	58.71	755.00	0.100
Smart Water	4.43	19.30	59.32	748.00	0.100
Smart Water	4.51	19.40	59.63	737.00	0.100
Smart Water	4.59	19.40	59.63	733.00	0.100
Smart Water	4.67	19.40	59.63	717.00	0.100
Smart Water	5.10	19.60	60.24	688.00	0.100
Smart Water	5.67	19.80	60.86	666.00	0.100
Smart Water	7.87	19.80	60.86	593.00	0.100

C.4 pH of Effluent During Acid Flooding

Table C.7: pH measurements of effluent from the acid flooding for core SK1 are given vs pore volume injected.

Flooding at 70°C						Flooding at 130°C			
H ₂ SO ₄ (12 mM)		H ₂ SO ₄ (15 mM)		H ₂ SO ₄ (18 mM)		H ₂ SO ₄ (6 mM)		H ₂ SO ₄ (8 mM)	
PV	pH	PV	pH	PV	pH	PV	pH	PV	pH
0.00	8.61	0.00	8.52	0.00	8.15	0.00	7.38	0.00	7.06
0.38	8.65	0.49	9.09	0.38	7.99	0.36	7.20	0.37	7.12
0.78	8.79	0.87	8.82	0.79	8.06	0.75	7.52	0.77	7.21
1.18	7.67	1.27	6.97	1.20	6.63	1.12	7.18	1.16	6.91
1.58	6.43	1.67	6.34	1.60	6.27	1.51	6.38	1.56	6.28
1.98	6.25	2.06	6.16	2.01	6.03	1.89	6.32	1.95	6.28
2.37	6.22	2.46	6.14	2.42	6.12	2.26	6.31	2.34	6.22
2.75	6.19	2.88	6.09	2.83	6.05	2.65	6.29	2.74	6.16
3.14	6.22	3.28	6.15	3.24	6.09	3.03	6.23	3.13	6.05
3.52	6.18	3.67	6.12	3.65	6.07	3.41	6.15	3.53	5.97
3.90	6.17	4.04	6.13	4.06	6.05	3.79	6.23	3.92	5.95
4.28	6.19	4.45	6.08	4.46	6.04	4.17	6.10	4.32	5.98
4.67	6.25	4.86	6.10	4.87	6.07	4.55	6.11	4.71	5.92
5.18	N/A	5.27	6.09	5.28	6.02	4.93	6.13	5.11	5.93
5.41	6.23	5.66	6.08						

C.5 Ion Chromatography Results

C.5.1 IC Analysis of Effluent from 6 mM H₂SO₄ (130°)

Table C.8

PV (ml)	Na ⁺ (mM)	K ⁺ (mM)	Mg ²⁺ (mM)	Ca ²⁺ (mM)	Cl ⁻ (mM)	SO ₄ ²⁻ (mM)
0.127	3.355	0.143	0.429	4.136	2.286	2.052
0.512	2.525	1.117	0.236	2.442	1.829	1.864
0.893	15.156	1.242	0.627	5.763	6.613	5.457
1.272	4.145	0.334	0.352	4.106	3.156	2.279
1.655	73.590	3.314	0.203	3.027	6.357	3.302
2.034	5.245	0.420	0.207	2.339	3.033	1.961
2.413	56.317	0.134	0.116	2.254	1.138	3.369
2.795	4.748	0.363	0.342	3.473	3.111	2.225
3.175	55.958	0.134	0.154	1.830	2.498	3.919
3.559	27.397	0.105	0.477	4.905	3.145	4.031
3.938	5.668	0.946	0.583	7.388	4.439	4.520
4.316	87.606	1.012	0.207	3.819	6.390	5.828
4.698	7.330	0.382	0.313	6.736	1.561	4.632
5.087	1.490	0.392	0.227	5.403	0.914	4.717

C.5.2 IC Analysis of Effluent from 8 mM H₂SO₄ (130°)

Table C.9

PV (ml)	Na ⁺ (mM)	K ⁺ (mM)	Mg ²⁺ (mM)	Ca ²⁺ (mM)	Cl ⁻ (mM)	SO ₄ ²⁻ (mM)
0.130	0.110	0.278	0.207	1.953	0.416	2.567
0.529	0.142	0.404	0.157	2.007	0.404	2.553
0.921	1.528	N/A	0.276	3.003	2.369	2.933
1.318	0.087	0.224	0.138	2.057	0.555	2.769
1.708	0.906	0.179	0.166	2.469	1.202	3.026
2.103	3.859	0.682	0.281	3.138	3.363	3.181
2.497	3.190	0.108	0.345	3.811	2.820	3.101
2.891	3.198	0.251	0.387	4.298	2.739	4.718
3.286	2.961	N/A	0.483	6.458	2.554	7.172
3.681	3.284	N/A	0.474	7.248	2.785	7.795
4.075	1.032	N/A	0.239	6.351	0.740	8.034
4.473	3.828	0.126	0.497	7.305	3.421	7.870
4.871	1.425	N/A	0.258	6.327	1.190	8.039
5.264	2.237	0.197	0.350	8.212	1.456	8.395

C.5.3 IC Analysis of Effluent from 12 mM H₂SO₄ (70°)

Table C.10

PV (ml)	Na ⁺ (mM)	K ⁺ (mM)	Mg ²⁺ (mM)	Ca ²⁺ (mM)	Cl ⁻ (mM)	SO ₄ ²⁻ (mM)
0.138	3.330	0.701	0.207	2.463	0.984	2.010
0.540	16.120	1.814	0.188	2.384	5.025	2.022
0.942	10.866	0.377	0.157	2.129	1.813	2.367
1.340	13.018	0.147	0.179	3.084	2.058	2.869
1.738	6.981	1.472	0.546	4.072	2.531	3.162
2.136	48.343	0.106	0.364	6.909	0.688	11.231
2.521	23.718	0.265	0.521	11.564	3.264	9.852
2.904	92.107	0.253	0.268	5.765	0.740	12.444
3.287	45.159	N/A	0.318	7.525	0.699	11.395
3.669	24.838	0.194	0.410	12.993	2.835	10.743
4.053	8.542	0.159	0.176	9.253	0.740	9.798
4.433	107.589	0.165	0.185	6.386	0.910	14.257
4.815	18.521	4.122	0.481	13.283	6.372	9.725
5.203	11.141	0.353	0.225	10.093	0.910	10.234

C.5.4 IC Analysis of Effluent from 15 mM H₂SO₄ (70°)

Table C.11

PV (ml)	Na ⁺ (mM)	K ⁺ (mM)	Mg ²⁺ (mM)	Ca ²⁺ (mM)	Cl ⁻ (mM)	SO ₄ ²⁻ (mM)
0.135	6.750	0.194	0.410	4.407	4.716	2.810
0.516	8.115	0.194	0.325	4.198	5.083	3.008
0.897	4.678	0.175	0.207	2.447	3.144	2.819
1.310	10.439	N/A	0.368	6.111	6.622	3.722
1.693	6.373	0.148	0.457	8.988	3.590	8.844
2.084	3.854	0.129	0.382	13.677	2.363	14.146
2.497	2.292	N/A	0.452	14.370	1.338	14.043
2.914	6.765	0.185	0.476	16.881	4.047	14.308
3.308	5.847	0.148	0.372	14.995	3.612	14.330
3.687	4.615	N/A	0.382	15.039	2.921	14.658
4.077	4.607	N/A	0.401	14.531	2.854	14.694
4.479	3.414	N/A	0.424	14.434	2.185	14.824
4.898	2.362	N/A	0.330	13.640	1.349	14.837
5.301	3.218	N/A	0.514	13.062	2.096	14.667

C.5.5 IC Analysis of Effluent from 18 mM H₂SO₄ (70°)

Table C.12

PV (ml)	Na ⁺ (mM)	K ⁺ (mM)	Mg ²⁺ (mM)	Ca ²⁺ (mM)	Cl ⁻ (mM)	SO ₄ ²⁻ (mM)
0.135	28.522	0.282	0.156	1.045	2.380	2.966
0.541	6.363	0.198	0.284	3.160	3.916	3.053
0.951	2.487	0.141	0.161	1.496	2.029	2.498
1.360	3.505	0.113	0.222	3.785	2.270	3.392
1.765	2.092	N/A	0.407	11.306	1.525	13.801
2.175	7.279	0.094	0.440	15.100	4.629	16.808
2.585	3.742	N/A	0.464	15.758	3.082	17.157
2.994	2.605	N/A	0.360	13.926	2.292	16.529
3.403	5.676	0.894	0.350	13.859	3.817	16.611
3.811	4.973	0.499	0.364	14.152	3.970	16.694
4.217	6.063	1.092	0.393	14.868	3.400	17.060
4.625	2.274	0.132	0.341	14.131	1.974	16.730
5.033	2.242	0.151	0.307	13.469	1.919	16.707
5.430	3.584	0.113	0.369	14.606	3.038	16.753

D | PHREEQC

D.1 PHREEQC - SO_4^{2-} equilibrated with $\text{CaCO}_3(\text{s})$

Table D.1: The table show mM of precipitated $\text{CaSO}_4(\text{s})$ at different temperatures for solutions containing various amounts of SO_4^{2-} equilibrated with $\text{CaCO}_3(\text{s})$.

$C_{\text{SO}_4^{2-}}$:	4 mM	6 mM	8 mM	10 mM	12 mM	16 mM	18 mM	20 mM
Temp °C	Precipitated CaSO_4 (mM)	Precipitated CaSO_4 (mM)	Precipitated CaSO_4 (mM)	Precipitated CaSO_4 (mM)	Precipitated CaSO_4 (mM)	Precipitated CaSO_4 (mM)	Precipitated CaSO_4 (mM)	Precipitated CaSO_4 (mM)
50	0	0	0	0	0	0	0	0
60	0	0	0	0	0	0	0	0.671
70	0	0	0	0	0	1.289	2.17	2.989
80	0	0	0	0.2444	1.342	3.246	4.077	4.846
90	0	0	0.732	1.923	2.986	4.794	5.574	6.294
100	0	0.717	2.097	3.265	4.286	5.99	6.721	7.395
110	0.3604	1.86	3.183	4.32	5.293	6.891	7.574	8.207
120	1.199	2.73	4.04	5.139	6.059	7.552	8.193	8.789
130	1.856	3.405	4.71	5.764	6.626	8.022	8.625	9.19

D.2 PHREEQC - SO_4^{2-} and Mg^{2+} equilibrated with $\text{CaCO}_3(\text{s})$

Table D.2: The table show mM of precipitated $\text{CaSO}_4(\text{s})$ at different temperatures for solutions containing various amounts of SO_4^{2-} and Mg^{2+} equilibrated with $\text{CaCO}_3(\text{s})$.

$C_{\text{SO}_4^{2-}} = C_{\text{Mg}^{2+}}$:	4 mM	6 mM	8 mM	10 mM	12 mM	16 mM	18 mM	20 mM
Temp °C	Precipitated CaSO_4 (mM)	Precipitated CaSO_4 (mM)	Precipitated CaSO_4 (mM)	Precipitated CaSO_4 (mM)	Precipitated CaSO_4 (mM)	Precipitated CaSO_4 (mM)	Precipitated CaSO_4 (mM)	Precipitated CaSO_4 (mM)
50	0	0	0	0	0	0	0	0
60	0	0	0	0	0	0	0	0
70	0	0	0	0	0	0	0	0
80	0	0	0	0	0	0	0	0
90	0	0	0	0	0	0.008581	0.5753	1.038
100	0	0	0	0	0.4296	1.501	1.985	2.44
110	0	0	0.3267	0.9854	1.588	2.656	3.133	3.578
120	0	0.5148	1.26	1.932	2.539	3.598	4.065	4.499
130	0.3908	1.26	2.029	2.711	3.32	4.365	4.821	5.242